
RamanBench: A Large-Scale Benchmark for Machine Learning on Raman Spectroscopy

Mario Koddenbrock^{1,*} Christoph Lange^{2,*} Robin Legner³ Martin Jaeger⁴
Martin Kögler⁵ Mariano N. Cruz Bournazou² Peter Neubauer²
Felix Bießmann^{6,7} Erik Rodner^{1,8}

¹HTW Berlin ²TU Berlin ³KWS SAAT, Einbeck ⁴HS Niederrhein, Krefeld
⁵VTT Finland, Oulu ⁶BHT Berlin ⁷Einstein Center Digital Future, Berlin
⁸Merantix Momentum, Germany *Equal contribution
mario.koddenbrock@htw-berlin.de christoph.lange@tu-berlin.de
erik.rodner@htw-berlin.de

Abstract

Machine Learning (ML) has transformed many scientific fields, yet key applications still lack standardized benchmarks. Raman spectroscopy, a widely used technique for non-invasive molecular analysis, is one such field where progress is limited by fragmented datasets, inconsistent evaluation, and models that fail to capture the structure of spectral data. We introduce **RamanBench**, the first large-scale, fully reproducible benchmark for ML on Raman spectroscopy, consisting of streamlined data access¹, evaluation protocols and code², as well as a live leaderboard³. It unifies 74 datasets (including 16 first released with this benchmark) across four domains, comprising 325,668 spectra and spanning classification and regression tasks under diverse experimental conditions. We benchmark 28 models under a standardized protocol, including classical methods (e.g., PLS), Raman-specific (e.g., RamanNet), Tabular Foundation Model (TFM) (e.g., TabPFN), and time-series approaches (e.g., ROCKET). TFM consistently outperform domain-specific and gradient boosting baselines, while time-series models remain competitive. However, no method generalizes across datasets, revealing a fundamental gap. Therefore, we invite the community to contribute new approaches to our living benchmark, with the potential to accelerate advances in critical applications such as medical diagnostics, biological research, and materials science.

1 Introduction

Raman spectroscopy is a well-established technique non-invasive inference the composition and molecular properties of materials. The underlying principle is based on exciting a sample with a monochromatic laser beam. A small fraction of the light is inelastically scattered by the vibrations of molecular bonds, shifting the energy of the photons and providing information about the molecular structure. The resulting Raman spectra, which record these energy shifts, are analyzed to identify the chemical composition and molecular structure of the sample [1]. Its versatility and non-invasive nature have led to widespread adoption across diverse domains, including material identification [2], bioprocess monitoring [3], medical diagnostics [4, 5], pharmaceutical quality control [6], and chemical process analysis [7]. Machine Learning (ML) has become central to automating spectral analysis,

¹<https://pypi.org/project/raman-data/>

²<https://pypi.org/project/raman-bench/>

³<https://huggingface.co/spaces/HTW-KI-Werkstatt/RamanBench>

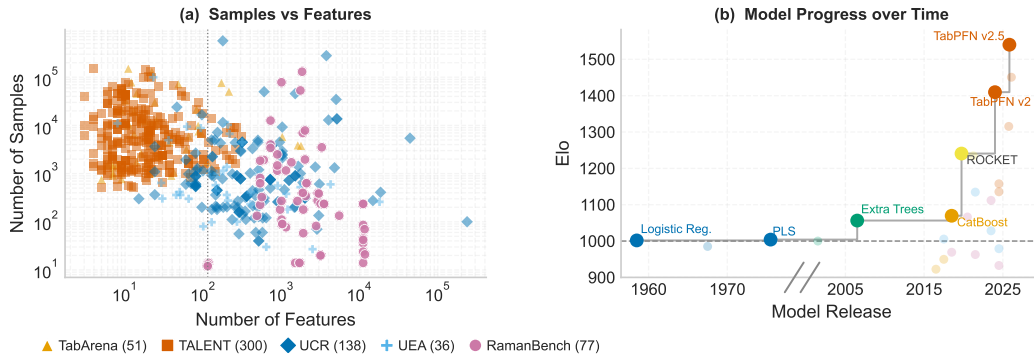


Figure 1: **RamanBench: High dimensional, low sample ML.** **Left:** Sample count vs. feature count for **RamanBench** (pink) and four reference benchmark collections; **RamanBench** occupies a distinct high-dimensional, low-sample regime. TabArena [9] and TALENT [10]: tabular ML; UCR [11] and UEA [12]: Time Series Classification (TSC). **Right:** Model performance (Elo) vs. release year. **RamanBench** enables a retrospective view: Partial Least Squares (PLS), the long-standing domain standard, would have been State-of-the-Art (SOTA) for most of the past decades; only recently have modern methods begun to clearly surpass it, with the SOTA frontier still advancing.

Table 1: **Existing benchmarks and dataset collections for ML on Raman spectroscopy.** Red cells mark a violation of **RamanBench**’s inclusion criteria (synthetic or non-Raman data, restricted/unavailable access); yellow signals a partial concern (multi-spectral scope, i.e. not exclusively Raman, or partial availability). No prior collection combines real measured spectra, Raman-only scope, and fully public access at this scale; most are also limited to a single task type.

Name	Datasets	Tasks	Data	Scope	Availability	In RamanBench
RRUFF Database [2]	1	Clf.	Real	Raman	Public	✓
MP Raman DB [15]	1	Reg.	Synth.	Raman	Public	×
ML Raman Open Dataset (MLROD) [16]	1	Clf.	Real	Raman	Public	✓
SynthSpec [17]	1	Clf.	Synth.	Multi-spectral	Public	×
DSCARNet [18]	12	Clf.	Real	Raman	Partial	Partial
RamanSPy [19]	7	Both	Real	Raman	Partial	Partial
Monte Carlo Peaks [20]	1	Both	Synth.	Multi-spectral	Public	×
Pharma Raman [6]	1	Clf.	Real	Raman	Public	✓
Bioprocess DL [21]	1	Reg.	Real	Raman	Public	✓
8-Spectrometer [22]	8	Reg.	Real	Raman	Public	✓
Validation Study [23]	4	Clf.	Real	Raman	Upon Req.	×
SpectrumWorld [24]	30+	Both	Both	Multi-spectral	Partial	×
DSCF / ComFile [25]	11	Both	Both	Multi-spectral	Partial	Partial
Open DL Bench [26]	3	Clf.	Real	Raman	Public	✓
RamanBench (ours)	74	Both	Real	Raman	Public	

with applications ranging from material classification and disease detection to quantitative prediction of chemical concentrations [8].

Despite its significance, scientific progress in ML for Raman spectroscopy is limited by several factors. Most importantly, comprehensive and standardized evaluation frameworks are lacking. Public Raman datasets are fragmented across platforms such as Kaggle, HuggingFace, Zenodo, and institutional repositories, often in diverse formats (e.g., CSV, MAT, SPC, OPJ), and with sometimes restricted or unreliable access. A comprehensive review of the open Raman data ecosystem by Coca-Lopez et al. [13] confirms this picture: most available databases are not FAIR-compliant[14], lack robust curation, and remain disconnected from reproducible analysis workflows. In Table 1, we summarize prior dataset collections, illustrating the heterogeneity of available resources. This lack of standardization leads to isolated evaluations and hides genuine progress. Many works report results on a single dataset [27, 28] and compare only against simple baselines such as PLS [29] or Support Vector Machine (SVM) [30], while broader comparisons remain limited in scope [26, 21, 13].

Standardized benchmarks have driven progress across many domains, including computer vision [31], natural language processing [32], and tabular data [33]. Unfortunately, Raman spectroscopy cannot

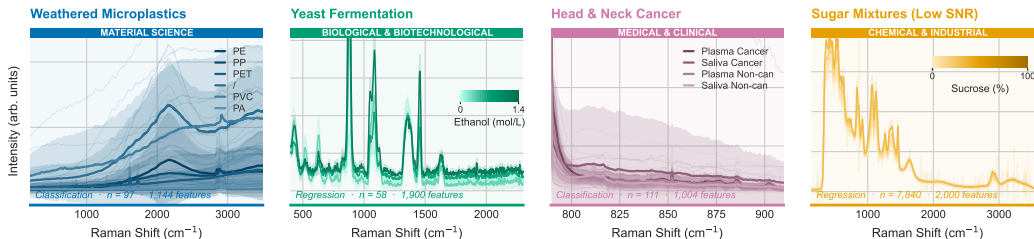


Figure 2: **Representative Raman spectra from the four application domains in RamanBench.** Each panel shows spectra from one domain, colored by class (classification) or by the target analyte value (regression, gradient from low to high). The thick line is the mean spectrum; shaded bands show ± 1 standard deviation. Spectral ranges, sample sizes, noise levels, and analytical tasks differ substantially across domains, illustrating the breadth and heterogeneity of **RamanBench**.

directly benefit from these benchmarks, as the data properties differ fundamentally from those of vision, language, or general tabular settings.

Compared to other benchmarks (Fig. 1, left), Raman spectroscopy data is characterized by typically smaller sample sizes and high feature dimensionality. Each Raman spectrum is a high-dimensional 1D intensity signal where the difference between the exciting and incoming photon is indexed by wavenumber (cm^{-1}). As peaks originate from fuzzy molecular vibrations (Fig. 2), adjacent wavenumber intensities are strongly correlated. On a broader scale, the spectra exhibit peak patterns that reflect the low-rank properties of the underlying molecular structure. These signals are superimposed on a dominant non-linear baseline that changes within a dataset, resulting in a low effective signal-to-noise ratio. While the underlying physical patterns transfer across datasets, both peaks and the baseline are distorted by the optical pathway of each measurement setup [34, 13].

We hypothesize that the statistical dependency patterns inherent to Raman spectroscopy data require dedicated modeling approaches or at least a broader evaluation with more recent models. In particular, modern model classes, including Tabular Foundation Model (TFM) and architectures exploiting spectral structure with non-linear embeddings [35, 36], have received little systematic evaluation across datasets. Ideal ML algorithms for Raman data should handle *high-dimensional* settings across the full spectrum of dataset sizes (from small experimental collections to large spectral libraries (Fig. 1, left)) exploit the shared ordered physical feature space, leverage high local correlations among peak intensities, and learn transferable representations across instruments, sample types, and domains. These requirements are not captured by existing tabular benchmarks such as TabArena [9] and TALENT [10], since tabular data is semantically more heterogeneous, comprising both categorical and numerical features, is unordered, and does not exhibit peak structures or share consistent semantic meaning across datasets. Time series benchmarks such as UCR Time Series Classification Archive (UCR) [11] and UEA Multivariate Time Series Archive (UEA) [12] provide the gold standard for temporal pattern recognition, but cover classification only and each series originates from a different sensor domain.

Inspired by recent advances in the tabular domain [9, 10], we present **RamanBench**, a large-scale, reproducible, and living benchmark for ML on Raman spectroscopy data, covering both classification and regression tasks across diverse instruments, sample types, and experimental conditions. Our main contributions are:

1. **Large-scale unified dataset collection.** We curate and standardize 74 public Raman datasets spanning 163 prediction targets and provide an open-source Python API for unified access.
2. **New datasets.** We publish 16 original Raman datasets for the first time, adding 67 new benchmark tasks (41 % of the total).
3. **Comprehensive evaluation.** We benchmark 28 models, from the longstanding domain standard PLS to modern foundation models (TabPFN, TabICL) and time series classifiers (ROCKET, Arsenal), across all datasets and tasks using standardized evaluation protocols.

Fig. 1 (right) tells two stories at once: First, PLS, the de-facto standard for quantitative Raman analysis, held its ground for a remarkably long time. While tree based approaches offer only a

slight improvement over PLS in the last decade, neural networks have begun to clearly surpass it. Second, even today’s best models leave substantial room for improvement (see Fig. 10), a gap that substantially exceeds the near-saturation seen on general tabular benchmarks and underscores **RamanBench** as an open challenge for the ML community. Beyond the rankings themselves, the figure illustrates that progress in ML for Raman spectroscopy has been scattered across isolated and methodologically inconsistent studies, leaving the field without a coherent performance history. By evaluating all models on the same unified benchmark, **RamanBench** makes this retrospective view possible for the first time: we can now trace which approaches would have led the field at any point in time and quantify how much progress has actually been made.

2 Related Work

Machine Learning (ML) for Raman spectroscopy. ML has been applied to Raman spectroscopy for over two decades, progressing from classical chemometric approaches — Principal Component Analysis (PCA)/Partial Least Squares (PLS) with Support Vector Machine (SVM) or Linear Discriminant Analysis (LDA) [37, 38] — to 1D Convolutional Neural Networks (CNNs) [39–41], transformers [42, 43], and self-supervised pretraining [44, 25]. Despite rich methodological diversity, evaluation remains fragmented: most studies compare only with classical baselines on small, private, or upon-request-only datasets, making it impossible to assess whether the reported gains reflect genuine architectural advances or differences in data and preprocessing [26].

Two concurrent studies partially address this gap. Sineesh and Kamsali [26] benchmark five Raman-specific classifiers on three datasets under a unified protocol. Lange et al. [21] frame Raman spectra as tabular data and compare 11 models (including gradient boosting, tabular neural networks, and TabPFN v1 [45]) on a single regression dataset, finding that CNN-based architectures perform best overall. **RamanBench** extends both efforts to 74 datasets, 28 models, and both classification and regression. Across this broader scope, we confirm Lange et al. [21]’s finding that PLS lags behind more expressive models, but find that Tabular Foundation Models (TFMs) occupy the top of the leaderboard on both tasks; the inconsistency of the original TabPFN v1 reported by Lange et al. [21] does not persist for v2/v2.5. For classification, SANet (the top-performing model in Sineesh and Kamsali [26]) not only ranks below TFMs and time-series classifiers across **RamanBench**, but is also outperformed by Deep CNN among the Raman-specific architectures themselves, suggesting that conclusions drawn from three datasets do not generalize and that the model scope of Sineesh and Kamsali [26] (five Raman-specific DL architectures) is too narrow.

Tabular and time-series benchmarks. Standardized benchmarks have driven progress across ML: ImageNet [31] for vision, GLUE [32] for NLP, and TALENT [10] or TabArena [9] for tabular data. While earlier tabular benchmarks [33] report tree-based methods as strong baselines, more recently TFM such as TabPFN [45, 46] and TabICL [47, 48] have emerged as strong contenders. For Time Series Classification (TSC), UCR Time Series Classification Archive (UCR) [11] and UEA Multivariate Time Series Archive (UEA) [12] are the standard benchmarks, with ROCKET [49] and its ensemble variant Arsenal (itself the core component of the HIVE-COTE [50] meta-ensemble) being among the top-performing methods. Raman spectra are structurally comparable to time series in that both are ordered 1D signals, yet differ fundamentally: all Raman spectra share the same underlying physics, with peak positions determined by molecular vibrational modes and a wavenumber axis that carries absolute physical meaning, a property not present in arbitrary time series. **RamanBench** is the first benchmark to directly compare TSC methods with Raman-specific architectures.

Spectroscopy benchmarks and datasets. In adjacent spectral modalities, MassSpecGym [51] curates 231k tandem Mass spectrometry (MS) spectra for molecular structure tasks, and NMRNet [52] standardizes Nuclear Magnetic Resonance (NMR) chemical shift prediction. No comparable benchmark exists for Raman spectroscopy. RamanSPy [19] offers preprocessing tools and seven curated datasets, but is primarily a spectral analysis toolbox rather than a data access layer; its datasets require manual downloading from their original sources, several of which are no longer publicly accessible. Our `raman-data` package provides unified API access to a broad collection of 89 publicly available Raman datasets.

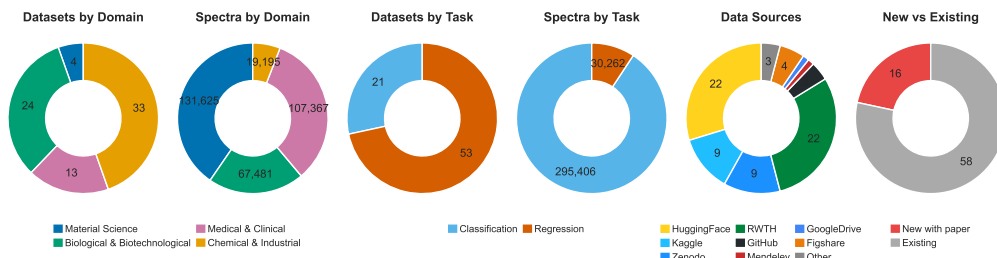


Figure 3: Benchmark composition overview: domain distribution (left two donuts), task distribution (center two), data sources (fifth), and new vs. existing datasets (sixth). **Domain:** Chemical & Industrial has the most datasets; Material Science dominates by spectrum count. **Tasks:** Regression datasets outnumber classification, yet classification accounts for 91 % of spectra. **Sources:** Datasets from eight platforms. **New vs. existing:** 16 datasets released for the first time with this paper.

3 Datasets

RamanBench consists of a curated collection of publicly available Raman spectroscopy datasets, specifically selected to provide a rigorous and comprehensive benchmark for Machine Learning (ML) models. The collection spans a wide range of spectral resolutions, excitation wavelengths (from 532 nm to 1064 nm), and experimental substrates, covering both classification and regression tasks. We provide all datasets in a consistent format via `raman-data` while preserving the unique noise profiles and artifacts characteristic of their respective application domains.

3.1 Inclusion Criteria

To be included, a dataset must be (1) **freely accessible**, (2) consist of **experimentally acquired** (not simulated) Raman spectra, and (3) provide **labels or regression targets** for supervised learning. Beyond these baseline requirements, each dataset must also satisfy:

4. **Minimum size.** At least 10 labeled spectra per dataset. For classification, classes with fewer than 9 spectra are removed (\dagger); if fewer than 2 classes remain, the dataset is excluded.
5. **Learnability.** Each regression target must achieve $R^2 > 0.05$ and each classification dataset must exceed the majority-class baseline by $\Delta F1 > 0.05$ with at least one model; details and exclusions in Section A.6.

Applied to the 89 datasets in `raman-data` (a curated subset of Table 1), these criteria yield 74 benchmark datasets; the remainder were excluded for insufficient size or failed learnability.

Small datasets. Datasets with fewer than 50 spectra are retained in **RamanBench**, as limited sample sizes are common in Raman spectroscopy [7, 53, 54]. However, datasets with fewer than 9 spectra per class are excluded.⁴ Following PMLBmini [58], which emphasizes the importance of benchmarking in data-scarce tabular settings, we further analyze which models are best suited to this regime in Section A.5.

3.2 Dataset Summary

RamanBench comprises **74 datasets**, spanning four application domains: Material Science, Biotechnology, Medical & Clinical, and Chemical & Industrial. Together, they contain **325k+ spectra** and define **163 independent benchmark tasks** (Fig. 3).

Scale diversity. Dataset sizes range from 12 spectra (Time-Gated *E. coli* Fermentation) to 130,061 spectra (MLROD), spanning over four orders of magnitude, with a median of only 235 spectra, reflecting the typical scarcity of labeled data in experimental spectroscopy. Classification datasets account for 91 % of total spectra (295,406 of 325,668), while regression datasets are more numerous

⁴This excludes the RamanBioLib reference library [55], the FT-Raman illicit adulterants subset [56], and the organic compounds dataset [57], each of which contains primarily a single spectrum per compound.

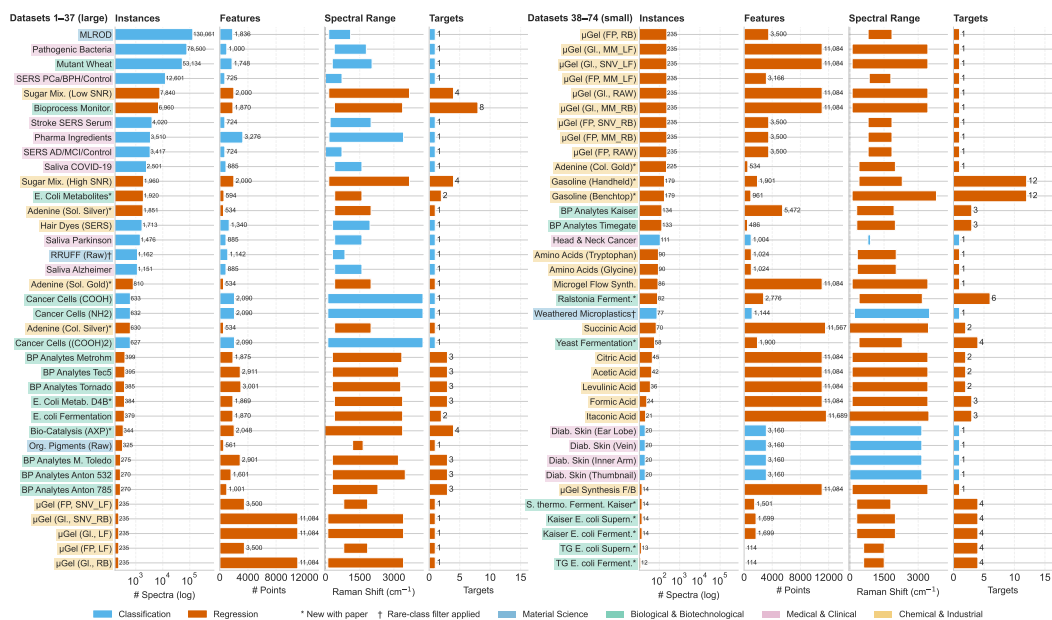


Figure 4: **RamanBench**: 74 datasets, 163 targets and 325,668 spectra across 4 application domains. The overview shows per-dataset characteristics sorted by size (largest top) and split into two halves. Each half shows four panels: **Instances** (spectrum count, log scale), **Features** (number of wavenumber points), **Spectral Range** (cm^{-1}), and **Targets** (regression targets, or 1 for classification). The colors of the dataset names indicate the application domain and the bar colors encode the task types.

(53 of 74) but predominantly small (87 % under 500 samples), demanding data-efficient learning methods (Fig. 4, left).

Spectral diversity. Raman shift coverage ranges from -32 to $4,278 \text{ cm}^{-1}$ (Fig. 4, center)⁵, and feature dimensionality ranges from 114 to 11,689 wavenumber points (median 1,951), placing **RamanBench** firmly in the high-dimensional regime where features outnumber training samples; this is most extreme in the Microgel Size datasets (11,689 points across 235 spectra, a 50:1 feature-to-sample ratio).

Task complexity. Classification difficulty ranges from binary screening (Diabetes, COVID-19) to fine-grained mineral identification with 79 classes (RRUFF raw). On the regression side, 31 of 53 datasets involve multi-target prediction, with up to 12 simultaneous physicochemical properties (Gasoline Properties, Fig. 4, right), yielding 163 distinct prediction tasks in total.

Domain and instrument diversity. The four domains contribute very different numbers of spectra: Material Science accounts for 40 % of spectra (131,625), driven by RRUFF and MLROD; Medical & Clinical 33 % (107,367); Biological & Biotechnological 21 % (67,481); and Chemical & Industrial 6 % (19,195) (Fig. 3). Excitation wavelengths span 532 nm to 1064 nm across benchtop, portable, and process instruments; the Bioprocess Analytes collection uniquely provides the same analytes measured across eight different instruments. Of the 74 datasets, 16 are released for the first time with this paper (marked *; full list in Table 11 in Section A.12), while the remaining 58 originate from HuggingFace, Kaggle, Zenodo, and other repositories.

Detailed per-dataset descriptions, including representative spectra, are provided in Section A.14.

4 Benchmark

To facilitate standardized and reproducible evaluation of Machine Learning (ML) models on Raman spectroscopy data, we developed ramanbench, an open-source benchmarking framework, which

⁵Negative Raman shifts arise in the anti-Stokes region, where scattered photons have higher energy than the excitation laser.

implements the complete benchmarking pipeline, covering data access, splitting, model training, metric computation, and statistical comparison. Implementation details are provided in Section A.3.

4.1 Model Selection

We evaluate 28 models in total from 7 different categories (full list in Section A.2). We choose (a) traditional ML models and (b) tree-based approaches as a reference, (c) Gradient Boosted Trees due to their tabular performance [59], (d) Deep Learning Models including the top-performing architectures from Lange et al. [21](ReZeroNet [60], FCResNeXt [61], and CoAtNet [62]), all recent (e) Tabular Foundation Model (TFM) (TabPFN [45, 46], TabICL [47, 48], MITRA [63], TabDPT [64] and TabM [65]), (f) Raman-specific architectures benchmarked in [26] (Deep CNN [39], SANet [40], RamanNet [41], RamanFormer [42], and RamanTransformer [66]), and (g) Time Series Classification (TSC) models (ROCKET [49] and Arsenal [50]). The two TSC models (classification-only) are providing the first direct comparison between time-series classifiers and Raman-specific architectures at benchmark scale. Additionally, we ran AutoGluon 1.5 [67] with the `extreme_quality` preset and a 4-hour time limit. All models are evaluated on fixed 80/20 train/test splits over 3 different seeds; full details of the splitting procedure and training setup are given in Section A.2.

4.2 Evaluation Metrics

Per-dataset performance is measured by macro-averaged F1-score for classification and RMSE for regression. Because raw metrics are not directly comparable across datasets with different scales and task types, we report two primary aggregate metrics, following Salinas and Erickson [68]: *normalized score* and *Elo rating*.

Normalized score. Each per-dataset raw score is rescaled so that the best model receives 1 and the median model 0; values below zero are clipped. Averaging these values across datasets yields a scale-invariant summary of overall performance.

Elo rating. Elo ratings are derived from pairwise comparisons on seed-averaged per-dataset metrics. For each dataset, raw metrics are first rescaled to $[0, 1]$ so that every dataset contributes equally, and each model pair is treated as a match whose winner is determined by the lower rescaled loss. Starting from a common prior and calibrated so that $RF = 1000$, ratings are updated iteratively across all datasets, yielding a ranking that aggregates evidence without being dominated by any single outlier. Confidence intervals (95 %) are obtained by bootstrapping over datasets.

For completeness, Table 8 also reports average rank and improvability; the improvability–runtime trade-off is visualized in Fig. 10. Statistical significance of pairwise ranking differences is assessed via Critical Difference (CD) diagrams [69], provided in Section A.11. Full metrics definitions and the statistical methodology are given in Section A.1.

4.3 Living Benchmark

RamanBench is designed as a *living benchmark*: results are versioned, the dataset collection grows over time, and the leaderboard is updated as new models and datasets are added. **RamanBench** v0.1 is the initial release presented in this paper. Protocols for contributing datasets and models, versioning, and long-term maintenance are described in Section A.3.4.

5 Results

Leaderboard. Fig. 5 shows the Elo score for each model with 95 % bootstrap confidence intervals. TFMs form the leading group; the only models that enter this group are time-series classifiers (Arsenal, ROCKET), and only on classification tasks, where they also rank above all gradient boosting methods. This is consistent with the two benchmarks discussed in Section 2. Across our broader benchmark, we confirm Lange et al. [21]’s finding that Partial Least Squares (PLS) lags behind more expressive models, and we find that the model scope in Sineesh and Kamsali [26] is too narrow to generalize. Raman-specific architectures are competitive on individual datasets, collectively accounting for 18 wins (see Table 8), but rank below foundation models across the full benchmark. ReZeroNet stands out as the first non-foundation model to challenge the TFM block in the combined regression and

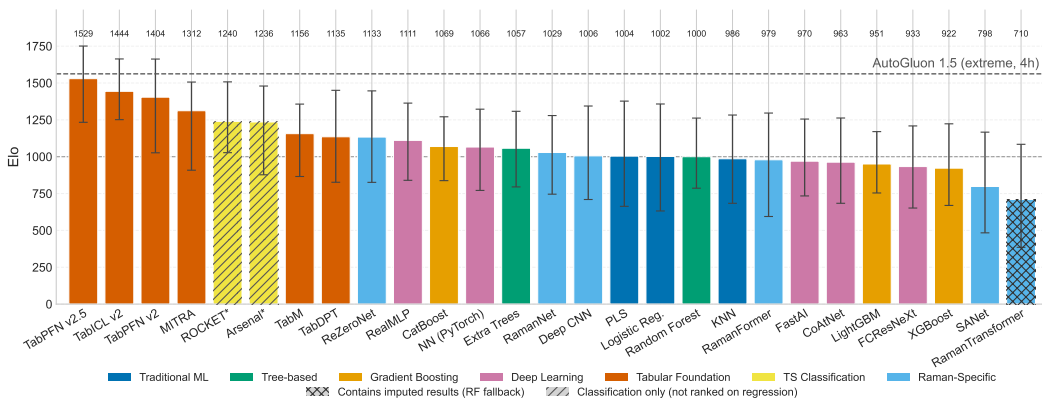


Figure 5: **RamanBench-v0.1 Leaderboard**. The top tier is dominated by Tabular Foundation Models (TFMs). The only models that can keep up are the time-series classifiers Arsenal and ROCKET (*=only evaluated on classification tasks). Over the full benchmark, ReZeroNet is the highest-ranking Raman-specific architecture and the first to challenge the TFM block. Elo ratings are anchored at Random Forest = 1 000, with 95 % bootstrap confidence intervals.

classification leaderboard, contributing 5 of those wins. The confidence intervals reveal that several groups of models are statistically indistinguishable, particularly in the mid-range of the ranking.

TFM. Despite operating beyond their recommended feature and row-count limits on several datasets (details in Section A.2), TFMs remain competitive, as confirmed by the ablation in Section A.7. Notably, TFMs also outperform all other model categories on small datasets with fewer than 50 training samples (Table 2).

The role of PLS. PLS [29] is the de facto standard model in Raman spectroscopy and serves as the primary baseline throughout **RamanBench**. As Fig. 1 (right) illustrates, **RamanBench** allows us to assess this retrospectively: PLS would have been State-of-the-Art (SOTA) for most of the past decades, with modern methods only recently beginning to clearly surpass it. Despite ranking 17th overall by Elo, PLS achieves 6 first-place finishes (see Table 8) across individual prediction targets, jointly the most among non-FM models.

Performance–efficiency trade-off. Fig. 6 places each model in the performance–efficiency space: normalized F1 (classification) and normalized RMSE (regression) versus mean total runtime (train + predict, log scale) measured on a single NVIDIA A100 GPU. Traditional and tree-based methods, such as PLS, k -Nearest Neighbors (kNN), and Random Forest, occupy the low-latency region but fail to reach the Pareto-optimal frontier. In contrast, TFMs (specifically TabPFN v2.5 and TabICL v2) establish the top performance tier at a moderate computational cost. However, we have to keep in mind that they perform in-context learning and we did not consider their training time on synthetic priors. High-cost architectures like RealMLP and Deep CNN require significantly more time yet offer lower predictive performance. All Raman-specific architectures except ReZeroNet show relative inefficiency, being slower than tree-based methods and less accurate than TFMs. Finally, while TabPFN v2.5 achieves a peak score of approximately 0.8 on regression tasks, it remains notably below the 1.0, indicating that no current model fully dominates the benchmark.

Improvability. To complement the scale-free Elo ranking as well as the clipped normalized scores, we report the *improvability* [9] of each model in Table 8: the mean fraction of a model’s error gap to the lowest error on each dataset (formal definition in Section A.1). TabPFN v2.5 achieves the lowest mean improvability at 19.0 %; the next best models (TabICL v2: 26.6 %, TabPFN v2: 30.5 %) are already substantially higher, and all other models exceed 40 %. These values are 2–3× higher than those of top models on TabArena [9] (5–9 %), indicating substantial room for algorithmic progress on Raman spectroscopy tasks, progress that **RamanBench** is designed to track. The improvability vs. training time trade-off is shown in Fig. 10.

Detailed per-dataset and per-model breakdowns, extended results tables, and Critical Difference (CD) diagrams are provided in Section A.11.

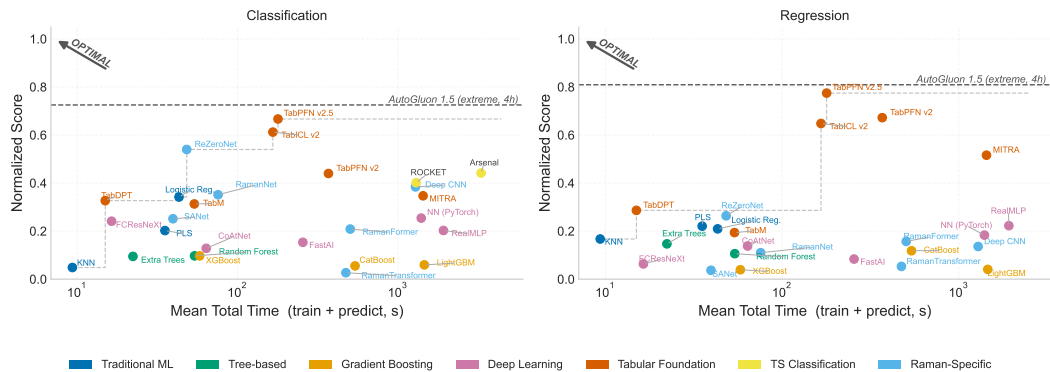


Figure 6: **TFM define the high-performance end of the Pareto frontier; ReZeroNet is the only non-TFM contender, while KNN qualifies through speed alone.** Normalized F1 (classification, left) and normalized RMSE (regression, right) vs. mean total runtime (train + predict, log scale). Metrics normalized per dataset following Salinas and Erickson [68]: best = 1, median = 0, clipped at 0. Runtime excludes TFM model pretraining costs.

6 Conclusion

RamanBench v0.1 represents the first large-scale Machine Learning (ML) benchmark for Raman spectroscopy, encompassing 74 datasets and 163 prediction targets across four application domains and evaluating 28 distinct models. Notably, TFMs lead the rankings for both small and large datasets, despite being originally designed for a different data modality. This trend is mirrored by the Time Series Classification (TSC) models Arsenal and ROCKET, which frequently outperform traditional ML methods, standard deep learning, and even specialized Raman architectures. While the potential of TFMs for Raman spectra has already surfaced in [21], our results cannot confirm the dominance of CNN approaches as suggested in [16, 21, 26].

Overall, the variety of winning model types (Table 8) and the significant improvability margin of the leading model (19.0%) compared to tabular data [9] underscore that Raman spectroscopy tasks are too heterogeneous for any single approach to dominate. This diversity reflects the field’s unique challenges: high dimensionality, limited sample sizes, inherent physical constraints, and low signal-to-noise ratios. This complexity establishes **RamanBench** as a necessary living benchmark—guiding practitioners toward the optimal method for each new task while challenging the community to bridge existing performance gaps.

Limitations and Future Work. **RamanBench** currently covers only 1D Raman spectra; 2D formats such as spectral images or hyperspectral cubes are not included. During model training and inference, we used a NVIDIA A100 GPU, which is more powerful than hardware typically available in wet labs. Even on this setup, some models have prohibitively high inference costs: MITRA (~ 626 s/1K) and Arsenal ($\sim 2,800$ s/1K) are unlikely to be practical in real-world deployments (more details in Section A.11.2). Preprocessing steps (baseline correction, denoising, Multiplicative Scatter Correction (MSC), Standard Normal Variate (SNV)) used in chemometric approaches [70] are not yet systematically ablated, so they are not fully disentangled from model performance in the current results; a systematic study would be an immediate next step. As this work provides an unprecedented amount of annotated Raman spectra from different instruments, it offers an opportunity for transfer learning, as demonstrated in [22] on a smaller scale.

As a living benchmark, **RamanBench** is designed to grow over time: we invite the community to contribute datasets from underrepresented domains, novel instrumentation, or larger sample sizes, as well as new models, following the guidelines in Section A.3.4 — in line with the open science and FAIR principles advocated for Raman spectroscopy [13].

Acknowledgments and Disclosure of Funding

Funding. Our work is funded by the Deutsche Forschungsgemeinschaft (DFG, German Research Foundation) – FIP-12 – Project-ID 528483508 and DFG’s project MEDEA (Grant No. 561489561).

Author Contributions. Author contributions are reported using the CRediT taxonomy [71]. M.Ko. and C.L. contributed equally and share first authorship; they led conceptualization, methodology, software development, formal analysis, data curation, writing of the original draft, and visualization. C.L., R.L., M.J., and M.Kö. conducted laboratory experiments and provided data resources. E.R. and F.B. provided supervision and contributed to conceptualization and methodology; E.R., F.B., M.N.C.B., and P.N. acquired funding. M.Ko., C.L., E.R., F.B., and P.N. reviewed and edited the manuscript.

Competing Interests. The authors declare no competing interests.

Impact Statement

This paper advances ML for Raman spectroscopy, a non-invasive analytical technique used across medicine, biology, chemistry, and materials science. By releasing a standardized benchmark with datasets, models, and evaluation code, we lower the barrier to applying state-of-the-art methods in these domains and may enable adoption in fields where the technology has not yet been widely used. Concrete benefits include improved disease detection, real-time bioprocess monitoring, safer industrial process control, and more reliable materials characterization. We are not aware of significant negative societal consequences specific to this work.

References

- [1] Miia Marika Jansson, Martin Kögler, Sohvi Hörkkö, Tero Ala-Kokko, and Lassi Rieppo. Vibrational spectroscopy and its future applications in microbiology. *Applied Spectroscopy Reviews*, 58(2):132–158, 2023.
- [2] Barbara Lafuente, Robert T Downs, Hexiong Yang, and Nate Stone. 1. the power of databases: The ruff project. In *Highlights in mineralogical crystallography*, pages 1–30. De Gruyter (O), 2015.
- [3] Karen A Esmonde-White, Maryann Cuellar, and Ian R Lewis. The role of raman spectroscopy in biopharmaceuticals from development to manufacturing. *Analytical and Bioanalytical Chemistry*, 414(2):969–991, 2022.
- [4] Chi-Sing Ho, Neal Jean, Catherine A Hogan, Lena Blackmon, Stefanie S Jeffrey, Mark Holodniy, Niaz Banaei, Amr AE Saleh, Stefano Ermon, and Jennifer Dionne. Rapid identification of pathogenic bacteria using raman spectroscopy and deep learning. *Nature communications*, 10(1):4927, 2019.
- [5] Dario Bertazioli, Marco Piazza, Cristiano Carlomagno, Alice Gualerzi, Marzia Bedoni, and Enza Messina. An integrated computational pipeline for machine learning-driven diagnosis based on raman spectra of saliva samples. *Computers in Biology and Medicine*, 171:108028, 2024.
- [6] Aaron R Flanagan and Frank G Glavin. Open-source raman spectra of chemical compounds for active pharmaceutical ingredient development. *Scientific Data*, 12(1):498, 2025.
- [7] Alexander Echtermeyer, Caroline Marks, Alexander Mitsos, and Jörn Viell. Inline raman spectroscopy and indirect hard modeling for concentration monitoring of dissociated acid species. *Applied spectroscopy*, 75(5):506–519, 2021.
- [8] Ruihao Luo, Juergen Popp, and Thomas Bocklitz. Deep learning for raman spectroscopy: A review. *Analytica*, 3(3):287–301, 2022.
- [9] Nick Erickson, Lennart Purucker, Andrej Tschalzev, David Holzmüller, Prateek Mutalik Desai, David Salinas, and Frank Hutter. Tabarena: A living benchmark for machine learning on tabular data. In *Proceedings of the 39th Conference on Neural Information Processing Systems (NeurIPS)*, 2025. URL <https://arxiv.org/abs/2506.16791>.

- [10] Si-Yang Liu, Hao-Run Cai, Qi-Le Zhou, Huai-Hong Yin, Tao Zhou, Jun-Peng Jiang, and Han-Jia Ye. TALENT: A tabular analytics and learning toolbox. *Journal of Machine Learning Research*, 26(226):1–16, 2025.
- [11] Hoang Anh Dau, Anthony Bagnall, Kaveh Kamgar, Chin-Chia Michael Yeh, Yan Zhu, Shaghayegh Gharghabi, Chotirat Ann Ratanamahatana, and Eamonn Keogh. The ucr time series archive. *IEEE/CAA Journal of Automatica Sinica*, 6(6):1293–1305, 2019.
- [12] Anthony Bagnall, Hoang Anh Dau, Jason Lines, Michael Flynn, James Large, Aaron Bostrom, Paul Southam, and Eamonn Keogh. The uea multivariate time series classification archive, 2018. *arXiv preprint arXiv:1811.00075*, 2018.
- [13] Nicolas Coca-Lopez, Victor Alcolea-Rodriguez, Miguel A Bañares, Sandor Brockhauser, Julien Gorenflot, Alex Henderson, Ron Hildebrandt, Nina Jeliaskova, Nikolay Kochev, Enrique Lozano Diz, et al. Artificial intelligence-powered raman spectroscopy through open science and fair principles. *ACS nano*, 19(44):38189–38218, 2025.
- [14] Mark D Wilkinson, Michel Dumontier, IJsbrand Jan Aalbersberg, Gabrielle Appleton, Myles Axton, Arie Baak, Niklas Blomberg, Jan-Willem Boiten, Luiz Bonino da Silva Santos, Philip E Bourne, et al. The fair guiding principles for scientific data management and stewardship. *Scientific data*, 3(1):1–9, 2016.
- [15] Qiaohao Liang, Shyam Dwaraknath, and Kristin A. Persson. High-throughput computation and evaluation of Raman spectra. *Scientific Data*, 6:135, 2019. doi: 10.1038/s41597-019-0138-y.
- [16] Genesis Berlanga, Quentin Williams, and Nathan Temiquel. Convolutional neural networks as a tool for raman spectral mineral classification under low signal, dusty mars conditions. *Earth and Space Science*, 9(10):e2021EA002125, 2022.
- [17] J. Schuetzke, N. J. Szymanski, and M. Reischl. Validating neural networks for spectroscopic classification on a universal synthetic dataset. *npj Computational Materials*, 9:100, 2023. doi: 10.1038/s41524-023-01055-y.
- [18] Songlin Lu, Yuanfang Huang, Wan Xiang Shen, Yu Lin Cao, Mengna Cai, Yan Chen, Ying Tan, Yu Yang Jiang, and Yu Zong Chen. Raman spectroscopic deep learning with signal aggregated representations for enhanced cell phenotype and signature identification. *PNAS Nexus*, 3(8):pgae268, 2024. doi: 10.1093/pnasnexus/pgae268.
- [19] Dimitar Georgiev, Simon Vilms Pedersen, Ruoxiao Xie, Álvaro Fernández-Galiana, Molly M Stevens, and Mauricio Barahona. Ramanspy: An open-source python package for integrative raman spectroscopy data analysis. *Analytical chemistry*, 96(21):8492–8500, 2024.
- [20] Jaume Béjar-Grimalt, Ángel Sánchez-Illana, Guillermo Quintás, Hugh J. Byrne, and David Pérez-Guaita. Monte Carlo peaks: Simulated datasets to benchmark machine learning algorithms for clinical spectroscopy. *Chemometrics and Intelligent Laboratory Systems*, 2025. doi: 10.1016/j.chemolab.2025.105548.
- [21] Christoph Lange, Madeline Altmann, Daniel Stors, Simon Seidel, Kyle Moynahan, Linda Cai, Stefan Born, Peter Neubauer, and M Nicolas Cruz Bournazou. Deep learning for raman spectroscopy: Benchmarking models for upstream bioprocess monitoring. *Measurement*, page 118884, 2025.
- [22] Christoph Lange, Maxim Borisyak, Martin Kögler, Stefan Born, Andreas Ziehe, Peter Neubauer, and M. Nicolas Cruz Bournazou. Comparing machine learning methods on Raman spectra from eight different spectrometers. *Spectrochimica Acta Part A: Molecular and Biomolecular Spectroscopy*, 334:125861, 2025. doi: 10.1016/j.saa.2025.125861.
- [23] J. Lilek et al. Machine learning of Raman spectroscopic data: Comparison of different validation strategies. *Journal of Raman Spectroscopy*, 56(9):867–877, 2025. doi: 10.1002/jrs.6842.
- [24] Zhuo Yang, Jiaqing Xie, Shuaike Shen, Daolang Wang, Yeyun Chen, Ben Gao, Shuzhou Sun, Biqing Qi, Dongzhan Zhou, Lei Bai, et al. Spectrumworld: Artificial intelligence foundation for spectroscopy. *arXiv preprint arXiv:2508.01188*, 2025.

- [25] Bingsen Xue, Xinyuan Bi, Zheyi Dong, Yunzhe Xu, Minghui Liang, Xin Fang, Yizhe Yuan, Ruoxi Wang, Shuyu Liu, Rushi Jiao, et al. Deep spectral component filtering as a foundation model for spectral analysis demonstrated in metabolic profiling. *Nature Machine Intelligence*, 7(5):743–757, 2025.
- [26] Adithya Sineesh and Akshita Kamsali. Benchmarking deep learning models for raman spectroscopy across open-source datasets. *arXiv preprint arXiv:2601.16107*, 2026.
- [27] Jeppe Hagedorn, Guilherme Ramos, Miguel Ressurreição, Ernst Broberg Hansen, Michael Sokolov, Carlos Casado Vázquez, and Christos Panos. Raman-enabled predictions of protein content and metabolites in biopharmaceutical *saccharomyces cerevisiae* fermentations. *Engineering in Life Sciences*, 24(12):e202400045, 2024.
- [28] Fabian Feidl, Simone Garbellini, Martin F Luna, Sebastian Vogg, Jonathan Souquet, Hervé Broly, Massimo Morbidelli, and Alessandro Butté. Combining mechanistic modeling and raman spectroscopy for monitoring antibody chromatographic purification. *Processes*, 7(10):683, 2019.
- [29] Herman Wold. Soft modeling: the basic design and some extensions. *Systems under indirect observation, Part II*, 2:36–37, 1982.
- [30] Corinna Cortes and Vladimir Vapnik. Support-vector networks. *Machine learning*, 20(3):273–297, 1995.
- [31] Jia Deng, Wei Dong, Richard Socher, Li-Jia Li, Kai Li, and Li Fei-Fei. Imagenet: A large-scale hierarchical image database. In *2009 IEEE conference on computer vision and pattern recognition*, pages 248–255. Ieee, 2009.
- [32] Alex Wang, Amanpreet Singh, Julian Michael, Felix Hill, Omer Levy, and Samuel Bowman. Glue: A multi-task benchmark and analysis platform for natural language understanding. In *Proceedings of the 2018 EMNLP workshop BlackboxNLP: Analyzing and interpreting neural networks for NLP*, pages 353–355, 2018.
- [33] Léo Grinsztajn, Edouard Oyallon, and Gaël Varoquaux. Why do tree-based models still outperform deep learning on typical tabular data? *Advances in neural information processing systems*, 35:507–520, 2022.
- [34] Günter G Hoffmann. *Infrared and Raman Spectroscopy: Principles and Applications*. Walter de Gruyter GmbH & Co KG, 2023.
- [35] Myung Jun Kim, Léo Grinsztajn, and Gaël Varoquaux. Carte: pretraining and transfer for tabular learning. *arXiv preprint arXiv:2402.16785*, 2024.
- [36] Myung Jun Kim, Félix Lefebvre, Gaëtan Brison, Alexandre Perez-Lebel, and Gaël Varoquaux. Table foundation models: on knowledge pre-training for tabular learning. *arXiv preprint arXiv:2505.14415*, 2025.
- [37] Katarína Rebrošová, Martin Šiler, Ota Samek, Filip Růžička, Silvie Bernatová, Veronika Holá, Jan Ježek, Pavel Zemánek, Jana Sokolová, and Petr Petráš. Rapid identification of staphylococci by raman spectroscopy. *Scientific reports*, 7(1):14846, 2017.
- [38] Thomas Bocklitz, Angela Walter, Katharina Hartmann, Petra Rösch, and Jürgen Popp. How to pre-process raman spectra for reliable and stable models? *Analytica chimica acta*, 704(1-2):47–56, 2011.
- [39] Jinchao Liu, Margarita Osadchy, Lorna Ashton, Michael Foster, Christopher J Solomon, and Stuart J Gibson. Deep convolutional neural networks for raman spectrum recognition: a unified solution. *Analyst*, 142(21):4067–4074, 2017.
- [40] Lin Deng, Yuzhong Zhong, Maoning Wang, Xiujuan Zheng, and Jianwei Zhang. Scale-adaptive deep model for bacterial raman spectra identification. *IEEE Journal of Biomedical and Health Informatics*, 26(1):369–378, 2021.

- [41] Nabil Ibtehaz, Muhammad EH Chowdhury, Amith Khandakar, Serkan Kiranyaz, M Sohel Rahman, and Susu M Zughaier. Ramannet: a generalized neural network architecture for raman spectrum analysis. *Neural Computing and Applications*, 35(25):18719–18735, 2023.
- [42] Onur Can Koyun, Reyhan Kevser Keser, Safa Onur Sahin, Damla Bulut, Mustafa Yorulmaz, Veysel Yucesoy, and Behcet Ugur Toreyin. Ramanformer: A transformer-based quantification approach for raman mixture components. *ACS omega*, 9(22):23241–23251, 2024.
- [43] Zilong Wang, Yunfeng Li, Jinglei Zhai, Siwei Yang, Biao Sun, and Pei Liang. Deep learning-based raman spectroscopy qualitative analysis algorithm: A convolutional neural network and transformer approach. *Talanta*, 275:126138, 2024.
- [44] Pengju Ren, Ri-gui Zhou, and Yaochong Li. A self-supervised learning method for raman spectroscopy based on masked autoencoders. *Expert Systems with Applications*, page 128576, 2025.
- [45] Noah Hollmann, Samuel Müller, Katharina Eggenberger, and Frank Hutter. TabPFN: A transformer that solves small tabular classification problems in a second. In *International Conference on Learning Representations*, 2023.
- [46] Noah Hollmann, Samuel Müller, Lennart Purucker, Arjun Krishnakumar, Max Körfer, Shi Bin Hoo, Robin Tibor Schirrmeyer, and Frank Hutter. Accurate predictions on small data with a tabular foundation model. *Nature*, 637(8045):319–326, 2025. doi: 10.1038/s41586-024-08328-6.
- [47] Jingang Qu, David Holzmüller, Gaël Varoquaux, and Marine Le Morvan. TabICL: A tabular foundation model for in-context learning on large data. In *International Conference on Machine Learning*, 2025.
- [48] Jingang Qu, David Holzmüller, Gaël Varoquaux, and Marine Le Morvan. TabICLv2: A better, faster, scalable, and open tabular foundation model. *arXiv preprint arXiv:2602.11139*, 2026.
- [49] Angus Dempster, Petitjean François, and Geoffrey I Webb. Rocket: exceptionally fast and accurate time series classification using random convolutional kernels. *Data Mining and Knowledge Discovery*, 34(5):1454–1495, 2020.
- [50] Matthew Middlehurst, James Large, Michael Flynn, Jason Lines, Aaron Bostrom, and Anthony Bagnall. Hive-cote 2.0: a new meta ensemble for time series classification. *Machine Learning*, 110(11):3211–3243, 2021.
- [51] Roman Bushuiev, Anton Bushuiev, Niek F de Jonge, Adamo Young, Fleming Kretschmer, Raman Samusevich, Janne Heirman, Fei Wang, Luke Zhang, Kai Dührkop, et al. Massspecgym: A benchmark for the discovery and identification of molecules. *Advances in Neural Information Processing Systems*, 37:110010–110027, 2024.
- [52] Fanjie Xu, Wentao Guo, Feng Wang, Lin Yao, Hongshuai Wang, Fujie Tang, Zhifeng Gao, Linfeng Zhang, Weinan E, Zhong-Qun Tian, et al. Toward a unified benchmark and framework for deep learning-based prediction of nuclear magnetic resonance chemical shifts. *Nature Computational Science*, 5(4):292–300, 2025.
- [53] Luise F Kaven, Hanna JM Wolff, Lukas Wille, Matthias Wessling, Alexander Mitsos, and Joern Viell. In-line monitoring of microgel synthesis: flow versus batch reactor. *Organic Process Research & Development*, 25(9):2039–2051, 2021.
- [54] Martin Kögler, Andrea Paul, Emmanuel Anane, Mario Birkholz, Alex Bunker, Tapani Viitala, Michael Maiwald, Stefan Junne, and Peter Neubauer. Comparison of time-gated surface-enhanced raman spectroscopy (tg-sers) and classical sers based monitoring of escherichia coli cultivation samples. *Biotechnology progress*, 34(6):1533–1542, 2018.
- [55] Marcelo Terán, José Javier Ruiz, Pablo Loza-Alvarez, David Masip, and David Merino. Open raman spectral library for biomolecule identification. *Chemometrics and Intelligent Laboratory Systems*, 264:105476, 2025.

- [56] Serena Rizzo, Yannick Weesepeel, Sara Erasmus, Joost Sinkeldam, Anna Lisa Piccinelli, and Saskia van Ruth. Dataset of raman and surface-enhanced raman spectroscopy spectra of illicit adulterants added to dietary supplements. 2023.
- [57] Rui Zhang, Huimin Xie, Shuning Cai, Yong Hu, Guo-kun Liu, Wenjing Hong, and Zhong-qun Tian. Transfer-learning-based raman spectra identification. *Journal of Raman Spectroscopy*, 51(1):176–186, 2020.
- [58] Ricardo Knauer, Marvin Grimm, and Erik Rodner. Pmlbmini: A tabular classification benchmark suite for data-scarce applications. *arXiv preprint arXiv:2409.01635*, 2024.
- [59] Yury Gorishniy, Ivan Rubachev, Valentin Khruikov, and Artem Babenko. Revisiting deep learning models for tabular data. *Advances in neural information processing systems*, 34:18932–18943, 2021.
- [60] Thomas Bachlechner, Bodhisattwa Prasad Majumder, Henry Mao, Gary Cottrell, and Julian McAuley. Rezero is all you need: Fast convergence at large depth. In *Uncertainty in artificial intelligence*, pages 1352–1361. PMLR, 2021.
- [61] Guri Zabërgja, Arlind Kadra, Christian MM Frey, and Josif Grabocka. Tabular data: Is deep learning all you need? *arXiv preprint arXiv:2402.03970*, 2024.
- [62] Zihang Dai, Hanxiao Liu, Quoc V Le, and Mingxing Tan. Coatnet: Marrying convolution and attention for all data sizes. *Advances in neural information processing systems*, 34:3965–3977, 2021.
- [63] Xiyuan Zhang, Danielle C Maddix, Junming Yin, Nick Erickson, Abdul Fatir Ansari, Boran Han, Shuai Zhang, Leman Akoglu, Christos Faloutsos, Michael W Mahoney, et al. Mitra: Mixed synthetic priors for enhancing tabular foundation models. *arXiv preprint arXiv:2510.21204*, 2025.
- [64] Junwei Ma, Valentin Thomas, Rasa Hosseinzadeh, Alex Labach, Hamidreza Kamkari, Jesse C Cresswell, Keyvan Golestan, Guangwei Yu, Anthony L Caterini, and Maksims Volkovs. Tabdpt: Scaling tabular foundation models on real data. *arXiv preprint arXiv:2410.18164*, 2024.
- [65] Yury Gorishniy, Akim Kotelnikov, and Artem Babenko. TabM: Advancing Tabular Deep Learning with Parameter-Efficient Ensembling, February 2025. URL <http://arxiv.org/abs/2410.24210>. arXiv:2410.24210 [cs].
- [66] Bo Liu, Kunxiang Liu, Xiaoqing Qi, Weijia Zhang, and Bei Li. Classification of deep-sea cold seep bacteria by transformer combined with raman spectroscopy. *Scientific Reports*, 13(1):3240, 2023.
- [67] Nick Erickson, Jonas Mueller, Alexander Shirkov, Hang Zhang, Pedro Larroy, Mu Li, and Alexander Smola. Autogluon-tabular: Robust and accurate automl for structured data. *arXiv preprint arXiv:2003.06505*, 2020.
- [68] David Salinas and Nick Erickson. TabRepo: A large scale repository of tabular model evaluations and its AutoML applications. In *AutoML Conference 2024 (ABCD Track)*, 2024.
- [69] Janez Demšar. Statistical comparisons of classifiers over multiple data sets. *Journal of Machine learning research*, 7(Jan):1–30, 2006.
- [70] Sara Mostafapour, Thomas Dörfer, Ralf Heinke, Petra Rösch, Jürgen Popp, and Thomas Bocklitz. Investigating the effect of different pre-treatment methods on raman spectra recorded with different excitation wavelengths. *Spectrochimica Acta Part A: Molecular and Biomolecular Spectroscopy*, 302:123100, 2023.
- [71] Amy Brand, Liz Allen, Micah Altman, Marjorie Hlava, and Jo Scott. Beyond authorship: attribution, contribution, collaboration, and credit. *Learned Publishing*, 28(2):151–155, 2015. doi: <https://doi.org/10.1087/20150211>. URL <https://onlinelibrary.wiley.com/doi/abs/10.1087/20150211>.

- [72] Arpad E Elo. The proposed uscf rating system, its development, theory, and applications. *Chess life*, 22(8):242–247, 1967.
- [73] Steffen Herbold. Autorank: A Python package for automated ranking of classifiers. *Journal of Open Source Software*, 5(48):2173, 2020. doi: 10.21105/joss.02173.
- [74] François Chollet. Xception: Deep learning with depthwise separable convolutions. In *Proceedings of the IEEE conference on computer vision and pattern recognition*, pages 1251–1258, 2017.
- [75] Mengxin Sun, Kunhong Liu, Qingqi Hong, and Beizhan Wang. A new ecoc algorithm for multiclass microarray data classification. In *2018 24th International Conference on Pattern Recognition (ICPR)*, pages 454–458. IEEE, 2018.
- [76] Christoph Lange, Simon Seidel, Madeline Altmann, Daniel Stors, Annina Kemmer, Linda Cai, Stefan Born, Peter Neubauer, and M Nicolas Cruz Bournazou. A setup for automatic raman measurements in high-throughput experimentation. *Biotechnology and Bioengineering*, 122(10):2751–2769, 2025.
- [77] Robin Legner, Alexander Wirtz, Tim Koza, Till Tetzlaff, Anna Nickisch-Hartfiel, and Martin Jaeger. Application of green analytical chemistry to a green chemistry process: Magnetic resonance and raman spectroscopic process monitoring of continuous ethanolic fermentation. *Biotechnology and bioengineering*, 116(11):2874–2883, 2019.
- [78] Christoph Lange, Isabel Thiele, Lara Santolin, Sebastian L Riedel, Maxim Borisyak, Peter Neubauer, and Mariano Nicolas Cruz-Bournazou. Data augmentation scheme for raman spectra with highly correlated annotations. In *Computer Aided Chemical Engineering*, volume 53, pages 3055–3060. Elsevier, 2024.
- [79] Melanie Voigt, Robin Legner, Simon Haefner, Anatoli Friesen, Alexander Wirtz, and Martin Jaeger. Using fieldable spectrometers and chemometric methods to determine ron of gasoline from petrol stations: A comparison of low-field 1h nmr@ 80 mhz, handheld raman and benchtop nir. *Fuel*, 236:829–835, 2019.
- [80] Robin Legner, Melanie Voigt, Alexander Wirtz, Anatoli Friesen, Simon Haefner, and Martin Jaeger. Using compact proton nuclear magnetic resonance at 80 mhz and vibrational spectroscopies and data fusion for research octane number and gasoline additive determination. *Energy & Fuels*, 34(1):103–110, 2019.
- [81] Stefano Fornasaro, Fatima Alsamad, Monica Baia, Luis AE Batista de Carvalho, Claudia Beleites, Hugh J Byrne, Alessandro Chiadò, Mihaela Chis, Malama Chisanga, Amuthachelvi Daniel, et al. Surface enhanced raman spectroscopy for quantitative analysis: results of a large-scale european multi-instrument interlaboratory study. *Analytical chemistry*, 92(5):4053–4064, 2020.
- [82] Wim Fremout and Steven Saverwyns. Identification of synthetic organic pigments: the role of a comprehensive digital raman spectral library. *Journal of Raman spectroscopy*, 43(11): 1536–1544, 2012.
- [83] Mingtan Dong, Qiaoqiao Zhang, Xinli Xing, Wei Chen, Zhenbing She, and Zejiao Luo. Raman spectra and surface changes of microplastics weathered under natural environments. *Science of the Total Environment*, 739:139990, 2020.
- [84] M Erzina, A Trelin, O Guselnikova, B Dvorankova, K Strnadova, A Perminova, P Ulbrich, D Mares, V Jerabek, R Elashnikov, et al. Precise cancer detection via the combination of functionalized sers surfaces and convolutional neural network with independent inputs. *Sensors and Actuators B: Chemical*, 308:127660, 2020.
- [85] Ayse Sen, Ibrahim Kecoglu, Muhammad Ahmed, Ugur Parlattan, and Mehmet Burcin Unlu. Differentiation of advanced generation mutant wheat lines: Conventional techniques versus raman spectroscopy. *Frontiers in Plant Science*, 14:1116876, 2023.

- [86] Edgar Guevara, Juan Carlos Torres-Galván, Miguel G Ramírez-Elías, Claudia Luevano-Contreras, and Francisco Javier González. Use of raman spectroscopy to screen diabetes mellitus with machine learning tools. *Biomedical Optics Express*, 9(10):4998–5010, 2018.
- [87] Hanna J Koster, Antonio Guillen-Perez, Juan Sebastian Gomez-Diaz, Maria Navas-Moreno, Andrew C Birkeland, and Randy P Carney. Fused raman spectroscopic analysis of blood and saliva delivers high accuracy for head and neck cancer diagnostics. *Scientific Reports*, 12(1): 18464, 2022.
- [88] Stefano Rini and Hirotsugu Hiramatsu. An efficient label-free analyte detection algorithm for time-resolved spectroscopy. *arXiv preprint arXiv:2011.07470*, 2020.
- [89] Samantha Higgins and Dmitry Kurouski. Surface-enhanced raman spectroscopy enables highly accurate identification of different brands, types and colors of hair dyes. *Talanta*, 251:123762, 2023.
- [90] Eleni D Koronaki, Luise F Kaven, Johannes MM Faust, Ioannis G Kevrekidis, and Alexander Mitsos. Nonlinear manifold learning determines microgel size from raman spectroscopy. *AIChE Journal*, 70(10):e18494, 2024.
- [91] Luise F Kaven, Artur M Schweidtmann, Jan Keil, Jana Israel, Nadja Wolter, and Alexander Mitsos. Data-driven product-process optimization of n-isopropylacrylamide microgel flow-synthesis. *Chemical Engineering Journal*, 479:147567, 2024.
- [92] Dimitar Georgiev, Álvaro Fernández-Galiana, Simon Vilms Pedersen, Georgios Papadopoulos, Ruoxiao Xie, Molly M Stevens, and Mauricio Barahona. Hyperspectral unmixing for raman spectroscopy via physics-constrained autoencoders. *Proceedings of the National Academy of Sciences*, 121(45):e2407439121, 2024.

NeurIPS Paper Checklist

1. Claims

Question: Do the main claims made in the abstract and introduction accurately reflect the paper’s contributions and scope?

Answer: [Yes]

Justification: Our main claims: (a) **RamanBench** introduce the first large-scale Raman Benchmark as shown in comparison to the existing benchmarks in Table 1 (b) It contains 74 datasets including 58 publicly available and 16 newly released as shown in Table 11. (c) We provide a Python package for the data(Section A.3.1) and for the benchmark(Section A.3.2). (d) We compare 28 model types on that data as shown in Table 8.

Guidelines:

- The answer [N/A] means that the abstract and introduction do not include the claims made in the paper.
- The abstract and/or introduction should clearly state the claims made, including the contributions made in the paper and important assumptions and limitations. A [No] or [N/A] answer to this question will not be perceived well by the reviewers.
- The claims made should match theoretical and experimental results, and reflect how much the results can be expected to generalize to other settings.
- It is fine to include aspirational goals as motivation as long as it is clear that these goals are not attained by the paper.

2. Limitations

Question: Does the paper discuss the limitations of the work performed by the authors?

Answer: [Yes]

Justification: We discuss limitations in Section 6.

Guidelines:

- The answer [N/A] means that the paper has no limitation while the answer [No] means that the paper has limitations, but those are not discussed in the paper.
- The authors are encouraged to create a separate “Limitations” section in their paper.
- The paper should point out any strong assumptions and how robust the results are to violations of these assumptions (e.g., independence assumptions, noiseless settings, model well-specification, asymptotic approximations only holding locally). The authors should reflect on how these assumptions might be violated in practice and what the implications would be.
- The authors should reflect on the scope of the claims made, e.g., if the approach was only tested on a few datasets or with a few runs. In general, empirical results often depend on implicit assumptions, which should be articulated.
- The authors should reflect on the factors that influence the performance of the approach. For example, a facial recognition algorithm may perform poorly when image resolution is low or images are taken in low lighting. Or a speech-to-text system might not be used reliably to provide closed captions for online lectures because it fails to handle technical jargon.
- The authors should discuss the computational efficiency of the proposed algorithms and how they scale with dataset size.
- If applicable, the authors should discuss possible limitations of their approach to address problems of privacy and fairness.
- While the authors might fear that complete honesty about limitations might be used by reviewers as grounds for rejection, a worse outcome might be that reviewers discover limitations that aren’t acknowledged in the paper. The authors should use their best judgment and recognize that individual actions in favor of transparency play an important role in developing norms that preserve the integrity of the community. Reviewers will be specifically instructed to not penalize honesty concerning limitations.

3. Theory assumptions and proofs

Question: For each theoretical result, does the paper provide the full set of assumptions and a complete (and correct) proof?

Answer: [N/A]

Justification: We do not provide any theoretical results in this manuscript.

Guidelines:

- The answer [N/A] means that the paper does not include theoretical results.
- All the theorems, formulas, and proofs in the paper should be numbered and cross-referenced.
- All assumptions should be clearly stated or referenced in the statement of any theorems.
- The proofs can either appear in the main paper or the supplemental material, but if they appear in the supplemental material, the authors are encouraged to provide a short proof sketch to provide intuition.
- Inversely, any informal proof provided in the core of the paper should be complemented by formal proofs provided in appendix or supplemental material.
- Theorems and Lemmas that the proof relies upon should be properly referenced.

4. Experimental result reproducibility

Question: Does the paper fully disclose all the information needed to reproduce the main experimental results of the paper to the extent that it affects the main claims and/or conclusions of the paper (regardless of whether the code and data are provided or not)?

Answer: [Yes]

Justification: All information required to reproduce the main results is provided. The `raman-data` package (publicly available on PyPI) gives unified access to all datasets. The `ramanbench` package implements the full evaluation pipeline. The evaluation protocol — fixed 80/20 train/test splits, 3 random seeds, AutoGluon with the `extreme_quality` preset and a 4-hour time limit on a single NVIDIA A100 GPU — is described in Section 4 and Section A.2.

Guidelines:

- The answer [N/A] means that the paper does not include experiments.
- If the paper includes experiments, a [No] answer to this question will not be perceived well by the reviewers: Making the paper reproducible is important, regardless of whether the code and data are provided or not.
- If the contribution is a dataset and/or model, the authors should describe the steps taken to make their results reproducible or verifiable.
- Depending on the contribution, reproducibility can be accomplished in various ways. For example, if the contribution is a novel architecture, describing the architecture fully might suffice, or if the contribution is a specific model and empirical evaluation, it may be necessary to either make it possible for others to replicate the model with the same dataset, or provide access to the model. In general, releasing code and data is often one good way to accomplish this, but reproducibility can also be provided via detailed instructions for how to replicate the results, access to a hosted model (e.g., in the case of a large language model), releasing of a model checkpoint, or other means that are appropriate to the research performed.
- While NeurIPS does not require releasing code, the conference does require all submissions to provide some reasonable avenue for reproducibility, which may depend on the nature of the contribution. For example
 - (a) If the contribution is primarily a new algorithm, the paper should make it clear how to reproduce that algorithm.
 - (b) If the contribution is primarily a new model architecture, the paper should describe the architecture clearly and fully.
 - (c) If the contribution is a new model (e.g., a large language model), then there should either be a way to access this model for reproducing the results or a way to reproduce the model (e.g., with an open-source dataset or instructions for how to construct the dataset).

- (d) We recognize that reproducibility may be tricky in some cases, in which case authors are welcome to describe the particular way they provide for reproducibility. In the case of closed-source models, it may be that access to the model is limited in some way (e.g., to registered users), but it should be possible for other researchers to have some path to reproducing or verifying the results.

5. Open access to data and code

Question: Does the paper provide open access to the data and code, with sufficient instructions to faithfully reproduce the main experimental results, as described in supplemental material?

Answer: [Yes]

Justification: All datasets are publicly accessible through the `raman-data` package (<https://pypi.org/project/raman-data/>). The full benchmark code, including configuration files and scripts to reproduce all experiments, is released at <https://github.com/ml-lab-htw/RamanBench>.

Guidelines:

- The answer [N/A] means that paper does not include experiments requiring code.
- Please see the NeurIPS code and data submission guidelines (<https://neurips.cc/public/guides/CodeSubmissionPolicy>) for more details.
- While we encourage the release of code and data, we understand that this might not be possible, so [No] is an acceptable answer. Papers cannot be rejected simply for not including code, unless this is central to the contribution (e.g., for a new open-source benchmark).
- The instructions should contain the exact command and environment needed to run to reproduce the results. See the NeurIPS code and data submission guidelines (<https://neurips.cc/public/guides/CodeSubmissionPolicy>) for more details.
- The authors should provide instructions on data access and preparation, including how to access the raw data, preprocessed data, intermediate data, and generated data, etc.
- The authors should provide scripts to reproduce all experimental results for the new proposed method and baselines. If only a subset of experiments are reproducible, they should state which ones are omitted from the script and why.
- At submission time, to preserve anonymity, the authors should release anonymized versions (if applicable).
- Providing as much information as possible in supplemental material (appended to the paper) is recommended, but including URLs to data and code is permitted.

6. Experimental setting/details

Question: Does the paper specify all the training and test details (e.g., data splits, hyperparameters, how they were chosen, type of optimizer) necessary to understand the results?

Answer: [Yes]

Justification: The evaluation protocol is described in Section 4: fixed 80/20 train/test splits, 3 random seeds, fixed hyperparameters, AutoGluon with the `extreme_quality` preset and a 4-hour time limit. Full model-specific hyperparameters and training details are provided in Section A.2.

Guidelines:

- The answer [N/A] means that the paper does not include experiments.
- The experimental setting should be presented in the core of the paper to a level of detail that is necessary to appreciate the results and make sense of them.
- The full details can be provided either with the code, in appendix, or as supplemental material.

7. Experiment statistical significance

Question: Does the paper report error bars suitably and correctly defined or other appropriate information about the statistical significance of the experiments?

Answer: [Yes]

Justification: Elo ratings are reported with 95 % confidence intervals obtained via 200 bootstrap sub-samples of the dataset pool (2.5 % and 97.5 % quantiles); the procedure is described in Section A.1. Statistical significance of ranking differences is assessed using Critical Difference diagrams based on the Friedman test followed by the Nemenyi post-hoc test at $\alpha = 0.05$, as described in Section A.1.

Guidelines:

- The answer [N/A] means that the paper does not include experiments.
- The authors should answer [Yes] if the results are accompanied by error bars, confidence intervals, or statistical significance tests, at least for the experiments that support the main claims of the paper.
- The factors of variability that the error bars are capturing should be clearly stated (for example, train/test split, initialization, random drawing of some parameter, or overall run with given experimental conditions).
- The method for calculating the error bars should be explained (closed form formula, call to a library function, bootstrap, etc.)
- The assumptions made should be given (e.g., Normally distributed errors).
- It should be clear whether the error bar is the standard deviation or the standard error of the mean.
- It is OK to report 1-sigma error bars, but one should state it. The authors should preferably report a 2-sigma error bar than state that they have a 96% CI, if the hypothesis of Normality of errors is not verified.
- For asymmetric distributions, the authors should be careful not to show in tables or figures symmetric error bars that would yield results that are out of range (e.g., negative error rates).
- If error bars are reported in tables or plots, the authors should explain in the text how they were calculated and reference the corresponding figures or tables in the text.

8. Experiments compute resources

Question: For each experiment, does the paper provide sufficient information on the computer resources (type of compute workers, memory, time of execution) needed to reproduce the experiments?

Answer: [Yes]

Justification: All models are evaluated on a single NVIDIA A100 GPU. Per-model mean runtimes (train + predict) are reported in Fig. 6 in Section 5. Compute resources are provided by the HPC clusters at HTW Berlin and TU Berlin.

Guidelines:

- The answer [N/A] means that the paper does not include experiments.
- The paper should indicate the type of compute workers CPU or GPU, internal cluster, or cloud provider, including relevant memory and storage.
- The paper should provide the amount of compute required for each of the individual experimental runs as well as estimate the total compute.
- The paper should disclose whether the full research project required more compute than the experiments reported in the paper (e.g., preliminary or failed experiments that didn't make it into the paper).

9. Code of ethics

Question: Does the research conducted in the paper conform, in every respect, with the NeurIPS Code of Ethics <https://neurips.cc/public/EthicsGuidelines>?

Answer: [Yes]

Justification: This work presents a benchmark for ML on Raman spectroscopy data. It does not include sensitive personal data, or dual-use risks, and fully conforms with the NeurIPS Code of Ethics.

Guidelines:

- The answer [N/A] means that the authors have not reviewed the NeurIPS Code of Ethics.

- If the authors answer [No], they should explain the special circumstances that require a deviation from the Code of Ethics.
- The authors should make sure to preserve anonymity (e.g., if there is a special consideration due to laws or regulations in their jurisdiction).

10. Broader impacts

Question: Does the paper discuss both potential positive societal impacts and negative societal impacts of the work performed?

Answer: [Yes]

Justification: We include an Impact Statement discussing the potential of this work to accelerate reliable analytical methods in biotechnology, chemistry, materials science, and medicine. We do not identify specific negative societal impacts arising from a benchmark for Raman spectroscopy data.

Guidelines:

- The answer [N/A] means that there is no societal impact of the work performed.
- If the authors answer [N/A] or [No], they should explain why their work has no societal impact or why the paper does not address societal impact.
- Examples of negative societal impacts include potential malicious or unintended uses (e.g., disinformation, generating fake profiles, surveillance), fairness considerations (e.g., deployment of technologies that could make decisions that unfairly impact specific groups), privacy considerations, and security considerations.
- The conference expects that many papers will be foundational research and not tied to particular applications, let alone deployments. However, if there is a direct path to any negative applications, the authors should point it out. For example, it is legitimate to point out that an improvement in the quality of generative models could be used to generate Deepfakes for disinformation. On the other hand, it is not needed to point out that a generic algorithm for optimizing neural networks could enable people to train models that generate Deepfakes faster.
- The authors should consider possible harms that could arise when the technology is being used as intended and functioning correctly, harms that could arise when the technology is being used as intended but gives incorrect results, and harms following from (intentional or unintentional) misuse of the technology.
- If there are negative societal impacts, the authors could also discuss possible mitigation strategies (e.g., gated release of models, providing defenses in addition to attacks, mechanisms for monitoring misuse, mechanisms to monitor how a system learns from feedback over time, improving the efficiency and accessibility of ML).

11. Safeguards

Question: Does the paper describe safeguards that have been put in place for responsible release of data or models that have a high risk for misuse (e.g., pre-trained language models, image generators, or scraped datasets)?

Answer: [N/A]

Justification: The released assets are a benchmark dataset collection and evaluation code for Raman spectroscopy. They pose no meaningful risk of misuse and do not require special safeguards.

Guidelines:

- The answer [N/A] means that the paper poses no such risks.
- Released models that have a high risk for misuse or dual-use should be released with necessary safeguards to allow for controlled use of the model, for example by requiring that users adhere to usage guidelines or restrictions to access the model or implementing safety filters.
- Datasets that have been scraped from the Internet could pose safety risks. The authors should describe how they avoided releasing unsafe images.
- We recognize that providing effective safeguards is challenging, and many papers do not require this, but we encourage authors to take this into account and make a best faith effort.

12. Licenses for existing assets

Question: Are the creators or original owners of assets (e.g., code, data, models), used in the paper, properly credited and are the license and terms of use explicitly mentioned and properly respected?

Answer: [Yes]

Justification: Every dataset is cited with its original publication in the per-dataset tables in Section A.14, and license information is reported for all 74 datasets. The majority are released under permissive open licenses (CC BY 4.0, CC0 1.0). MLROD uses a BY-NC license (non-commercial use only; this paper is academic research). The RRUFF mineral database does not carry a formal license identifier, but its founding paper [2] explicitly states that the data is provided with free access; we treat this as a grant of free academic use. For the Amino Acid LC dataset (Kaggle), no license is stated by the authors; we have contacted them for clarification (see <https://www.kaggle.com/datasets/sergioalejandrod/raman-spectroscopy/discussion/690923>). Similarly, the three Saliva datasets (COVID-19, Alzheimer, Parkinson) from Bertazioli et al. [5] carry no explicit license; we have opened a clarification request with the authors (see <https://github.com/piazzam/Robust-SVM-Raman/issues/1>).

Guidelines:

- The answer [N/A] means that the paper does not use existing assets.
- The authors should cite the original paper that produced the code package or dataset.
- The authors should state which version of the asset is used and, if possible, include a URL.
- The name of the license (e.g., CC-BY 4.0) should be included for each asset.
- For scraped data from a particular source (e.g., website), the copyright and terms of service of that source should be provided.
- If assets are released, the license, copyright information, and terms of use in the package should be provided. For popular datasets, paperswithcode.com/datasets has curated licenses for some datasets. Their licensing guide can help determine the license of a dataset.
- For existing datasets that are re-packaged, both the original license and the license of the derived asset (if it has changed) should be provided.
- If this information is not available online, the authors are encouraged to reach out to the asset's creators.

13. New assets

Question: Are new assets introduced in the paper well documented and is the documentation provided alongside the assets?

Answer: [Yes]

Justification: All newly released datasets are hosted on Hugging Face and accompanied by Croissant metadata files documenting dataset structure, splits, and provenance. The benchmark code is documented at github.com/ml-lab-htw/RamanBench and a full list is provided in Section A.13 and github.com/ml-lab-htw/RamanBench/blob/main/NEW_DATASETS.md.

Guidelines:

- The answer [N/A] means that the paper does not release new assets.
- Researchers should communicate the details of the dataset/code/model as part of their submissions via structured templates. This includes details about training, license, limitations, etc.
- The paper should discuss whether and how consent was obtained from people whose asset is used.
- At submission time, remember to anonymize your assets (if applicable). You can either create an anonymized URL or include an anonymized zip file.

14. Crowdsourcing and research with human subjects

Question: For crowdsourcing experiments and research with human subjects, does the paper include the full text of instructions given to participants and screenshots, if applicable, as well as details about compensation (if any)?

Answer: [N/A]

Justification: This paper does not involve crowdsourcing or research with human subjects.

Guidelines:

- The answer [N/A] means that the paper does not involve crowdsourcing nor research with human subjects.
- Including this information in the supplemental material is fine, but if the main contribution of the paper involves human subjects, then as much detail as possible should be included in the main paper.
- According to the NeurIPS Code of Ethics, workers involved in data collection, curation, or other labor should be paid at least the minimum wage in the country of the data collector.

15. Institutional review board (IRB) approvals or equivalent for research with human subjects

Question: Does the paper describe potential risks incurred by study participants, whether such risks were disclosed to the subjects, and whether Institutional Review Board (IRB) approvals (or an equivalent approval/review based on the requirements of your country or institution) were obtained?

Answer: [N/A]

Justification: This paper does not involve crowdsourcing or research with human subjects. No IRB approval was required.

Guidelines:

- The answer [N/A] means that the paper does not involve crowdsourcing nor research with human subjects.
- Depending on the country in which research is conducted, IRB approval (or equivalent) may be required for any human subjects research. If you obtained IRB approval, you should clearly state this in the paper.
- We recognize that the procedures for this may vary significantly between institutions and locations, and we expect authors to adhere to the NeurIPS Code of Ethics and the guidelines for their institution.
- For initial submissions, do not include any information that would break anonymity (if applicable), such as the institution conducting the review.

16. Declaration of LLM usage

Question: Does the paper describe the usage of LLMs if it is an important, original, or non-standard component of the core methods in this research? Note that if the LLM is used only for writing, editing, or formatting purposes and does *not* impact the core methodology, scientific rigor, or originality of the research, declaration is not required.

Answer: [N/A]

Justification: LLMs are not used as a component of the core methodology. No declaration is required.

Guidelines:

- The answer [N/A] means that the core method development in this research does not involve LLMs as any important, original, or non-standard components.
- Please refer to our LLM policy in the NeurIPS handbook for what should or should not be described.

A Appendix

Contents

A.1	Evaluation Metrics	25
A.2	Model Descriptions	27
A.3	Software	29
A.3.1	raman-data — Unified Dataset Library	30
A.3.2	raman-bench — Reproducible Benchmarking Pipeline	30
A.3.3	Online Leaderboard	31
A.3.4	Living Benchmark Protocols	31
A.4	Handling Foul Play and Dataset Contamination	31
A.5	Ablation: Small vs. Larger Datasets	32
A.6	Learnability Verification	34
A.7	Foundation Model Recommended Size Limits	37
A.8	Combined Ranking	39
A.9	Extended Results Tables	39
A.10	Pairwise Win Rates	39
A.11	Detailed Results	39
A.11.1	Model Ranking	39
A.11.2	Computational Efficiency	40
A.11.3	Improvability vs. Training Time	41
A.11.4	Statistical Significance — Critical Difference Diagrams	41
A.12	Dataset Overview Table	41
A.13	New Datasets: Measurement Details	41
A.13.1	<i>E. coli</i> Fermentation: Kaiser and Time-Gated Raman Measurements	42
A.13.2	<i>S. thermophilus</i> Fermentation: Kaiser and Time-Gated Raman Measurements	47
A.13.3	<i>E. coli</i> Metabolites: High-Throughput Raman Measurements	48
A.13.4	Bio-Catalysis Monitoring of Adenosine Phosphates (AXP)	49
A.13.5	Ethanolc Yeast Fermentation	50
A.13.6	<i>R. eutropha</i> Copolymer Fermentations	50
A.13.7	Gasoline Properties: Benchtop and Handheld Raman Measurements	51
A.13.8	Adenine SERS: European Multi-Instrument Interlaboratory Study	53
A.14	Dataset Descriptions	54
A.14.1	Material Science	54
A.14.2	Biological & Biotechnological	56
A.14.3	Medical & Clinical	60
A.14.4	Chemical & Industrial	65

A.1 Evaluation Metrics

Throughout this section, *prediction target* (or simply *target*) refers to a single labeled output column: classification datasets contribute one target each, while multi-target regression datasets contribute one target per output variable (e.g. glucose concentration, fructose concentration). Every metric — F1, RMSE, Elo match, normalized score, improbability — is computed independently per target; results are never aggregated across the targets of the same dataset before ranking.

Classification. Per-dataset classification performance is primarily measured by the **macro-averaged F1-score**:

$$F1_{\text{macro}} = \frac{1}{C} \sum_{c=1}^C \frac{2TP_c}{2TP_c + FP_c + FN_c},$$

where C is the number of classes and TP_c, FP_c, FN_c are the true positives, false positives, and false negatives for class c , respectively. Macro-averaging weights each class equally regardless of its frequency, which is appropriate for the highly imbalanced multi-class tasks in **RamanBench** (e.g. RRUFF with 79 mineral classes after rare-class filtering). Higher F1 is better; a random classifier achieves $F1_{\text{macro}} \approx 1/C$ for balanced classes. F1 is used as the primary metric for Elo, Score, Avg Rank, Improbability, and CD diagram aggregation.

The classification leaderboard additionally reports **balanced accuracy** — the average per-class recall. It ranges from 0 to 1 (chance level = $1/C$ for C balanced classes) and is complementary to F1 in that it is insensitive to class imbalance and directly reflects discrimination ability across all classes.

We do not report the area under the ROC curve (AUC-ROC) as a primary metric. For multiclass problems, AUC-ROC requires one-vs-rest or one-vs-one averaging over predicted class probabilities; several models in **RamanBench** (e.g. Arsenal) use a ridge classifier that does not produce calibrated probabilities, making cross-model AUC comparison unreliable.

Regression. Per-target regression performance is primarily measured by the **root mean squared error** (RMSE):

$$RMSE = \sqrt{\frac{1}{n} \sum_{i=1}^n (y_i - \hat{y}_i)^2},$$

where y_i are the ground-truth target values and \hat{y}_i the model predictions. RMSE is reported in the original physical units of each target (e.g. concentration in g/L, absorbance units). RMSE is used as the primary metric for Elo, Score, Avg Rank, and Improbability aggregation.

The regression leaderboard additionally reports the **coefficient of determination** (R^2) — the proportion of variance in the target explained by the model. $R^2 = 1$ indicates a perfect fit; $R^2 = 0$ means the model performs no better than the target mean; negative values indicate worse-than-mean predictions. R^2 is not used as the primary ranking metric, but is reported alongside RMSE in the results tables.

Scale-invariant aggregation. Because F1 and RMSE are not comparable across targets with different scales and task types, overall model rankings are derived using scale-invariant aggregation methods, all operating on per-target scores: $F1 \uparrow$ for classification and $RMSE \downarrow$ for regression.

Elo Rating. Following the approach of TabArena [9], we evaluate models using the Elo rating system [72]. Before computing Elo, per-target (not per seed or per dataset) errors are rescaled to a $[0, 1]$ loss (lower is better) via

$$\ell_{\text{rescaled}} = \frac{\ell - \ell_{\text{best}}}{\ell_{\text{worst}} - \ell_{\text{best}}}, \quad \ell = \begin{cases} 1 - F1 & \text{classification} \\ RMSE & \text{regression,} \end{cases}$$

so that every target contributes equally, regardless of metric scale [9]. For every target, each pair of models then plays a pairwise “match”: the model with the lower rescaled loss wins; ties yield 0.5 points each. Ratings are updated using the standard Elo formula

$$R'_A \leftarrow R_A + K(W_{AB} - E_{AB}), \quad E_{AB} = \frac{1}{1 + 10^{(R_B - R_A)/400}},$$

where $W_{AB} \in \{0, 0.5, 1\}$ is the observed outcome, E_{AB} is the expected win probability, and $K = 32$ controls the magnitude of each rating update. A 400-point gap corresponds to a 10:1 (91 %) expected win rate. Because the final rating depends on the order in which comparisons are processed, we average over 200 randomly shuffled orderings of the full target pool to obtain stable estimates. Following Erickson et al. [9], we report Elo scores calibrated so that Random Forest achieves a rating of 1 000: all mean-centred Elo scores are shifted by $\Delta = 1000 - \text{Elo}_{\text{mean}}(\text{RF})$.

Elo Confidence Intervals. Following Erickson et al. [9], we bootstrap over the target pool to estimate ranking sensitivity: 200 resamples are drawn with replacement from the full set of prediction targets, and Elo is recomputed from scratch for each resample. The 2.5th and 97.5th percentiles yield a 95 % confidence interval for each model. This procedure treats benchmark targets as approximately exchangeable, so the intervals should be interpreted as reflecting variability due to the specific dataset collection in **RamanBench** rather than guaranteeing formal frequentist coverage. The RF-anchoring shift Δ is held fixed at the value from the full target pool and applied uniformly to both bounds, so all reported intervals remain on the RF = 1 000 scale.

Discussion. The confidence interval for RF does not collapse to a point even though RF defines the rating scale: the shift Δ is fixed at its value on the full target pool before bootstrapping, so each resample’s RF Elo fluctuates around 1 000 rather than being pinned to it. CIs are computed under mean-centering (all models averaged to zero) rather than RF-centering, because anchoring to a single reference model inflates variance; the Δ shift is added afterward. This yields tighter intervals for strong models, making relative Elo differences more interpretable.

Normalized Score. Following Salinas and Erickson [68], we linearly rescale per-target scores so that the best method achieves a normalized score of 1 and the median method achieves a normalized score of 0. Scores below zero are clipped to zero. Formally, let s_m be the raw score of model m on a given target, and let s_{best} and s_{median} denote the best and median scores across all models on that target (where “best” means highest F1 for classification and lowest RMSE for regression):

$$\tilde{s}_m = \max\left(0, \frac{s_m - s_{\text{median}}}{s_{\text{best}} - s_{\text{median}}}\right).$$

The normalized score is then averaged across all targets. This formulation ensures that each target contributes equally regardless of its absolute metric scale, and that the median-performing model serves as the zero baseline rather than the worst-performing model. Models that perform below the per-target median receive a score of 0; the best model always receives exactly 1. Because the per-target best is determined independently for each target, the mean normalized score of the strongest model is strictly below 1.0 whenever rankings differ across targets.

Wins. A model is credited with a *win* on a prediction target if it achieves the best score on that target after averaging over all random seeds. Wins are counted per target (not per seed or per dataset), so that each individual regression target in a multi-target dataset contributes independently — consistent with how targets are treated in all other metrics.

Improvability. Improvability was introduced by TabArena [9] and quantifies what fraction of a model’s current error could be eliminated by switching to the best available model on each target. Let $\ell_i(m)$ denote the error of model m on target i (where $\ell = 1 - \text{F1}$ for classification and $\ell = \text{RMSE}$ for regression), and let $\ell_i^* = \min_{m'} \ell_i(m')$ be the best error achieved by any model on target i . The *improvability* of model m on target i is

$$\mathcal{I}_i(m) = \frac{\ell_i(m) - \ell_i^*}{\ell_i(m)} \times 100 \%,$$

and the *mean improvability* is averaged across all targets. It lies in [0%, 100%]: 0% means the model is already optimal within the evaluated pool (or achieves zero error); values close to 100% indicate that the best model achieves nearly zero error while the current model does not. Unlike the Elo rating, improvability is sensitive to the *magnitude* of performance differences, making it more informative for practitioners who care about how much a method lags behind the best. Note that improvability is inherently *relative*: it quantifies the gap within the evaluated model pool and should be interpreted alongside absolute performance metrics. The AutoGluon ensemble is included in the model pool

when computing ℓ_j^* ; because it often achieves the lowest error on a target (by combining many models with a 4-hour time budget), individual models’ improvability partly reflects their distance from a strong ensemble rather than from the best single model. The performance–efficiency trade-off in terms of improvability vs. training time is visualized in Fig. 10.

Critical Difference (CD) Diagrams. To assess whether observed ranking differences are statistically significant, we use CD diagrams [69] generated with the AutoRank package [73]. AutoRank first applies the Friedman test to detect any overall difference across models; if significant, it follows up with the Nemenyi post-hoc test at $\alpha = 0.05$. Models are ranked per instance (target \times seed) using macro-averaged F1 for classification and RMSE for regression, and the average rank over all instances is shown on the axis (lower rank = better). Models connected by a horizontal bar are *not* significantly different at $\alpha = 0.05$.

Models that do not support a given task type (e.g. Arsenal and ROCKET for regression) are excluded from the corresponding diagram. For remaining models with isolated missing results, we assign the worst observed score on that instance so that every model participates in every rank computation without artificially dropping instances.

Sources of variability. Results in **RamanBench** are averaged over three independent repetitions with different random seeds. Each seed controls a distinct source of variability:

- **Data split randomness.** Each seed produces a different stratified (classification) or group-aware (grouped datasets) 80/20 train/test split via `sklearn’s train_test_split / GroupShuffleSplit` with `random_state=seed`.
- **Model randomness.** At the start of each seed iteration the pipeline calls `random.seed`, `numpy.random.seed`, `torch.manual_seed`, and `torch.cuda.manual_seed_all` with the current seed, ensuring consistent weight initialisation for PyTorch-based deep learning models across runs. For sklearn-compatible models (Random Forest, gradient boosting, Partial Least Squares (PLS), etc.) and AutoGluon, the seed is additionally passed as `random_state`. Residual non-determinism from GPU kernel scheduling (e.g. cuDNN) is not suppressed, as enabling `torch.use_deterministic_algorithms` would prohibit several operations used by the benchmarked architectures.
- **Evaluation randomness.** Elo ratings are computed by averaging over 200 randomly shuffled target orderings (seeded with 42) to suppress order dependence. Bootstrap confidence intervals resample the target pool 200 times with replacement (same fixed seed). Metric computation (F1, RMSE) is deterministic given the predictions.

Discussion. Each aggregation metric captures a different aspect of model performance. **Elo** treats every target equally regardless of the magnitude of performance gaps, providing a robust overall ranking that is insensitive to outliers. **Improvability** captures the magnitude of performance differences: a model with low improvability is close to optimal on every target, regardless of whether it wins outright. **Rank-based metrics** (mean rank, CD diagrams) are robust to outliers and scale independently of the metric units. A known limitation of Elo is that it is based solely on pairwise win/loss outcomes and therefore ignores the *magnitude* of performance differences: a model that barely loses every match scores the same as one that loses by large margins. We deliberately complement Elo with **normalized score** and **improvability**, both of which are sensitive to the size of performance gaps, so that readers can assess whether ranking differences are practically meaningful. This design mirrors the recommendation from the TabArena review process [9], where reviewers raised the same concern and the authors added improvability to address it.

A.2 Model Descriptions

All models are trained and evaluated through **AutoGluon 1.5** [67]. Each model is wrapped as a custom or built-in AutoGluon model so that training, validation splitting, and prediction follow a uniform interface. The sole exception is the AutoGluon ensemble (see below), which is allocated a time budget of 14,400 s (4 h) to run its full stacking and ensembling pipeline. ROCKET and Arsenal are integrated via `sktime` and registered as AutoGluon-compatible custom models; they support classification only. All remaining models support both classification and regression.

Baseline. **Dummy** predicts using simple strategies such as the mean (regression) or the most frequent class (classification), serving as a lower-bound reference.

Traditional ML. **k -Nearest Neighbors** is an instance-based model (it retains all training samples and performs no parameter learning) that predicts based on the majority class or mean value of the k closest training samples in feature space. **Linear / Logistic Regression** uses ordinary least squares for regression or the logistic function for classification. **Partial Least Squares (PLS)** projects spectra and targets into a shared latent space to maximize their covariance; for classification tasks it is applied as PLS Discriminant Analysis (PLS-DA) with one-hot encoded class labels.

Tree-based. **Random Forest** is an ensemble of decision trees trained on bootstrap samples with random feature subsets, aggregated via averaging (regression) or voting (classification). **Extra Trees** uses random split thresholds instead of optimal splits, trading slight bias for reduced variance.

Gradient Boosting. **CatBoost** uses gradient boosting on decision trees with native support for categorical features and ordered boosting to reduce overfitting. **LightGBM** is a gradient boosting framework using histogram-based tree learning for efficient training on large-scale and high-dimensional data. **XGBoost** is a gradient boosting framework using regularized tree learning with efficient parallel computation and built-in handling of sparse data.

Deep Learning. **FastAI Neural Network** is a fully connected neural network, trained using the FastAI library with learning rate scheduling and dropout. **PyTorch Neural Network** is a Multilayer Perceptron (MLP) implemented in PyTorch with configurable architecture, dropout, and batch normalization. **RealMLP** is a modern MLP architecture with improved training techniques including learning rate warmup, weight decay, and feature preprocessing. **FCResNeXt** is a fully connected residual network with ResNeXt-style parallel MLP branches introduced in version 1 of [61]. Average pooling reduces the input dimension, followed by four residual blocks each containing multiple parallel bottleneck MLPs whose outputs are summed with the identity shortcut. Ranked 2nd ($R^2 = 0.959$) in the benchmark of Lange et al. [21]. **CoAtNet** [62] is a CNN–Self-Attention hybrid that combines a depthwise-separable convolutional encoder (four stride-2 blocks) with multi-head self-attention on the compressed representation, followed by global average pooling and a two-layer classification/regression head. Ranked 3rd ($R^2 = 0.958$) in the benchmark of Lange et al. [21].

Tabular Foundation Model (TFM). **Mitra** [63] is a TFM pre-trained on mixed synthetic priors, combining in-context learning with fine-tuning for strong performance on small datasets. Natively limited to 10 classes; for datasets with more classes we wrap Mitra with an Error-Correcting Output Codes (ECOC) classifier from the `tabPFN-extensions` library [46], enabling evaluation on all **RamanBench** classification tasks. **TabPFN v2** [46] is a tabular prior-fitted network that performs in-context learning on tabular data, limited to datasets with ≤ 500 features. Natively limited to 10 classes; for datasets with more classes we apply the same ECOC wrapper as for Mitra. **TabPFN v2.5** [46] is an updated version of TabPFN with improved prior distributions and architecture refinements. Same 10-class native limit; extended with the ECOC many-class wrapper for larger class sets. All **RamanBench** classification datasets exceed TabPFN v2’s 500-feature limit; we lifted this constraint without feature subsampling. To prevent out-of-memory errors on an NVIDIA A100 (80 GB), row-count subsampling was applied in two cases: TabPFN v2 on *Bacteria Identification* and *MLROD*, and TabPFN v2.5 on *MLROD*. Performance under these constraints is validated in Section A.7. **TabDPT** [64] is a deep prior transformer for tabular data that leverages pretraining on synthetic datasets for improved few-shot performance. **TabICL v2** [48] is a tabular in-context learning model that uses a transformer to perform prediction directly from the training context without explicit parameter fitting. Version 2 extends the original classification-only model to support both classification and regression. AutoGluon 1.5 ships only TabICL v1, which lacks regression support; we therefore forked AutoGluon, upgraded the bundled TabICL to v2, and added a native `TabICLModel` wrapper that exposes both tasks. This limitation is expected to be resolved in AutoGluon 1.6. **TabM** [65] combines batch ensembling with a modified MLP architecture for efficient and accurate tabular prediction.

Raman-Specific Architectures. **Deep CNN** [39] is a LeNet-5-inspired 1D Convolutional Neural Network (CNN) consisting of three convolutional layers with kernel sizes 21, 11, and 5 interleaved with max-pooling, followed by a dense classification head. We selected the number of filters

following [26]. **ReZeroNet** [60] is a CNN with ReZero residual blocks and depthwise-separable convolutions [74]. Eight residual blocks use learnable scaling factors (initialized to zero) on the residual branch, ELU activations, and stride-2 max-pooling for progressive downsampling. Ranked 1st ($R^2 = 0.960$) in the [21] benchmark. **SANet** [40] is a Scale-Adaptive Network with multi-scale 1D convolutional blocks (kernel sizes 3–13) and squeeze-excitation channel attention, designed to capture Raman peaks of varying widths. Five blocks progressively increase channel depth (16→192) with stride-2 downsampling. Selected following [26]. **RamanFormer** [42] is a transformer encoder for Raman spectra that patchifies the spectrum into non-overlapping segments, applies three transformer encoder layers with convolutional post-processing, and pools to a classification or regression head. Originally proposed for mixture quantification; adapted here for classification following [26]. **RamanNet** [41] is a sliding-window MLP that splits the spectrum into overlapping windows, each processed by an independent perceptron, avoiding the translational equivariance of standard convolutions. Features are concatenated and passed through dense layers with decreasing dropout. **RamanTransformer** [66] is a Vision Transformer (ViT) adapted for 1D Raman spectra, with patch tokenization, a learnable class token, positional encoding, and 12 transformer encoder blocks with 12-head self-attention. Selected following [26].

Time-Series Classifiers. **ROCKET** [49] applies 10,000 random convolutional kernels with varying lengths, dilations, and biases to the input signal, extracts two summary statistics per kernel (proportion of positive values and max), and trains a RidgeClassifierCV on the resulting features. Achieves near-state-of-the-art accuracy at a fraction of deep learning’s computational cost. Classification only. **Arsenal** [50] is an ensemble of multiple ROCKET transforms, each trained with a RidgeClassifierCV and combined via cross-validation-weighted voting. Unlike plain ROCKET, Arsenal produces well-calibrated probability estimates and forms one of the four components of HIVE-COTE 2.0. Classification only.

Ensemble. **AutoGluon Ensemble** runs AutoGluon’s full ensemble mode, which automatically selects and combines predictions from its built-in model portfolio via multi-layer stacking and weighted ensembling. The candidate pool consists of the 16 built-in AutoGluon models: CatBoost, FastAI, LightGBM, k -Nearest Neighbors (kNN), Linear/Logistic Regression, Mitra, PyTorch NN, RealMLP, TabPFN v2, TabPFN v2.5, Random Forest, TabDPT, TabICL v2, TabM, XGBoost, and Extra Trees. Custom models (PLS, all Raman-specific deep learning architectures, ROCKET, and Arsenal) are *not* included in the ensemble pool, as AutoGluon’s stacking mechanism operates only over its native model registry. Serves as an upper-bound reference for the built-in model portfolio.

Data Augmentation for Deep Learning Models. The eight deep learning architectures (Deep CNN, CoAtNet, FCResNeXt, RamanFormer, RamanNet, RamanTransformer, ReZeroNet, and SANet) are trained with augmentation applied once before training: the training split is expanded threefold by appending noise-augmented copies of each spectrum ($\sigma_{\text{noise}} = 0.01 \cdot \sigma_X$, i.e. 1% of the training-set standard deviation). This ensures that even very small training splits (e.g. $n < 20$) produce enough samples per mini-batch to stabilize batch normalization statistics and reduce gradient variance. Augmentation is disabled for training splits exceeding 2,000 samples, where the regularization benefit is marginal. This additive Gaussian noise strategy is the standard regularization approach for spectral deep learning models [26].

Training-Set Subsampling for Memory-Constrained Models. TabPFN v2 and TabPFN v2.5 encounter GPU out-of-memory (OOM) errors on an NVIDIA A100 (80 GB) for specific large-scale dataset combinations. The affected training splits are capped at 10,000 spectra; stratified sampling is used (only classification datasets affected). The affected combinations are: TabPFN v2 on Bacteria Identification and MLROD; and TabPFN v2.5 on MLROD. The test split is never modified; evaluation is always performed on the full held-out set. All other model–dataset combinations use the complete training data without modification.

A.3 Software

RamanBench is implemented as two complementary open-source Python packages.

A.3.1 raman-data — Unified Dataset Library

A key obstacle to reproducible Raman spectroscopy research is *data fragmentation*: the 74 datasets in **RamanBench** are distributed across eleven heterogeneous platforms (HuggingFace, Zenodo, Figshare, Mendeley Data, Kaggle, GitHub, Google Drive, RWTH cloud storage, and institutional mirrors), each with its own access API and file format (CSV, TSV, MATLAB .mat, SPC, XLSX, binary NumPy). Without a unified interface, every researcher who wants to reproduce or extend our results must independently resolve these integration details — a substantial and error-prone overhead. `raman-data` resolves this by wrapping all repository-specific access and format parsing behind a single consistent API, with transparent local caching after the first download. The package is fully standalone and can be used independently of the benchmarking pipeline in any research context requiring Raman spectroscopy data.

Installation. `pip install raman-data`

Links.

- PyPI: <https://pypi.org/project/raman-data/>
- GitHub: https://github.com/ml-lab-htw/raman_data

API.

```
from raman_data import raman_data, TASK_TYPE, APPLICATION_TYPE

# List all available dataset identifiers
names = raman_data()

# Filter by task type or domain
clf_names = raman_data(task_type=TASK_TYPE.Classification)
bio_names = raman_data(application_type=APPLICATION_TYPE.Biological)

# Load a specific dataset
dataset = raman_data("bioprocess_substrates")
X = dataset.spectra          # (N, W) float64
shifts = dataset.raman_shifts # (W,) cm-1 axis
y = dataset.targets         # (N,) or (N, T)
```

Design. Each dataset is described by a `DatasetInfo` dataclass that stores the task type (`TASK_TYPE.Classification` / `Regression`), application domain (`APPLICATION_TYPE`), provenance metadata (source URL, citation, licence), and a loader function encapsulating the dataset-specific ingestion logic.

The returned `RamanDataset` object exposes:

- `spectra` — $(N \times W)$ intensity matrix,
- `raman_shifts` — wavenumber axis in cm^{-1} ,
- `targets` — scalar or vector labels / concentrations,
- `target_names` — human-readable target descriptions,
- `metadata` — provenance dict (source, paper DOI, licence).

A.3.2 raman-bench — Reproducible Benchmarking Pipeline

`raman-bench` is the open-source evaluation framework underlying every result in this paper. It standardizes preprocessing, train/test splitting, hyperparameter optimization, and metric computation across all evaluated model families and datasets, ensuring that every reported number can be reproduced from a single configuration file.

Installation. `pip install raman-bench`

Links.

- GitHub: <https://github.com/ml-lab-htw/RamanBench>
- PyPI: <https://pypi.org/project/raman-bench/>

Core modules.

<code>benchmark.RamanBenchmark</code>	Loads datasets via <code>raman-data</code> , applies preprocessing, performs train/test splits with fixed seeds, and caches prepared splits to disk for reproducible re-evaluation.
<code>model.RamanModel</code>	Wraps each model family (classical chemometrics, gradient boosting, deep networks, Tabular Foundation Model (TFM)) in a uniform sklearn-compatible interface, including HPO via AutoGluon’s search-space mechanism.
<code>evaluation</code>	Computes per-dataset, per-model metrics (F1, balanced accuracy, RMSE, R^2 , training time, inference latency, peak memory, energy) and aggregates them across folds and repetitions.

A.3.3 Online Leaderboard

Hugging Face Spaces. <https://huggingface.co/spaces/HTW-KI-Werkstatt/RamanBench>

The **RamanBench** leaderboard provides an interactive, always-up-to-date view of benchmark results. It is hosted as a Hugging Face Space and displays Elo ratings, normalized scores, mean ranks, improvability, and efficiency metrics for all evaluated models, with filters by model category and individual columns.

Computational setup. All experiments are run on an HPC cluster at HTW Berlin. Each model is submitted as a separate SLURM job and allocated one NVIDIA A100 GPU (80 GB HBM2e) and 256 GB of CPU RAM. Reported train and inference times reflect single-GPU execution on an A100 and are not directly comparable to results obtained on different hardware.

A.3.4 Living Benchmark Protocols

Maintenance. **RamanBench** is jointly maintained by KI-Werkstatt HTW Berlin (Mario Koddenbrock) and the Dept. of Biotechnology, TU Berlin (Christoph Lange). Maintainer responsibilities include reviewing dataset and model submissions, re-running evaluations on new contributions, publishing leaderboard snapshots, and handling corrections or retractions.

Versioning. Each update that adds datasets or models, changes evaluation protocols, or corrects errors is tagged as a new version (e.g., v0.2). Version changelogs are maintained on GitHub and HuggingFace. Results from prior versions remain accessible so that comparisons are possible.

Contributing datasets. New datasets must satisfy the same inclusion criteria as the existing collection (see Section 3.1): real measured Raman spectra, unrestricted public access, a minimum of 10 samples, and a learnable prediction target verified by the learnability check (Section A.6). Contributions are submitted as GitHub pull requests; required metadata fields and a submission template are provided at <https://github.com/ml-lab-htw/RamanBench>.

Contributing models. New models may be submitted in one of three forms: (1) a reproducible training script implementing the `RamanModel` interface (Section A.3.2), (2) publicly released pre-trained weights with an inference wrapper, or (3) an open-source API endpoint with a `RamanModel`-compatible wrapper. Upon acceptance, the maintainers run the submitted model on the standard hardware setup and publish the results on the leaderboard. Models that require closed APIs or non-reproducible configurations are not eligible.

A.4 Handling Foul Play and Dataset Contamination

A fundamental limitation of any open benchmark is the risk that reported results reflect foul play or dataset contamination rather than genuine generalisation. Model developers could selectively tune hyperparameters on **RamanBench**’s datasets, or include them as pretraining data for a foundation model. We discuss both concerns in turn; a parallel discussion in the context of tabular Machine Learning (ML) can be found in Erickson et al. [9].

Avoiding foul play. Foul play will inevitably occur as **RamanBench** grows in visibility. Two structural guards reduce this risk:

1. **Transparent submissions and maintainer scrutiny.** All accepted submission forms (training scripts, pretrained weights, and open API endpoints) must be publicly accessible and are re-run by the maintainers on standard hardware. Outlier results trigger manual inspection of the submitted code or weights; models with confirmed irregularities are flagged on a separate leaderboard.
2. **Living benchmark updates.** Regular updates (new datasets, adjusted splits, and changed random seeds) make targeted overfitting progressively harder to sustain across all targets.

Active maintenance is a precondition for both guards; we therefore regard keeping **RamanBench** alive and regularly updated as the best long-term protection against foul play.

Possible data contamination. At the time of this writing, data contamination is unlikely to have affected results in **RamanBench**: the datasets are specialist Raman spectroscopy measurements that have not, to our knowledge, been included in any model’s pretraining corpus. All benchmarked Tabular Foundation Model (TFM) — MITRA [63], TabPFN v2/v2.5 [46], TABDPT [64], and TABICL v2 [48] — were trained on synthetic data or general-purpose tabular benchmarks, none of which include Raman spectroscopy data. Once **RamanBench** is publicly released this situation will change; the guards described above are designed for that scenario, and we will annotate the leaderboard with contamination information as it becomes available.

A.5 Ablation: Small vs. Larger Datasets

Raman spectroscopy datasets span roughly four orders of magnitude in size, with a substantial fraction of **RamanBench** falling into a *small-data regime* (fewer than 50 spectra in total). This is not a collection artefact but reflects the practical reality of the field: acquiring labelled Raman spectra is often costly, time-consuming, or limited by the availability of reference material. The importance of benchmarking under such data scarcity has recently been emphasized in the tabular ML community by Knauer et al. [58], who introduce PMLBmini for this setting. **RamanBench** extends this perspective to spectroscopy, where small datasets are common rather than exceptional. Understanding which model families remain reliable under these conditions is therefore essential.

We partition all benchmark datasets into two groups:

- **Small** (16 datasets): $N < 50$ spectra (training + test combined).
- **Larger** (62 datasets): $N \geq 50$ spectra.

To enable comparison across classification and regression tasks, we report a *mean normalized score*, as described in Section A.1. We further report $\Delta = \overline{\text{Score}}_{\text{Small}} - \overline{\text{Score}}_{\text{Larger}}$: a positive Δ (\uparrow) indicates relatively stronger performance on small datasets, while a negative Δ (\downarrow) reflects improved performance with increasing data. Models are sorted by performance on small datasets (descending).

Classical methods remain competitive in the small-data regime (Table 2). While TFM dominate overall performance, their advantage narrows substantially on small datasets. **TabPFN v2.5** and **TabICL v2** still achieve the highest scores (0.56 and 0.51), but classical ensemble methods become competitive: **Extra Trees** reaches 0.38 (4th overall), followed by **TabPFN v2** (0.36) and **Random Forest** (0.32). Both **Extra Trees** ($\Delta = +0.29$) and **Random Forest** ($\Delta = +0.26$) exhibit the strongest positive shifts, indicating that their relative performance is concentrated in the small-data regime. Other simple methods such as *k*-**Nearest Neighbors (kNN)** ($\Delta = +0.18$) and **Logistic Regression** ($\Delta = +0.12$) also benefit from limited data.

Foundation models benefit strongly from additional data (Table 2). Although foundation models perform well across both partitions, their advantage increases markedly with dataset size. **TabPFN v2.5** achieves the highest overall and large-dataset scores (0.79 and 0.83), while **TabPFN v2** shows the strongest scaling effect ($\Delta = -0.37$), improving from 0.36 on small datasets to 0.73 on larger ones. Similarly, **TabICL v2** benefits from additional data ($\Delta = -0.19$). Negative Δ values for these models reflect effective utilization of larger datasets rather than poor performance in the small-data regime.

Table 2: **Classical ensemble methods challenge Tabular Foundation Model (TFM) dominance on small datasets:** Mean normalized score per model across all, small ($N_{\text{total}} < 50$), and larger ($N_{\text{total}} \geq 50$) datasets (best model per dataset = 1, median = 0; classification: F1; regression: RMSE). $\Delta = \text{Score}_{\text{Small}} - \text{Score}_{\text{Larger}}$; \uparrow indicates $\Delta > 0.05$, \downarrow indicates $\Delta < -0.05$. Largest positive and negative Δ and best mean normalized score per partition in **bold**. Models are sorted by performance on small datasets.

Model	Mean Norm. Score (\uparrow)			Δ
	(All, $N=150$)	(Rest, $N=126$)	(Tiny, $N=24$)	
TabPFN v2.5	0.79	0.83	0.56	-0.27 \downarrow
TabICL v2	0.67	0.70	0.51	-0.19 \downarrow
MITRA	0.51	0.52	0.49	-0.03
Extra Trees	0.14	0.10	0.38	+0.29 \uparrow
TabPFN v2	0.67	0.73	0.36	-0.37 \downarrow
Logistic Reg.	0.23	0.21	0.33	+0.12 \uparrow
Random Forest	0.11	0.06	0.32	+0.26 \uparrow
KNN	0.16	0.13	0.31	+0.18 \uparrow
PLS	0.23	0.21	0.29	+0.08 \uparrow
NN (PyTorch)	0.20	0.20	0.23	+0.03
ReZeroNet	0.31	0.34	0.20	-0.14 \downarrow
RealMLP	0.23	0.23	0.20	-0.04
RamanTransformer	0.05	0.02	0.19	+0.17 \uparrow
RamanNet	0.15	0.14	0.19	+0.06 \uparrow
CoAtNet	0.14	0.14	0.16	+0.02
CatBoost	0.11	0.10	0.15	+0.04
FCResNeXt	0.09	0.08	0.14	+0.05 \uparrow
TabDPT	0.30	0.34	0.11	-0.23 \downarrow
XGBoost	0.05	0.04	0.10	+0.06 \uparrow
TabM	0.22	0.24	0.09	-0.15 \downarrow
FastAI	0.10	0.11	0.06	-0.04
RamanFormer	0.17	0.19	0.06	-0.14 \downarrow
LightGBM	0.04	0.04	0.05	+0.01
Deep CNN	0.18	0.20	0.05	-0.15 \downarrow
ROCKET	0.06	0.06	0.05	-0.01
Arsenal	0.06	0.07	0.03	-0.04
SANet	0.07	0.08	0.03	-0.05

Model behavior across regimes. Most classical and low-capacity models exhibit positive Δ , indicating robustness under limited data, whereas high-capacity and representation-heavy models tend to benefit from larger datasets. **MITRA** ($\Delta = -0.03$) stands out as largely insensitive to dataset size, maintaining stable performance across regimes.

A.6 Learnability Verification

A benchmark is only meaningful if its datasets contain learnable spectral signal — i.e. if the labels are actually correlated with the spectra. To verify this, we apply task-specific learnability checks.

Classification. For each dataset we compare the best non-Dummy model’s mean F1 against the Dummy majority-class baseline ($\Delta = \text{Best} - \text{Dummy}$). A dataset passes if $\Delta > 0.05$, a conservative threshold well within the range of practically meaningful improvement.

Regression. No separate Dummy comparison is needed for regression: $R^2 > 0$ by definition implies outperforming the constant mean predictor. We use a slightly stricter threshold of $R^2 > 0.05$ to filter out targets where the learned signal is negligible; a target passes if the best model achieves $R^2 > 0.05$.

Table 3: Learnability verification (classification). For each dataset, the best non-Dummy model’s mean F1 is compared to the Dummy majority-class baseline. $\Delta = \text{Best} - \text{Dummy}$. A dataset passes if $\Delta > 0.05$ (✓); otherwise it fails (×).

Dataset	Best Model	F1 (Best)	F1 (Dummy)	Δ	Pass
Alzheimer’s SERS Serum	TabICL v2	0.990	0.241	0.750	✓
Cancer Cell Metabolite ((COOH) ₂)	Deep CNN	1.000	0.019	0.981	✓
Cancer Cell Metabolite (COOH)	Deep CNN	0.995	0.019	0.976	✓
Cancer Cell Metabolite (NH ₂)	ReZeroNet	0.997	0.019	0.978	✓
Diabetes Skin (Ear Lobe)	ROCKET	0.689	0.333	0.356	✓
Diabetes Skin (Inner Arm)	FCResNeXt	0.656	0.333	0.322	✓
Diabetes Skin (Thumbnail)	PLS	0.411	0.333	0.078	✓
Diabetes Skin (Vein)	RamanNet	0.522	0.333	0.189	✓
Hair Dyes SERS	Deep CNN	1.000	0.269	0.731	✓
Head & Neck Cancer	PLS	0.704	0.180	0.524	✓
ML Raman Open Dataset (MLROD)	TabICL v2	0.990	0.033	0.957	✓
Mutant Wheat	TabPFN v2.5	0.921	0.127	0.794	✓
Pathogenic Bacteria	RamanNet	0.947	0.007	0.940	✓
Pharmaceutical Ingredients	Logistic Reg.	1.000	0.003	0.997	✓
Prostate Cancer SERS Serum	TabICL v2	0.998	0.210	0.788	✓
RRUFF Minerals (Raw)	Arsenal	0.953	0.002	0.950	✓
Saliva Alzheimer	TabPFN v2.5	0.975	0.659	0.316	✓
Saliva COVID-19	TabPFN v2.5	0.957	0.199	0.757	✓
Saliva Parkinson	TabPFN v2.5	0.953	0.443	0.509	✓
Stroke SERS Serum	RamanFormer	0.999	0.333	0.665	✓
Weathered Microplastics	Logistic Reg.	1.000	0.333	0.667	✓

Table 4: Learnability verification (regression). For each target, the best model’s mean R^2 is reported. Pass: $R^2 > 0.05$ (✓).

Dataset	Best Model	R^2 (Best)	Pass
Acetic Concentration — Acetic Acid (AA)	TabPFN v2.5	1.000	✓
— Acetate (AA-)	TabICL v2	1.000	✓
Adenine (Colloidal Gold)	TabPFN v2	0.922	✓
Adenine (Colloidal Silver)	TabICL v2	0.834	✓
Adenine (Solid Gold)	TabPFN v2.5	0.739	✓
Adenine (Solid Silver)	TabPFN v2.5	0.844	✓
Amino Acid LC (Glycine)	FastAI	0.101	✓
Amino Acid LC (Leucine)	XGBoost	-0.018	×
Amino Acid LC (Phenylalanine)	NN (PyTorch)	-0.010	×
Amino Acid LC (Tryptophan)	TabDPT	0.057	✓
Bio-Catalysis Monitoring of AXP — Adenosin	PLS	0.666	✓

Continued on next page

(continued from previous page)

Dataset	Best Model	R^2 (Best)	Pass
— ADP	PLS	0.741	✓
— AMP	PLS	0.766	✓
— ATP	TabPFN v2.5	0.832	✓
Bioprocess Analytes Anton 532 — Glucose	TabPFN v2	0.790	✓
— Acetate	TabPFN v2	0.457	✓
— MagnesiumSulfate	TabICL v2	0.948	✓
Bioprocess Analytes Anton 785 — Glucose	TabPFN v2.5	0.918	✓
— Acetate	TabPFN v2	0.808	✓
— MagnesiumSulfate	RealMLP	0.975	✓
Bioprocess Analytes E. Coli Metabolites — Glucose	TabPFN v2.5	0.946	✓
— Sodium_Acetate	TabPFN v2.5	0.935	✓
Bioprocess Analytes Kaiser — Glucose	TabDPT	0.837	✓
— Acetate	TabPFN v2.5	0.835	✓
— MagnesiumSulfate	KNN	0.815	✓
Bioprocess Analytes Metrohm — Glucose	TabPFN v2	0.890	✓
— Acetate	TabPFN v2	0.914	✓
— MagnesiumSulfate	KNN	0.992	✓
Bioprocess Analytes Mettler Toledo — Glucose	TabDPT	0.857	✓
— Acetate	TabPFN v2	0.855	✓
— MagnesiumSulfate	TabPFN v2.5	0.976	✓
Bioprocess Analytes Tec5 — Glucose	TabPFN v2.5	0.938	✓
— Acetate	TabDPT	0.768	✓
— MagnesiumSulfate	LightGBM	0.919	✓
Bioprocess Analytes Timigate — Glucose	PLS	0.818	✓
— Acetate	TabPFN v2.5	0.883	✓
— MagnesiumSulfate	TabICL v2	0.981	✓
Bioprocess Analytes Tornado — Glucose	TabPFN v2	0.947	✓
— Acetate	TabDPT	0.824	✓
— MagnesiumSulfate	Deep CNN	0.988	✓
Bioprocess Monitoring — Glucose	TabPFN v2.5	0.954	✓
— Glycerol	TabPFN v2	0.982	✓
— Acetate	TabPFN v2.5	0.909	✓
— EnPump	ReZeroNet	0.972	✓
— Nitrate	CoAtNet	0.983	✓
— Yeast_Extract	TabICL v2	0.962	✓
— total_phosphate	TabICL v2	0.976	✓
— total_sulfate	TabPFN v2.5	0.944	✓
Citric Concentration — Citric acid (CA)	TabPFN v2.5	0.998	✓
— Citrate 1 (CA-)	TabPFN v2.5	0.999	✓
E. Coli Fermentation — Glucose	TabPFN v2	0.971	✓
— Acetate	TabPFN v2	0.491	✓
E. Coli Metabolites Dig4Bio — Glucose (g/L)	TabPFN v2	0.929	✓
— Sodium Acetate (g/L)	TabPFN v2.5	0.870	✓
— Magnesium Acetate (g/L)	TabPFN v2.5	0.879	✓
Formic Concentration — Formic acid (FA)	TabPFN v2.5	0.998	✓
— Formiate (FA-)	Logistic Reg.	0.929	✓
— water	CoAtNet	0.894	✓
Gasoline Properties (Benchtop) — Research Octane Number	ReZeroNet	0.926	✓
— Motor Octane Number	TabPFN v2.5	0.952	✓
— Ethanol Content (— Ethyl Tert-Butyl Ether (ETBE)	ReZeroNet	0.964	✓
— Methyl Tert-Butyl Ether (MTBE)	ReZeroNet	0.944	✓
— Density at 15°C	TabPFN v2.5	0.798	✓
— Water Content	MITRA	0.551	✓
— Oxygenates Content	TabPFN v2.5	0.574	✓
— Oxygen Content	TabPFN v2	0.797	✓
— Olefins Content	TabPFN v2.5	0.956	✓
— Aromatics Content	Logistic Reg.	0.937	✓
— Benzene Content	TabPFN v2	0.964	✓
Gasoline Properties (Handheld) — Research Octane Number	TabPFN v2.5	0.906	✓
— Motor Octane Number	TabPFN v2	0.967	✓
— Ethanol Content (— Ethyl Tert-Butyl Ether (ETBE)	KNN	0.959	✓
— Methyl Tert-Butyl Ether (MTBE)	RamanFormer	0.886	✓
— Density at 15°C	MITRA	0.587	✓
— Water Content	TabPFN v2.5	0.474	✓
— Oxygenates Content	TabPFN v2.5	0.370	✓
— Oxygen Content	FCResNeXt	0.639	✓
— Olefins Content	TabPFN v2.5	0.909	✓
— Aromatics Content	TabPFN v2.5	0.900	✓
— Benzene Content	TabPFN v2	0.858	✓
Itaconic Concentration — Itaconic acid (IA)	TabICL v2	0.998	✓
— Itaconate 1 (IA-)	TabPFN v2.5	0.971	✓
— Itaconate 2 (IA2-)	TabPFN v2.5	0.998	✓
Kaiser Raman E. coli Fermentation — OD600	RamanTransformer	-0.457	×
— Glucose	Logistic Reg.	0.589	✓
— Acetate	TabDPT	-1.556	×
Kaiser Raman E. coli Fermentation Supernatant — OD600	Extra Trees	0.405	✓
— Glucose	XGBoost	0.278	✓
— Acetate	PLS	-1.299	×
Levulinic Concentration — pH	MITRA	0.908	✓
— Mass of NaOH	TabPFN v2.5	0.998	✓
Microgel Size (Linear Fit, FingerPrint)	TabPFN v2.5	0.164	✓
Microgel Size (Linear Fit, Global)	TabPFN v2	0.249	✓
Microgel Size (MinMax + Linear Fit, FingerPrint)	TabPFN v2.5	0.083	✓
Microgel Size (MinMax + Linear Fit, Global)	TabPFN v2	0.280	✓
Microgel Size (MinMax + Rubber Band, FingerPrint)	TabPFN v2	0.101	✓
Microgel Size (MinMax + Rubber Band, Global)	TabPFN v2	0.268	✓
Microgel Size (Raw, FingerPrint)	TabPFN v2.5	0.221	✓
Microgel Size (Raw, Global)	TabICL v2	0.276	✓

Continued on next page

(continued from previous page)

Dataset	Best Model	R^2 (Best)	Pass
Microgel Size (Rubber Band, FingerPrint)	TabICL v2	0.168	✓
Microgel Size (Rubber Band, Global)	TabPFN v2	0.232	✓
Microgel Size (SNV + Linear Fit, FingerPrint)	TabPFN v2	0.158	✓
Microgel Size (SNV + Linear Fit, Global)	TabICL v2	0.340	✓
Microgel Size (SNV + Rubber Band, FingerPrint)	TabPFN v2	0.132	✓
Microgel Size (SNV + Rubber Band, Global)	TabICL v2	0.323	✓
Microgel Synthesis Flow vs. Batch	TabDPT	0.664	✓
Microgel Synthesis in Flow	TabPFN v2.5	0.980	✓
R. eutropha Copolymer Fermentations — Cell Dry Weight [g/L]	TabPFN v2.5	0.985	✓
— Fructose HPLC [g/L]	TabPFN v2.5	0.991	✓
— Hhx [g/L]	TabPFN v2.5	0.979	✓
— HB [g/L]	MITRA	0.915	✓
— Residual CDW [g/L]	TabPFN v2.5	0.975	✓
— Urea kit [g/L]	TabDPT	0.963	✓
Streptococcus thermophilus Fermentations Kaiser — Lactose	CoAtNet	-9.415	×
— Galactose	TabPFN v2.5	0.547	✓
— Lactate	CoAtNet	-4.084	×
— OD600	CoAtNet	-0.237	×
Succinic Concentration — pH	TabPFN v2.5	0.985	✓
— Mass of NaOH	TabPFN v2.5	1.000	✓
Sugar Mixtures (High SNR) — Sucrose	TabICL v2	1.000	✓
— Fructose	TabICL v2	1.000	✓
— Maltose	TabPFN v2.5	1.000	✓
— Glucose	TabICL v2	0.999	✓
Sugar Mixtures (Low SNR) — Sucrose	TabICL v2	0.999	✓
— Fructose	TabICL v2	0.998	✓
— Maltose	TabPFN v2.5	0.987	✓
— Glucose	TabICL v2	0.982	✓
Synthetic Organic Pigments (Raw)	Deep CNN	0.255	✓
Time-Gated Raman E. coli Fermentation — OD600	FCResNeXt	-4.580	×
— Glucose	Logistic Reg.	0.406	✓
— Acetate	Extra Trees	0.232	✓
Time-Gated Raman E. coli Fermentation Supernatant — OD600	NN (PyTorch)	-3.644	×
— Glucose	RamanFormer	0.801	✓
— Acetate	KNN	-0.095	×
Time-Gated Streptococcus thermophilus Fermentations — Lactose	TabPFN v2	-14657.663	×
— Galactose	TabPFN v2	-308.511	×
— Lactate	TabPFN v2	-2367.421	×
— OD600	TabPFN v2	-1133.366	×
Yeast Fermentation — Glucose [mol / L]	TabPFN v2	0.580	✓
— Fructose [mol / L]	MITRA	0.703	✓
— Glycerol [mol / L]	NN (PyTorch)	0.731	✓
— Ethanol [mol / L]	RamanNet	0.896	✓

Classification (Table 3). All 21 classification datasets pass the $\Delta > 0.05$ threshold: the worst-performing dataset has $\Delta = 0.078$ (Diabetes Skin (Thumbnail)). This confirms that every classification task in **RamanBench** carries learnable spectral signal.

Regression (Table 4). Out of 148 regression targets evaluated for learnability (129 included in the benchmark plus 19 excluded candidates), 15 fail the $R^2 > 0.05$ threshold (shown in red in Table 4). The failures cluster around two themes:

- **Amino Acid LC — Leucine** ($R^2 = -0.018$) and **Phenylalanine** ($R^2 = -0.010$): both targets carry insufficient spectral variation relative to noise; the other two amino acid targets from the same dataset pass.
- **Fermentation analytes** in Kaiser *E. coli* Fermentation (OD600: $R^2 = -0.46$; Acetate: $R^2 = -1.56$), Kaiser *E. coli* Fermentation Supernatant (Acetate: $R^2 = -1.30$), *Streptococcus thermophilus* Fermentation — Kaiser (Lactose: $R^2 = -9.42$; Lactate: $R^2 = -4.08$; OD600: $R^2 = -0.24$), Time-Gated *E. coli* Fermentation (OD600: $R^2 = -4.58$), Time-Gated *E. coli* Fermentation Supernatant (OD600: $R^2 = -3.64$; Acetate: $R^2 = -0.10$), and *Streptococcus thermophilus* Fermentation — Timegate (Lactose: $R^2 = -126$; Galactose: $R^2 = -352$; Lactate: $R^2 = -3483$; OD600: $R^2 = -1315$): biomass and metabolite concentrations appear largely decorrelated from single-snapshot Raman spectra in these datasets.

In total, 15 regression targets and 1 complete dataset (*Streptococcus thermophilus* Fermentation — Timegate, all four targets failing) are excluded from all **RamanBench** metrics on learnability grounds.

A.7 Foundation Model Recommended Size Limits

TabPFN v2 and TabPFN v2.5 have documented recommended maximum dataset sizes; the models can process larger inputs, but were not specifically built or evaluated for them [46]. MITRA [63] and both TabPFN version have an architectural class-count constraint of 10.

Because Raman spectra are inherently high-dimensional, all 21 classification datasets exceed the recommended feature limit for TabPFN v2; models simply run without feature subsampling once limits are lifted. TabPFN v2.5 has a more permissive feature limit (2,000); 9 datasets fall within all its recommendations. For datasets with more than 10 classes, Error-Correcting Output Codes (ECOC) [75] was applied for all three models. Row-count subsampling was applied only for combinations that caused out-of-memory errors on the A100 (80 GB): TabPFN v2 on *Bacteria Identification* ($N = 78,500$) and *MLROD* ($N = 130,061$); TabPFN v2.5 on *MLROD* only. All other model-dataset combinations ran without any subsampling.

Table 5: Recommended maximum dataset sizes for three TFM used in **RamanBench**. MITRA has no documented row or feature limit. Limits are lifted via `ignore_pretraining_limits=True`; no feature subsampling is applied. ECOC [75] is used for $C > 10$.

Model	Max Rows	Max Features	Max Classes
TabPFN v2	10,000	500	10
TabPFN v2.5	50,000	2,000	10
MITRA	—	—	10

Table 6 reports macro-F1 (mean \pm std across three seeds) for all 21 datasets. Results shown in gray are *within* the model’s recommended limits; all other entries exceed at least one limit. N/F/C values in **bold** exceed the most restrictive limit across the three models ($N > 10\,000$, $F > 500$, $C > 10$). Superscripts on dataset names indicate the exceeded dimension(s): n = row count, f = feature count, c = class count. \ddagger = ECOC used.

Table 6: **Foundation models perform competitively beyond their recommended size limits.** Macro-F1 (mean \pm std over 3 seeds) for TabPFN v2, TabPFN v2.5, and MITRA on all 21 benchmark classification datasets. Gray entries are within the model’s recommended limits; all others exceed at least one limit. **Bold** N/F/C values exceed the strictest recommended limit ($N > 10\,000$, $F > 500$, $C > 10$). \ddagger ECOC used for $C > 10$ [75].

Dataset	N	F	C	TabPFN v2	TabPFN v2.5	MITRA	Best Model (F1)
Saliva Alzheimer ^f	1,151	885	2	0.961 \pm 0.005	0.975 \pm 0.003	0.950 \pm 0.005	0.975 (TabPFN v2.5)
Pathogenic Bacteria ^{c,f,n\ddagger}	78,500	1,000	30	0.888 \pm 0.002	0.899 \pm 0.001	0.714 \pm 0.008	0.947 (RamanNet)
Cancer Cell Metabolite ((COOH)2) ^{c,f\ddagger}	627	2,090	12	0.989 \pm 0.012	0.992 \pm 0.008	0.995 \pm 0.005	1.000 (Deep CNN)
Cancer Cell Metabolite (COOH) ^{c,f\ddagger}	633	2,090	12	0.977 \pm 0.021	0.992 \pm 0.008	0.982 \pm 0.020	0.995 (Deep CNN)
Cancer Cell Metabolite (NH2) ^{c,f\ddagger}	632	2,090	12	0.992 \pm 0.008	0.995 \pm 0.005	0.995 \pm 0.005	0.997 (ReZeroNet)
Stroke SERS Serum ^f	4,020	724	2	0.997 \pm 0.002	0.998 \pm 0.001	0.996 \pm 0.001	0.999 (RamanFormer)
Saliva COVID-19 ^f	2,501	885	3	0.901 \pm 0.014	0.957 \pm 0.007	0.821 \pm 0.019	0.957 (TabPFN v2.5)
Diabetes Skin (Ear Lobe) ^f	20	3,160	2	0.522 \pm 0.201	0.478 \pm 0.267	0.244 \pm 0.077	0.689 (ROCKET)
Diabetes Skin (Inner Arm) ^f	20	3,160	2	0.289 \pm 0.077	0.244 \pm 0.077	0.222 \pm 0.192	0.656 (FCResNeXt)
Diabetes Skin (Thumbnail) ^f	20	3,160	2	0.233 \pm 0.252	0.178 \pm 0.168	0.178 \pm 0.168	0.411 (PLS)
Diabetes Skin (Vein) ^f	20	3,160	2	0.467 \pm 0.231	0.378 \pm 0.308	0.422 \pm 0.278	0.522 (RamanNet)
Hair Dyes SERS ^f	1,713	1,340	4	0.999 \pm 0.002	0.999 \pm 0.002	0.998 \pm 0.003	1.000 (Deep CNN)
Head & Neck Cancer ^f	111	1,004	4	0.545 \pm 0.077	0.552 \pm 0.037	0.507 \pm 0.133	0.704 (PLS)
Weathered Microplastics ^f	77	1,144	3	0.841 \pm 0.035	0.937 \pm 0.001	0.893 \pm 0.038	1.000 (Logistic Reg.)
ML Raman Open Dataset (MLROD) ^{c,f,n\ddagger}	130,061	1,836	16	0.977 \pm 0.002	0.988 \pm 0.000	0.967 \pm 0.001	0.990 (TabICL v2)
Saliva Parkinson ^f	1,476	885	2	0.886 \pm 0.021	0.953 \pm 0.014	0.870 \pm 0.022	0.953 (TabPFN v2.5)
Pharmaceutical Ingredients ^{c,f\ddagger}	3,510	3,276	32	0.996 \pm 0.004	1.000	0.959 \pm 0.013	1.000 (Logistic Reg.)
RRUFF Minerals (Raw) ^{c,f\ddagger}	1,162	1,142	79	0.803 \pm 0.015	0.892 \pm 0.019	0.924 \pm 0.016	0.953 (Arsenal)
Alzheimer’s SERS Serum ^f	3,417	724	3	0.953 \pm 0.002	0.980 \pm 0.005	0.958 \pm 0.013	0.990 (TabICL v2)
Prostate Cancer SERS Serum ^{f,n}	12,601	725	3	0.990 \pm 0.002	0.996 \pm 0.002	0.964 \pm 0.004	0.998 (TabICL v2)
Mutant Wheat ^{f,n}	53,134	1,748	4	0.877 \pm 0.002	0.921 \pm 0.003	0.828 \pm 0.001	0.921 (TabPFN v2.5)

Gray = within recommended limits for that model; n row limit, f feature limit, c class limit exceeded. \ddagger ECOC used [75].

Key observations (classification). Despite exceeding the recommended limits, the three foundation models maintain competitive performance on the vast majority of datasets. On large datasets where row-count subsampling was applied due to OOM (*MLROD*, *Bacteria Identification*), TabPFN v2.5 — which has the most permissive row limit (50 000) — consistently outperforms TabPFN v2, as expected.

Exceeding only the feature limit (the majority of datasets) causes no systematic degradation. Among datasets with more than 10 classes, *Pathogenic Bacteria* (30 classes, $N = 78,500$) and *RRUFF Mineral Raw* (79 classes) show the largest gaps to the best model; for Bacteria Identification this is compounded by row-count subsampling. *Cancer Cell* (12 classes) and *Pharmaceutical Ingredients* (32 classes) are largely unaffected.

Regression (Table 7). For regression, the row-count limit is satisfied by all datasets in **RamanBench** (maximum $N = 7,840$ for Sugar Mixtures Low SNR, well below TabPFN v2’s limit of 10 000); no row-count subsampling was needed. The feature limit is exceeded for 50 of 53 regression datasets. We report mean R^2 averaged across all non-excluded targets per dataset for TabPFN v2 and TabPFN v2.5 (MITRA has no feature limit and is excluded from this comparison). Both models perform competitively on the majority of datasets despite the high feature counts, with performance consistent with other top models. Exceptions are low- R^2 fermentation datasets (*Kaiser E. coli Fermentation*, *Streptococcus thermophilus Fermentation*) where all models struggle, not specifically the TabPFN models.

Table 7: **TabPFN v2 and v2.5 perform competitively beyond their recommended feature limit on regression datasets.** All regression datasets fulfil the row-count limit ($N \leq 10,000$ for v2, $N \leq 50,000$ for v2.5). Gray = within the model’s recommended feature limit.

Dataset	N	F	TabPFN v2	TabPFN v2.5	Best Model (R^2)
Acetic Concentration ^f	42	11,084	0.998	1.000	0.999 (TabICL v2)
Adenine (Colloidal Gold) ^f	225	534	0.922	0.916	0.911 (TabICL v2)
Adenine (Colloidal Silver) ^f	630	534	0.828	0.832	0.834 (TabICL v2)
Adenine (Solid Gold) ^f	810	534	0.701	0.739	0.705 (MITRA)
Adenine (Solid Silver) ^f	1,851	534	0.819	0.844	0.834 (TabICL v2)
Amino Acid LC (Glycine) ^f	90	1,024	0.035	0.004	0.101 (FastAI)
Amino Acid LC (Tryptophan) ^f	90	1,024	-0.030	0.046	0.057 (TabDPT)
Bioprocess Analytes Anton 532 ^f	270	1,601	0.724	0.649	0.698 (TabDPT)
Bioprocess Analytes Anton 785 ^f	270	1,001	0.892	0.896	0.865 (MITRA)
Bioprocess Analytes Kaiser ^f	134	5,472	0.763	0.804	0.733 (TabICL v2)
Bioprocess Analytes Metrohm ^f	399	1,875	0.915	0.881	0.852 (ReZeroNet)
Bioprocess Analytes Mettler Toledo ^f	275	2,901	0.520	0.716	0.833 (TabDPT)
Bioprocess Analytes Tec5 ^f	395	2,911	0.785	0.733	0.841 (TabDPT)
Bioprocess Analytes Tornado ^f	385	3,001	0.897	0.774	0.828 (ReZeroNet)
Bioprocess Monitoring ^f	6,960	1,870	0.914	0.939	0.942 (TabICL v2)
Citric Concentration ^f	45	11,084	0.480	0.999	0.995 (RealMLP)
E. Coli Fermentation ^f	379	1,870	0.731	0.633	0.702 (Logistic Reg.)
Bioprocess Analytes E. Coli Metabolites ^f	1,920	594	0.938	0.940	0.935 (TabICL v2)
E. Coli Metabolites Dig4Bio ^f	384	1,869	0.890	0.892	0.871 (MITRA)
Microgel Synthesis in Flow ^f	86	11,084	0.965	0.980	0.967 (MITRA)
Formic Concentration ^f	24	11,084	0.554	0.720	0.721 (Extra Trees)
Gasoline Properties (Benchtop) ^f	179	961	0.838	0.851	0.817 (MITRA)
Gasoline Properties (Handheld) ^f	179	1,901	0.763	0.757	0.735 (MITRA)
Bio-Catalysis Monitoring of AXP ^f	344	2,048	0.661	0.700	0.732 (PLS)
Itaconic Concentration ^f	21	11,689	0.539	0.989	0.939 (TabICL v2)
Kaiser Raman E. coli Fermentation ^f	14	1,699	-1.479	-0.541	0.589 (Logistic Reg.)
Kaiser Raman E. coli Fermentation Supe... ^f	14	1,699	-2.186	-1.098	0.030 (Extra Trees)
Levulinic Concentration ^f	36	11,084	0.867	0.909	0.950 (MITRA)
Microgel Size (Linear Fit, FingerPrint) ^f	235	3,500	0.134	0.164	0.160 (MITRA)
Microgel Size (Linear Fit, Global) ^f	235	11,084	0.249	0.210	0.224 (TabICL v2)
Microgel Size (MinMax + Linear Fit, Fi... ^f	235	3,166	0.083	0.083	0.057 (MITRA)
Microgel Size (MinMax + Linear Fit, Gl... ^f	235	11,084	0.280	0.276	0.150 (TabICL v2)
Microgel Size (MinMax + Rubber Band, F... ^f	235	3,500	0.101	0.065	0.071 (TabICL v2)
Microgel Size (MinMax + Rubber Band, G... ^f	235	11,084	0.268	0.258	0.153 (TabM)
Microgel Size (Raw, FingerPrint) ^f	235	3,500	0.183	0.221	0.203 (TabICL v2)
Microgel Size (Raw, Global) ^f	235	11,084	0.261	0.215	0.276 (TabICL v2)
Microgel Size (Rubber Band, FingerPrint) ^f	235	3,500	0.064	0.064	0.168 (TabICL v2)
Microgel Size (Rubber Band, Global) ^f	235	11,084	0.232	0.193	0.210 (TabDPT)
Microgel Size (SNV + Linear Fit, Finge... ^f	235	3,500	0.158	0.068	0.092 (XGBoost)
Microgel Size (SNV + Linear Fit, Global) ^f	235	11,084	0.272	0.259	0.340 (TabICL v2)
Microgel Size (SNV + Rubber Band, Fing... ^f	235	3,500	0.132	0.048	0.081 (RamanNet)
Microgel Size (SNV + Rubber Band, Glob... ^f	235	11,084	0.263	0.254	0.323 (TabICL v2)
Microgel Synthesis Flow vs. Batch ^f	14	11,084	0.247	0.272	0.664 (TabDPT)
R. eutropha Copolymer Fermentations ^f	82	2,776	0.942	0.961	0.944 (TabICL v2)
Streptococcus thermophilus Fermentatio... ^f	14	1,501	-3.729	0.547	-0.115 (Deep CNN)
Succinic Concentration ^f	70	11,567	0.991	0.992	0.990 (MITRA)
Sugar Mixtures (High SNR) ^f	1,960	2,000	0.966	1.000	1.000 (TabICL v2)
Sugar Mixtures (Low SNR) ^f	7,840	2,000	0.945	0.985	0.991 (TabICL v2)
Synthetic Organic Pigments (Raw) ^f	325	561	0.202	0.231	0.255 (Deep CNN)
Yeast Fermentation ^f	58	1,900	0.687	0.655	0.713 (MITRA)

Gray = within recommended feature limit; ^f feature limit exceeded.

A.8 Combined Ranking

Table 8: **TabPFN v2.5 ranks first overall; no single model dominates across all datasets.** Combined model ranking sorted by Elo rating (RF = 1 000). RMSE and F1 are normalized per dataset following Salinas and Erickson [68]: best = 1, median = 0, clipped at 0 (higher is always better after normalization, including RMSE). Values are averaged across all datasets of the respective task type. Models marked with * are evaluated on classification only; dashes indicate task types not applicable.

Model	Elo (↑)	Mean Rank (↓)	Wins (↑)	Improvability (↓)	RMSE (↑)	R ² (↑)	F1 (↑)	Bal. Acc. (↑)
AutoGluon 1.5 (extreme, 4h)	1562 ± 371	3.9	—	14.4%	0.63	0.65	0.67	0.66
TabPFN v2.5	1529 ± 296	4.3	52	19.0%	0.58	0.60	0.62	0.63
TabICL v2	1444 ± 220	5.7	21	26.6%	0.51	0.53	0.55	0.55
TabPFN v2	1404 ± 377	6.3	25	30.5%	0.52	0.54	0.36	0.35
MITRA	1312 ± 403	8.1	5	37.2%	0.38	0.42	0.33	0.33
ROCKET*	1240 ± 268	10.5	1	55.5%	—	—	0.37	0.35
Arsenal*	1236 ± 358	10.5	1	58.3%	—	—	0.40	0.39
TabM	1156 ± 290	12.1	0	47.3%	0.17	0.22	0.28	0.29
TabDPT	1135 ± 315	11.9	6	44.5%	0.25	0.28	0.32	0.31
ReZeroNet	1133 ± 313	11.8	5	43.1%	0.17	0.19	0.48	0.48
RealMLP	1111 ± 271	13.0	0	47.4%	0.19	0.22	0.22	0.22
CatBoost	1069 ± 231	14.1	0	51.2%	0.15	0.20	0.08	0.08
NN (PyTorch)	1066 ± 294	14.1	1	48.6%	0.18	0.21	0.23	0.23
Extra Trees	1057 ± 262	14.3	1	50.8%	0.16	0.22	0.08	0.07
RamanNet	1029 ± 283	15.1	2	50.3%	0.10	0.11	0.31	0.30
Deep CNN	1006 ± 338	15.2	4	48.2%	0.12	0.12	0.39	0.39
PLS	1004 ± 373	15.3	6	50.0%	0.15	0.20	0.16	0.14
Logistic Reg.	1002 ± 370	14.9	6	49.5%	0.16	0.21	0.32	0.32
Random Forest	1000 ± 262	15.6	1	52.4%	0.13	0.17	0.10	0.10
KNN	986 ± 302	15.9	3	51.4%	0.13	0.17	0.09	0.09
RamanFormer	979 ± 385	16.5	4	52.1%	0.10	0.12	0.20	0.18
FastAI	970 ± 286	16.4	1	52.7%	0.08	0.12	0.15	0.15
CoAtNet	963 ± 300	16.4	1	52.7%	0.10	0.11	0.11	0.12
LightGBM	951 ± 220	17.0	1	55.0%	0.07	0.08	0.05	0.06
FCResNeXt	933 ± 281	17.4	2	54.8%	0.08	0.09	0.23	0.22
XGBoost	922 ± 301	17.9	1	55.4%	0.07	0.10	0.10	0.10
SANet	798 ± 369	20.5	0	61.7%	0.05	0.05	0.24	0.25
RamanTransformer [†]	710 ± 375	22.1	0	67.5%	0.08	0.10	0.02	0.03

*Classification-only model; ELO, Mean Rank and Improvability are computed on classification datasets only.

[†]RamanTransformer failed on 31 of 129 regression targets; missing results were imputed using RF as a fallback.

A.9 Extended Results Tables

The following tables report aggregated performance across all benchmark datasets. Models are sorted by combined Elo rating, highest first. All metrics are defined in Section A.1; after per-dataset normalization, higher is always better — including for RMSE. **Mean** reports the raw mean across all datasets and targets; **Wins** counts first-place finishes per prediction target. Best value per column is highlighted in **bold**.

A.10 Pairwise Win Rates

Fig. 7 shows the absolute number of target wins for every pair of models. Each cell reports how many targets the model on the **y-axis** beats the model on the **x-axis** (ties count as 0.5). Cell color encodes the win rate: green indicates a high win rate for the row model, red a low win rate. Only targets for which both models produce a prediction are counted; task-restricted models are compared on their supported subset only. Models are sorted by combined Elo rating, best at top-left.

A.11 Detailed Results

A.11.1 Model Ranking

Fig. 8 summarizes the combined ranking across all regression and classification targets. The left panel shows each model’s average rank pooled over all targets (rank 1 = best; regression ranked by RMSE, classification by F1); the right panel shows the total number of first-place finishes across all (target × seed) instances.

Average rank across all tasks (Fig. 8, left) confirms the performance ordering: AutoGluon 1.5 achieves the best average rank overall (≈3.9); among the main comparison models, TabPFN v2.5 leads (≈4.3), followed by TabICL v2 (≈5.7) and TabPFN v2 (≈6.3). MITRA (≈8.1) follows, with

Table 9: **TabPFN v2.5 leads on regression; TabPFN v2 and TabICL v2 follow closely, while MITRA ranks fourth despite its higher computational cost.** Elo and Mean Rank are computed over regression datasets only.

Model	Elo (\uparrow)	Mean Rank (\downarrow)	Mean Normalized		Wins		Mean Time (s)
			RMSE (\uparrow)	R ² (\uparrow)	RMSE (\uparrow)	R ² (\uparrow)	
AutoGluon 1.5 (extreme, 4h)	1607 \pm 370	3.6	0.63 \pm 0.37	0.65 \pm 0.37	—	—	1831.7 \pm 4499.2
TabPFN v2.5	1580 \pm 437	3.9	0.58 \pm 0.33	0.60 \pm 0.34	18	18	178.5 \pm 1852.4
TabICL v2	1465 \pm 242	5.3	0.51 \pm 0.33	0.53 \pm 0.33	8	8	165.8 \pm 1381.6
TabPFN v2	1445 \pm 378	5.7	0.52 \pm 0.33	0.54 \pm 0.34	12	13	368.3 \pm 2804.8
MITRA	1338 \pm 357	7.2	0.38 \pm 0.30	0.42 \pm 0.33	3	2	1433.2 \pm 10194.3
TabM	1142 \pm 300	12.0	0.17 \pm 0.20	0.22 \pm 0.26	0	0	53.7 \pm 251.9
TabDPT	1122 \pm 333	11.7	0.25 \pm 0.28	0.28 \pm 0.29	4	4	14.9 \pm 33.6
RealMLP	1115 \pm 370	12.7	0.19 \pm 0.25	0.22 \pm 0.30	0	0	1918.9 \pm 2447.8
ReZeroNet	1092 \pm 341	12.3	0.17 \pm 0.25	0.19 \pm 0.29	0	0	48.2 \pm 144.5
CatBoost	1080 \pm 246	13.6	0.15 \pm 0.19	0.20 \pm 0.26	0	0	539.4 \pm 929.3
Extra Trees	1069 \pm 294	13.6	0.16 \pm 0.23	0.22 \pm 0.29	0	2	22.3 \pm 39.6
PLS	1040 \pm 371	14.6	0.15 \pm 0.26	0.20 \pm 0.31	2	1	35.2 \pm 135.8
NN (PyTorch)	1038 \pm 329	14.2	0.18 \pm 0.26	0.21 \pm 0.30	0	0	1395.1 \pm 2305.1
Logistic Reg.	1016 \pm 367	15.1	0.16 \pm 0.26	0.21 \pm 0.30	2	2	43.1 \pm 167.1
KNN	1003 \pm 287	15.4	0.13 \pm 0.22	0.17 \pm 0.26	0	0	9.3 \pm 16.3
Random Forest	1000 \pm 273	15.2	0.13 \pm 0.21	0.17 \pm 0.27	1	0	53.9 \pm 119.8
RamanNet	992 \pm 321	15.4	0.10 \pm 0.18	0.11 \pm 0.21	0	0	75.5 \pm 325.2
CoAtNet	963 \pm 381	16.1	0.10 \pm 0.20	0.11 \pm 0.22	0	0	63.7 \pm 194.3
Deep CNN	961 \pm 347	15.7	0.12 \pm 0.21	0.12 \pm 0.23	0	1	1285.2 \pm 2034.5
FastAI	960 \pm 294	16.2	0.08 \pm 0.17	0.12 \pm 0.21	1	1	255.1 \pm 486.7
RamanFormer	945 \pm 369	16.3	0.10 \pm 0.22	0.12 \pm 0.25	2	1	503.4 \pm 2172.9
LightGBM	931 \pm 237	16.8	0.07 \pm 0.15	0.08 \pm 0.16	0	0	1458.1 \pm 2585.3
FCResNeXt	895 \pm 296	17.8	0.08 \pm 0.20	0.09 \pm 0.20	0	0	16.4 \pm 32.7
XGBoost	891 \pm 277	17.9	0.07 \pm 0.17	0.10 \pm 0.21	0	0	58.0 \pm 342.1
SANet	729 \pm 368	21.1	0.05 \pm 0.13	0.05 \pm 0.14	0	0	39.5 \pm 154.5
RamanTransformer [†]	685 \pm 422	21.7	0.08 \pm 0.18	0.10 \pm 0.22	0	0	473.0 \pm 1961.0

Models sorted by combined Elo (RF = 1 000), highest first. Mean Normalized [68]: best = 1, median = 0, clipped at 0 (higher = better for all metrics including RMSE). Wins: number of targets on which a model achieved the best seed-averaged raw score. Time: mean total (train + predict) time in seconds. [†]RamanTransformer failed on 31 of 129 regression targets; missing results were imputed using RF as a fallback.

the two time-series classifiers ROCKET and Arsenal at nearly identical average ranks (≈ 10.5 each) — notably ahead of all gradient boosting methods. TabDPT (≈ 11.9) and ReZeroNet (≈ 11.8) lead the next group, with TabM (≈ 12.1) close behind, followed by a dense mid-tier cluster spanning RealMLP, CatBoost, Extra Trees, NN (PyTorch), Logistic Regression, and most Raman-specific models (ranks 13–16). Gradient boosting methods perform surprisingly poorly: CatBoost (≈ 14.1), LightGBM (≈ 17.0), and XGBoost (≈ 17.9) rank well below foundation models. RamanTransformer (≈ 22.1) and SANet (≈ 20.5) are the lowest-ranked models.

First-place finishes (Fig. 8, right) are counted among the main comparison models only (AutoGluon is excluded as an upper baseline; it leads with 59 wins when included). Among main models, TabPFN v2.5 dominates (52 wins) followed by TabPFN v2 (25 wins) and TabICL v2 (21 wins). TabDPT, PLS, and Logistic Regression each achieve 6 target wins; ReZeroNet and MITRA achieve 5 each; Deep CNN achieves 4. Among tree-based models, Extra Trees, Random Forest, LightGBM, and XGBoost each achieve 1 win, while CatBoost achieves none.

A.11.2 Computational Efficiency

Fig. 9 shows all three efficiency dimensions.

Training time spans three orders of magnitude: KNN and PLS train fastest (~ 8 – 30 s); Arsenal is slowest ($\sim 2,900$ s), with RealMLP ($\sim 1,900$ s) and AutoGluon ($\sim 1,800$ s) also in the slowest tier. Tabular Foundation Model (TFM) vary widely: TabICL and TabDPT train in ~ 40 – ~ 90 s, while MITRA takes ~ 830 s.

Peak memory: AutoGluon and TabICL require the most (~ 26 GB each); most other models cluster at 1.5–4 GB.

Inference latency: XGBoost and tree-based methods achieve < 1 s/1K samples; MITRA (~ 626 s/1K) and Arsenal ($\sim 2,800$ s/1K) have the highest inference cost.

Table 10: **Foundation models dominate classification; TabPFN v2.5 achieves the highest normalized F1 while remaining competitive in training time.** Elo and Mean Rank are computed over classification datasets only.

Model	Elo (\uparrow)	Mean Rank (\downarrow)	Mean Normalized		Wins		Mean Time (s)
			Bal. Acc. (\uparrow)	F1 (\uparrow)	Bal. Acc. (\uparrow)	F1 (\uparrow)	
AutoGluon 1.5 (extreme, 4h)	1472 \pm 462	5.6	0.66 \pm 0.38	0.67 \pm 0.36	—	—	1831.7 \pm 4499.2
TabPFN v2.5	1397 \pm 348	7.1	0.63 \pm 0.37	0.62 \pm 0.37	4	4	178.5 \pm 1852.4
TabICL v2	1361 \pm 310	7.7	0.55 \pm 0.38	0.55 \pm 0.38	3	3	165.8 \pm 1381.6
ReZeroNet	1338 \pm 232	8.3	0.48 \pm 0.36	0.48 \pm 0.36	1	1	48.2 \pm 144.5
TabPFN v2	1265 \pm 204	10.2	0.35 \pm 0.36	0.36 \pm 0.36	0	0	368.3 \pm 2804.8
ROCKET	1255 \pm 251	10.5	0.35 \pm 0.35	0.37 \pm 0.34	1	1	1297.4 \pm 3236.2
Arsenal	1234 \pm 350	10.5	0.39 \pm 0.36	0.40 \pm 0.36	1	1	3292.4 \pm 2235.0
Deep CNN	1182 \pm 375	12.1	0.39 \pm 0.40	0.39 \pm 0.40	3	3	1285.2 \pm 2034.5
RamanNet	1168 \pm 377	13.2	0.30 \pm 0.37	0.31 \pm 0.37	2	2	75.5 \pm 325.2
TabM	1154 \pm 304	13.1	0.29 \pm 0.36	0.28 \pm 0.36	0	0	53.7 \pm 251.9
TabDPT	1149 \pm 334	13.4	0.31 \pm 0.38	0.32 \pm 0.37	0	0	14.9 \pm 33.6
NN (PyTorch)	1145 \pm 248	13.4	0.23 \pm 0.29	0.23 \pm 0.29	0	0	1395.1 \pm 2305.1
MITRA	1140 \pm 315	13.4	0.33 \pm 0.35	0.33 \pm 0.35	0	0	1433.2 \pm 10194.3
Logistic Reg.	1131 \pm 389	14.0	0.32 \pm 0.40	0.32 \pm 0.39	2	2	43.1 \pm 167.1
RealMLP	1113 \pm 281	14.7	0.22 \pm 0.30	0.22 \pm 0.30	0	0	1918.9 \pm 2447.8
FCResNeXt	1108 \pm 320	14.5	0.22 \pm 0.33	0.23 \pm 0.33	1	1	16.4 \pm 32.7
CatBoost	1019 \pm 242	17.3	0.08 \pm 0.23	0.08 \pm 0.23	0	0	539.4 \pm 929.3
CoAtNet	1013 \pm 325	18.0	0.12 \pm 0.25	0.11 \pm 0.24	0	0	63.7 \pm 194.3
FastAI	1011 \pm 289	17.3	0.15 \pm 0.30	0.15 \pm 0.29	0	0	255.1 \pm 486.7
SANet	1001 \pm 437	17.1	0.25 \pm 0.35	0.24 \pm 0.34	0	0	39.5 \pm 154.5
Random Forest	1000 \pm 335	18.1	0.10 \pm 0.26	0.10 \pm 0.26	0	0	53.9 \pm 119.8
XGBoost	978 \pm 368	18.0	0.10 \pm 0.24	0.10 \pm 0.24	0	0	58.0 \pm 342.1
LightGBM	974 \pm 286	18.4	0.06 \pm 0.17	0.05 \pm 0.15	1	0	1458.1 \pm 2585.3
KNN	957 \pm 280	19.1	0.09 \pm 0.23	0.09 \pm 0.22	0	0	9.3 \pm 16.3
Extra Trees	951 \pm 365	19.0	0.07 \pm 0.24	0.08 \pm 0.24	0	0	22.3 \pm 39.6
RamanFormer	935 \pm 476	18.2	0.18 \pm 0.33	0.20 \pm 0.33	1	1	503.4 \pm 2172.9
PLS	914 \pm 504	19.5	0.14 \pm 0.29	0.16 \pm 0.31	1	2	35.2 \pm 135.8
RamanTransformer	684 \pm 402	24.5	0.03 \pm 0.13	0.02 \pm 0.10	0	0	473.0 \pm 1961.0

Models sorted by combined Elo (RF = 1 000), highest first. Mean Normalized [68]: best = 1, median = 0, clipped at 0 (higher = better for all metrics). Wins: number of targets on which a model achieved the best seed-averaged raw score. Time: mean total (train + predict) time in seconds.

A.11.3 Improvability vs. Training Time

Fig. 10 visualizes the trade-off between mean improvability (%) and mean total time (training + prediction) separately for classification (left) and regression (right). A model in the lower-left region is both close to optimal within the evaluated pool (low improvability) and computationally cheap. The dashed Pareto frontier marks models that no other model simultaneously beats on both dimensions. ROCKET and Arsenal appear only in the classification panel as they do not support regression.

A.11.4 Statistical Significance — Critical Difference Diagrams

Critical Difference (CD) diagrams are computed following the procedure described in Section A.1 (Friedman test, Nemenyi post-hoc, $\alpha = 0.05$, AutoRank [73]). Models connected by a horizontal bar are not significantly different; task-restricted models (ROCKET, Arsenal) are excluded from the regression diagram. Results for regression (RMSE) and classification (macro-averaged F1) are shown in Fig. 11 and Fig. 12, respectively.

A.12 Dataset Overview Table

Table 11 provides a concise summary of all 74 datasets included in **RamanBench**, listing the application domain, task type, number of spectra, spectral range and resolution, and whether the dataset is newly released with this paper.

A.13 New Datasets: Measurement Details

This section provides detailed descriptions of the measurement setups, acquisition parameters, and sample preparation protocols for the previously unpublished datasets released as part of **RamanBench**. Datasets are grouped by experimental origin; relevant dataset identifiers are listed at the start of each subsection.

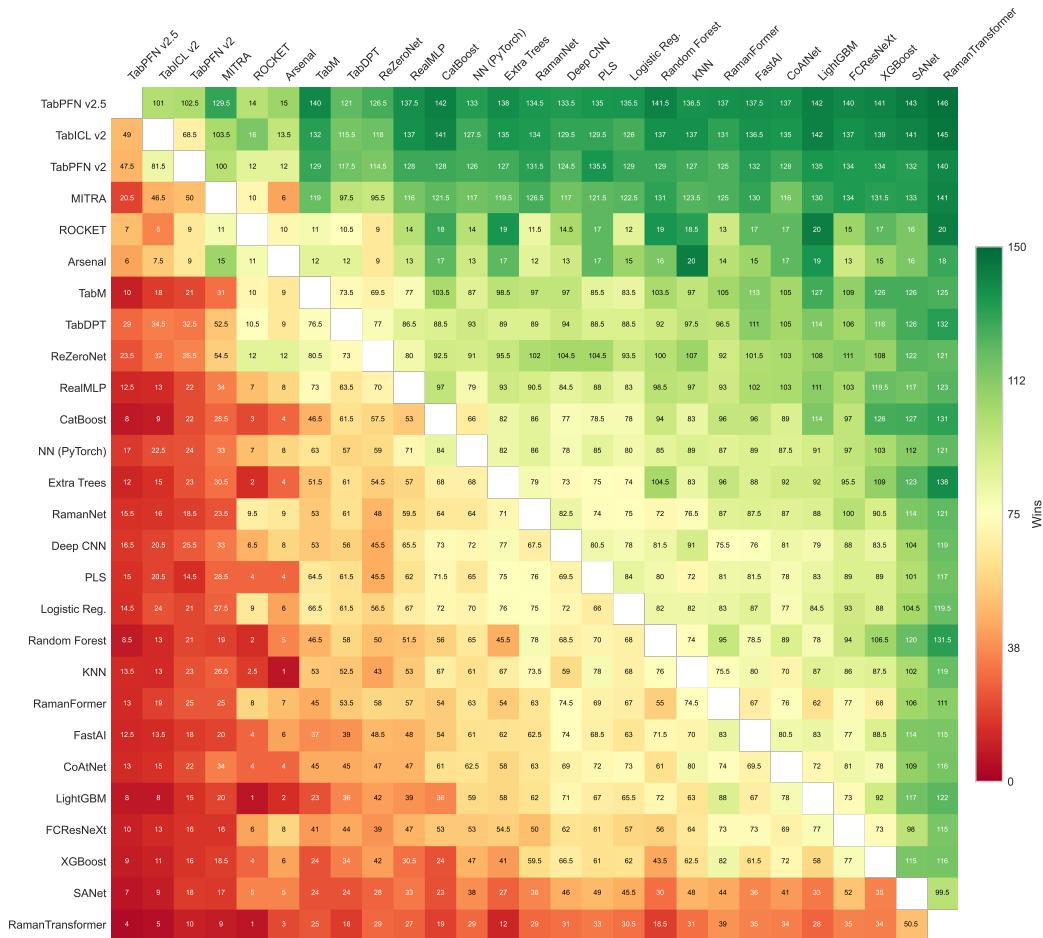


Figure 7: **Top-ranked models win broadly across the benchmark; lower-ranked models show consistent losses against most competitors.** Pairwise win counts across all 163 prediction targets. Each cell shows the number of targets on which the **y-axis model** outperforms the **x-axis model** (ties count as 0.5). Cell color encodes the win rate: green cells indicate a high win rate for the row model; red cells indicate a low win rate. The colorbar is labeled with absolute win counts. Models are sorted by combined Elo rating, best at top-left. Only targets for which both models produce a valid prediction are counted.

A.13.1 *E. coli* Fermentation: Kaiser and Time-Gated Raman Measurements

These four datasets originate from a study comparing two Raman spectroscopy approaches, continuous wave and time-gated Raman, for monitoring of *E. coli* fed-batch fermentation processes [54]. Each approach was applied to both the full fermentation broth and the cell-free supernatant, yielding four dataset variants.

NIR-Raman Measurements. Spectra were recorded using a Kaiser RXN1 spectrometer (Kaiser Optical Systems, Ann Arbor, MI, USA) equipped with a nonimmersion Raman MR process probe (NA = 0.29). The excitation wavelength was 785 nm at a laser power of 135 mW. Each spectrum was acquired with an integration time of 20 s and 5 accumulations per measurement. Spectral resolution was 4 cm^{-1} (FWHM) and detection was performed by a CCD cooled to $-40 \text{ }^\circ\text{C}$.

Time-Gated Raman Measurements. Spectra were recorded using a TimeGate TGM1 spectrometer (TimeGate Instruments, Oulu, Finland) equipped with a BWTek RPB 532 fiber-optic probe (NA = 0.22). The excitation source was a pulsed Nd:YVO₄ laser at 532 nm (pulse duration 100 ps) with an average power of approximately 30 mW. Time-gated detection used a temporal window of

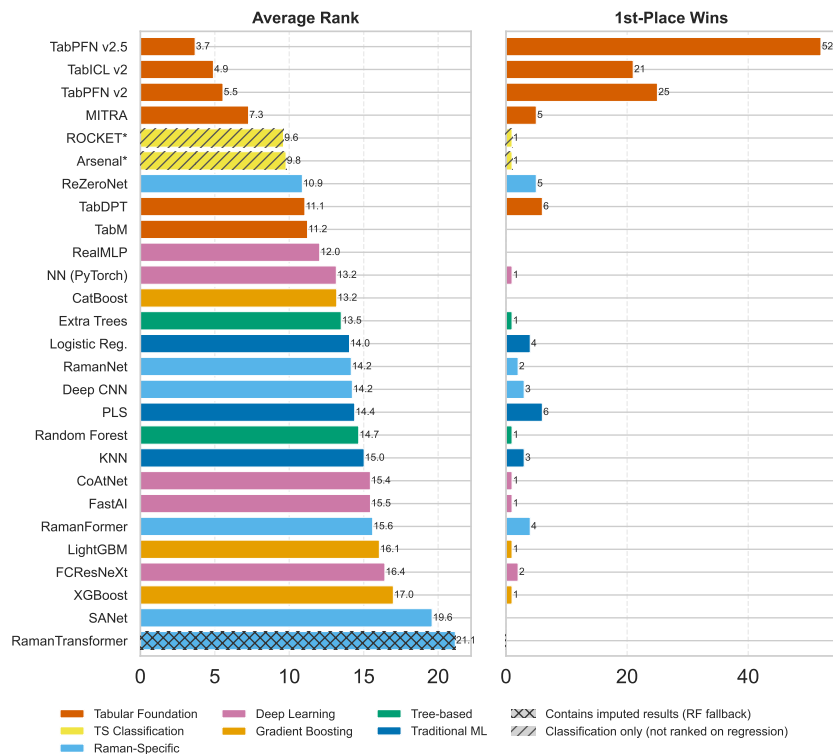


Figure 8: **Foundation models achieve the best average rank and dominate first-place finishes; tree-based models achieve at most one first-place finish each.** Combined model ranking across all regression and classification targets. Metrics are averaged over seeds per (target, model) before ranking, so each prediction target counts as exactly one win. **Left:** average rank pooled over all targets (rank 1 = best); regression targets are ranked by RMSE (lower is better) and classification targets by F1-score (higher is better). **Right:** total number of first-place finishes across all targets, excluding AutoGluon (upper baseline, 59 wins when included). Models are sorted by average rank (best at top) and color-coded by algorithmic family.

1.2–2.1 ns after the laser pulse to suppress fluorescence from the culture medium. A total collection time of approximately 15 min was required per well-resolved spectrum. The spectral resolution was 10 cm^{-1} (FWHM); detection used a non-cooled single-photon avalanche diode (SPAD) array.

Sample Preparation. Fermentation samples were collected at defined time points, centrifuged to obtain cell-free supernatant, and stored frozen at -80°C until measurement. Offline spectroscopic measurements were performed in aluminium microwell plates ($20 \mu\text{L}$ cavity per well). Reference concentrations for glucose and acetate were determined by standard enzymatic reference assays.

These datasets comprise newly released small-scale *E. coli* fermentation spectra recorded with a Kaiser Raman spectrometer [54]. The datasets capture fermentation broth and centrifuged supernatant, respectively, targeting OD600, glucose, acetate, and fermentation time. Statistics are given in Table 12; representative spectra are shown in Fig. 13.

Table 12: Dataset statistics for Kaiser Ecoli.

Dataset	Task	No. Targets	Samples	Features	Wavelength (cm^{-1})	License	Ref.
Fermentation	Regr.	4	14	1,699	301–1999	CC BY 4.0	[54]
Fermentation Supernatant	Regr.	4	14	1,699	301–1999		

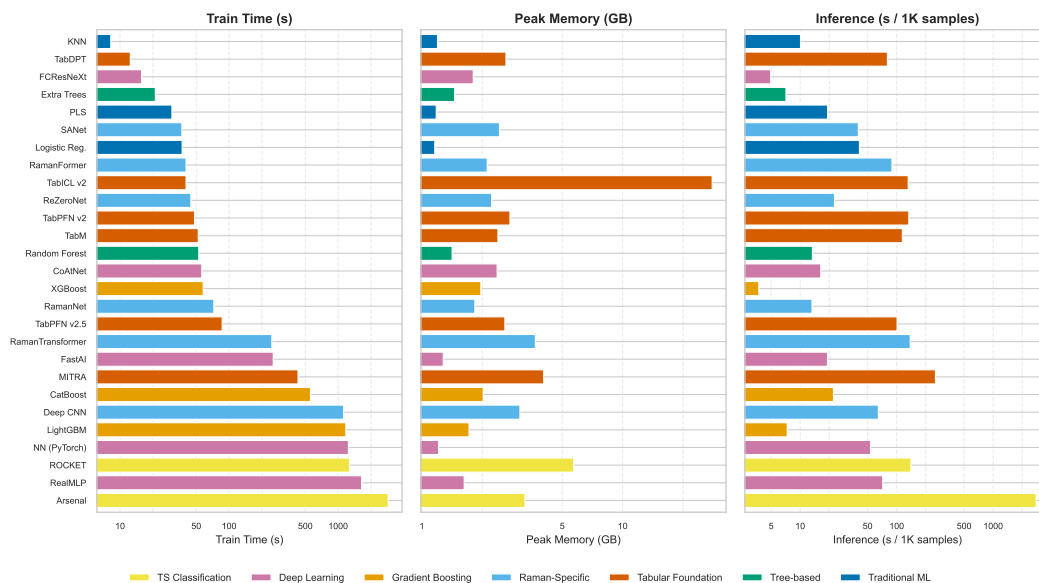


Figure 9: **Arsenal and RealMLP are the slowest models by training time; XGBoost and tree-based methods offer the lowest inference latency.** Computational efficiency of all evaluated models across three dimensions. **Training time** (left, log scale): total wall-clock time for fitting on the training split. **Peak memory** (center): maximum RAM/VRAM footprint during training in GB. **Inference latency** (right, log scale): mean prediction time in seconds per 1 000 samples. Models are sorted by training time.

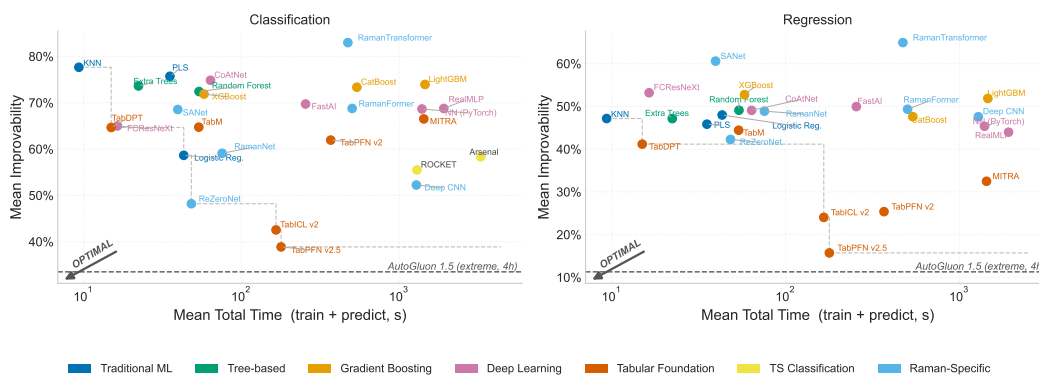


Figure 10: **TFM anchor the low-improvability end of the Pareto frontier; ReZeroNet is the only Raman-specific model near it, while KNN qualifies through speed alone.** Mean improvability (%) vs. mean total time (train + predict, s) on a log scale, shown separately for classification (left) and regression (right). Improvability of 0% indicates optimal performance within the evaluated model pool; higher values indicate larger room for improvement. The dashed line shows the Pareto frontier (lower-left is optimal). See Section A.1 for the formal definition of improvability.

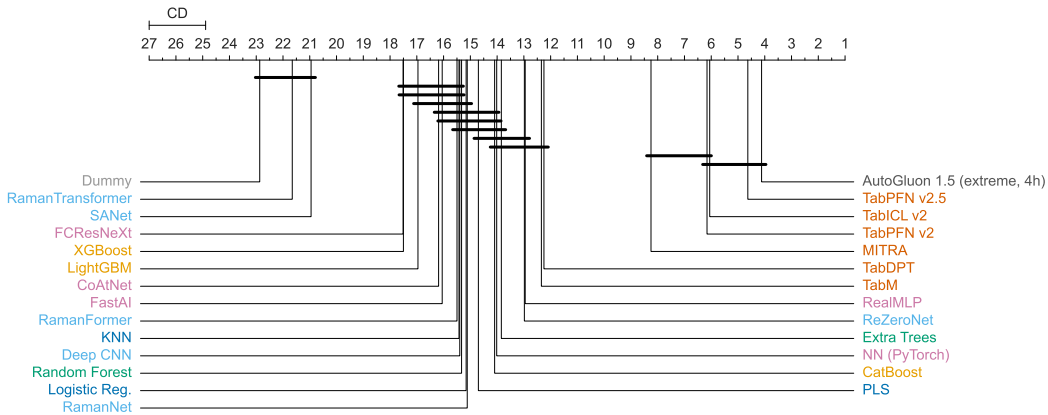


Figure 11: **Regression: both TabPFN variants, AutoGluon, and TabICL v2 form a statistically indistinguishable leading group of four; no model is significantly superior to this group.** CD diagram for RMSE across all regression targets (lower rank is better). Generated via Friedman test and Nemenyi post-hoc test ($\alpha = 0.05$) using AutoRank [73]. Models connected by a horizontal bar are not significantly different.

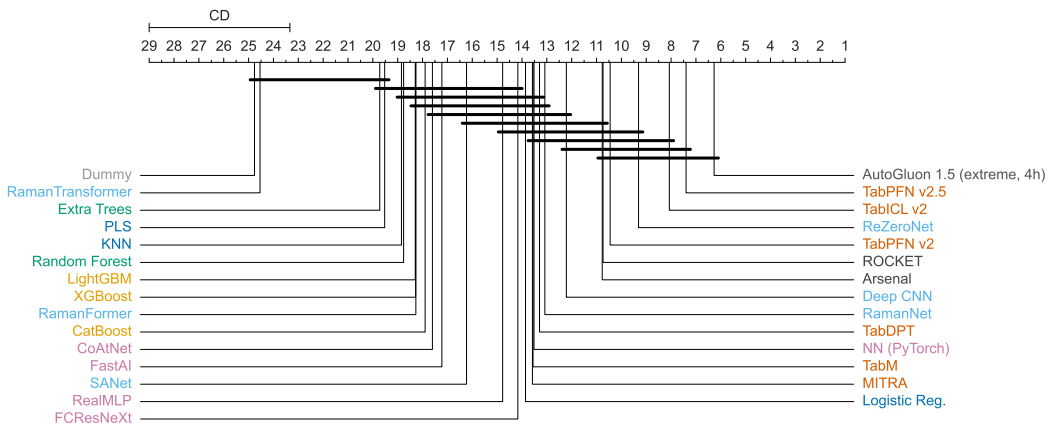


Figure 12: **Classification: seven models form a statistically indistinguishable leading group, remarkably, both time-series classifiers (Arsenal, ROCKET) as well as ReZeroNet rank within it alongside the three top performing TFM.** CD diagram for macro-averaged F1 across all classification targets (lower rank is better). Generated via Friedman test and Nemenyi post-hoc test ($\alpha = 0.05$) using AutoRank [73]. Models connected by a horizontal bar are not significantly different.

Table 11: **RamanBench** Overview: **Datasets**: number of individual benchmark datasets (e.g. different instruments or preprocessing variants). **Targets**: number of regression targets, or 1 for classification.

	Task	Datasets	Targets	Samples	Features	Range (cm ⁻¹)	Details
Material Science							
ML Raman Open Dataset (MLROD)	Class.	1	1	130,061	1,836	141–1100	Table 23
RRUFF Minerals (Raw) [†]	Class.	1	1	1,162	1,142	303–853	Table 24
Synthetic Organic Pigments (Raw)	Regr.	1	1	325	561	1189–1651	Table 25
Weathered Microplastics [†]	Class.	1	1	77	1,144	202–3498	Table 26
Biological & Biotechnological							
Bio-Catalysis Monitoring of AXP [*]	Regr.	1	4	344	2,048	-32–3385	Table 16
Bioprocess Analytes	Regr.	8	24	2,261	1,601	300–3500	Table 27
Bioprocess Monitoring	Regr.	1	8	6,960	1,870	391–3385	Table 28
Cancer Cell	Class.	3	3	1,892	2,090	100–4278	Table 29
E. coli Fermentation	Regr.	1	2	379	1,870	391–3385	Table 30
Ecoli Metabolites [*]	Regr.	2	5	2,304	594	402–1599	Table 15
Kaiser Ecoli [*]	Regr.	2	8	28	1,699	301–1999	Table 12
Mutant Wheat	Class.	1	1	53,134	1,748	296–2043	Table 31
R. eutropha Copolymer Fermentations [*]	Regr.	1	6	82	2,776	405–3180	Table 18
Streptococcus Thermophilus [*]	Regr.	1	4	14	1,501	300–1800	Table 14
Tg Ecoli [*]	Regr.	2	8	25	114	604–1508	Table 13
Yeast Fermentation [*]	Regr.	1	4	58	1,900	401–2300	Table 17
Medical & Clinical							
Alzheimer's SERS Serum	Class.	1	1	3,417	724	0–723	Table 32
Diabetes Skin	Class.	4	4	80	3,160	0–3159	Table 33
Head & Neck Cancer	Class.	1	1	111	1,004	789–910	Table 34
Pathogenic Bacteria	Class.	1	1	78,500	1,000	382–1792	Table 35
Pharmaceutical Ingredients	Class.	1	1	3,510	3,276	150–3425	Table 36
Prostate Cancer SERS Serum	Class.	1	1	12,601	725	0–724	Table 37
Saliva Alzheimer	Class.	1	1	1,151	885	401–1598	Table 39
Saliva COVID-19	Class.	1	1	2,501	885	401–1598	Table 38
Saliva Parkinson	Class.	1	1	1,476	885	401–1598	Table 40
Stroke SERS Serum	Class.	1	1	4,020	724	200–2000	Table 41
Chemical & Industrial							
Acetic Concentration	Regr.	1	2	42	11,084	100–3425	Table 42
Adenine Colloidal [*]	Regr.	2	2	855	534	400–1999	Table 21
Adenine Solid [*]	Regr.	2	2	2,661	534	400–1999	Table 22
Amino Acids	Regr.	2	2	180	1,024	326–2035	Table 43
Citric Concentration	Regr.	1	2	45	11,084	100–3425	Table 44
Formic Concentration	Regr.	1	3	24	11,084	100–3425	Table 45
Gasoline Properties (Benchtop) [*]	Regr.	1	12	179	961	98–3801	Table 19
Gasoline Properties (Handheld) [*]	Regr.	1	12	179	1,901	400–2300	Table 20
Hair Dyes SERS	Class.	1	1	1,713	1,340	309–1952	Table 46
Itaconic Concentration	Regr.	1	3	21	11,689	-37–3470	Table 47
Levulinic Concentration	Regr.	1	2	36	11,084	100–3425	Table 48
Microgel Size	Regr.	14	14	3,290	3,500	800–1850	Table 49
Microgel Synthesis Flow vs. Batch	Regr.	1	1	14	11,084	100–3425	Table 50
Microgel Synthesis in Flow	Regr.	1	1	86	11,084	100–3425	Table 51
Succinic Concentration	Regr.	1	2	70	11,567	-20–3450	Table 52
Sugar Mixtures	Regr.	2	8	9,800	2,000	142–3685	Table 53
Total		74	163	325,668			

Class. = Classification; Regr. = Regression; Range = spectral range (cm⁻¹).

* = dataset released for the first time with this paper. † = Sample count after removing classes with fewer than 10 samples.

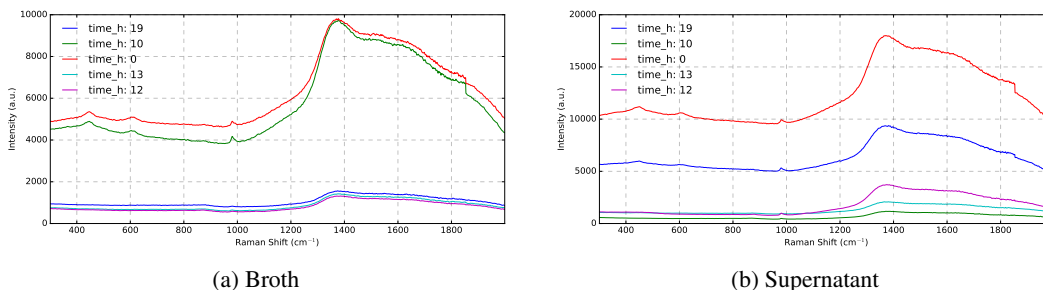


Figure 13: Representative Raman spectra from the Kaiser E. coli datasets, 5 random samples each.

These datasets contain newly released *E. coli* fermentation spectra acquired using time-gated Raman (Timegate) spectroscopy [54], which suppresses fluorescence background. As with the Kaiser E. coli datasets, broth and supernatant are measured separately across four targets (OD600, glucose, acetate, fermentation time). Statistics are given in Table 13; representative spectra are shown in Fig. 14.

Table 13: Dataset statistics for Tg Ecoli.

Dataset	Task	No. Targets	Samples	Features	Wavelength (cm ⁻¹)	License	Ref.
Fermentation	Regr.	4	12	114	604–1508	CC BY 4.0	[54]
Fermentation Supernatant	Regr.	4	13	114	604–1508		

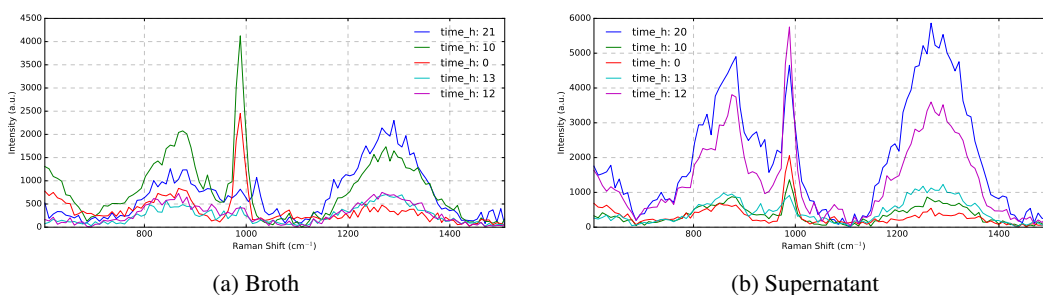


Figure 14: Representative Raman spectra from the Time-Gated E. coli datasets, 5 random samples each.

A.13.2 *S. thermophilus* Fermentation: Kaiser and Time-Gated Raman Measurements

These two datasets contain offline Raman spectra collected during batch cultivations of *Streptococcus thermophilus* in shake flasks. Each dataset covers two independent fermentation runs conducted over a 24-hour cultivation period.

Kaiser RXN1 Measurements. Spectra were recorded using a Kaiser RXN1 spectrometer (Kaiser Optical Systems) with 785 nm excitation. Acquisition parameters were analogous to those used for the *E. coli* Kaiser fermentation dataset (Section A.13.1).

Time-Gated Raman Measurements. Spectra were recorded using a Time-Gated Raman spectrometer with a pulsed 532 nm laser to suppress the fluorescence background characteristic of complex fermentation media. Acquisition parameters were analogous to those used for the *E. coli* Time-Gated fermentation dataset (Section A.13.1).

These datasets contain newly released *Streptococcus thermophilus* fermentation spectra recorded with Kaiser and Timegate spectrometers, targeting lactose, galactose, lactate, and OD600 concentrations. Both datasets fall in the tiny-data regime ($N < 50$), reflecting the challenge of online monitoring in small-scale fermentations. Statistics are given in Table 14; representative spectra are shown in Fig. 15.

Table 14: Dataset statistics for Streptococcus Thermophilus.

Dataset	Task	No. Targets	Samples	Features	Wavelength (cm ⁻¹)	License	Ref.
Fermentation Kaiser	Regr.	4	14	1,501	300–1800	CC BY 4.0	—

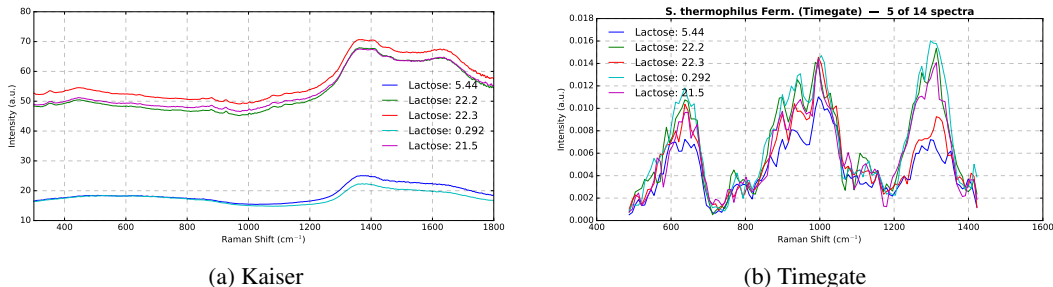


Figure 15: Representative Raman spectra from the Streptococcus Thermophilus datasets, 5 random samples each.

A.13.3 E. coli Metabolites: High-Throughput Raman Measurements

Both datasets contain Raman spectra of aqueous mixtures of key *E. coli* fermentation metabolites, acquired using an automated high-throughput Raman measurement system integrated into a liquid handling station [76]. The *ecoli_metabolites* dataset covers binary glucose–acetate mixtures; *ecoli_metabolites_dig4bio* extends the composition to include magnesium sulfate.

Instrument. A Metrohm Raman Plus 785 spectrometer (Metrohm AG, Herisau, Switzerland) equipped with a fiber-optic BAC102 Raman probe was used. The excitation wavelength was 785 nm at a laser power of 455 mW. Spectra were recorded from 65 to 3350 cm^{-1} (2048 data points) with an acquisition time of 10 s per spectrum. The measurement cell was a BCR100A Raman Cuvette Holder (Metrohm AG) accommodating an 18 μL flow-through cuvette (Hellma GmbH & Co. KG, Müllheim, Germany; Article No. 178128510-40) with a flat quartz window and a working distance of 5.9 mm.

Automated Liquid Handling. The spectrometer was integrated into a Tecan EVO 200 liquid handling station (Tecan Group, Männedorf, Switzerland) controlled via a microservice-based software stack. Samples were pipetted by a robotic arm into up to eight parallel wells of a sampling interface connected to the flow-through cuvette via PTFE tubing and a multiplexer valve (Elvesflow, Paris, France).

Sample Preparation. Mixtures of D-(+)-glucose monohydrate (Carl Roth, Karlsruhe, Germany), sodium acetate, and magnesium sulfate heptahydrate (Carl Roth, Karlsruhe, Germany) were prepared at concentration ranges typical of *E. coli* fed-batch fermentation processes. The concentrations that the liquid handling robot was supposed to pipet into the wells were assumed to be the ground truth. The consistency of these annotations with enzymatic assays was confirmed in [76].

These two datasets contain newly released in-line Raman spectra from *E. coli* cultivations, targeting key metabolite concentrations (glucose, sodium acetate, and magnesium sulfate). The Dig4Bio dataset extends the analyte panel to include magnesium sulfate; both datasets were acquired using the same automated measurement platform [76]. Statistics are given in Table 15; representative spectra are shown in Fig. 16.

Table 15: Dataset statistics for Ecoli Metabolites.

Dataset	Task	No. Targets	Samples	Features	Wavelength (cm^{-1})	License	Ref.
Ecoli Metabolites	Regr.	2	1,920	594	402–1599	CC BY 4.0	[76]
Dig4bio	Regr.	3	384	1,869	391–3384		

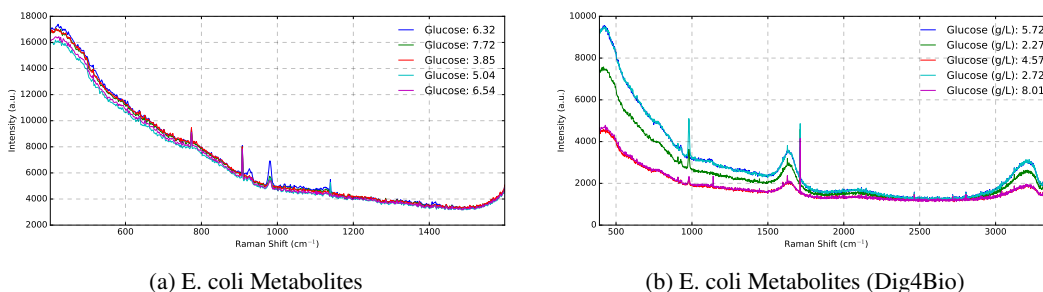


Figure 16: Representative Raman spectra from the E. coli Metabolites datasets, 5 random samples each.

A.13.4 Bio-Catalysis Monitoring of Adenosine Phosphates (AXP)

This dataset comprises high-throughput Raman spectra collected for real-time monitoring of biocatalytic reactions involving adenosine phosphates (AMP, ADP, ATP; collectively AXP). A distinctive feature of the reaction medium is the use of Deep Eutectic Solvents (DES), which serve as an alternative solvent system for the biocatalytic conversion. Moreover, all samples contain a Tris(hydroxymethyl)aminomethane buffer to fix the pH between 7 and 9. When training this dataset with a machine learning model, it can serve as an analytic method to evaluate the suitability of different enzymes.

Instrument. A Metrohm Raman Plus 785 spectrometer (Metrohm AG, Herisau, Switzerland) with a fiber-optic BAC102 Raman probe was used. The excitation wavelength was 785 nm at 455 mW laser power. Spectra were recorded with 25 s acquisition time per spectrum with an 18 μ L flow-through cuvette (Hellma GmbH & Co. KG, Müllheim, Germany) featuring a flat quartz window and 5.9 mm working distance as described in [76].

This dataset contains newly released in-line Raman spectra for monitoring adenosine phosphate concentrations during bio-catalytic reactions. The four regression targets cover the key phosphorylated forms of adenosine (adenosine, ADP, AMP, ATP). All samples contain a Tris(hydroxymethyl)aminomethane buffer to fix the pH between 7 and 9 and use a green Deep Eutectic Solvent (DES) as the reaction medium; a trained model for this dataset can serve as an analytical tool to evaluate enzyme suitability during biocatalytic conversion. Statistics are given in Table 16; representative spectra are shown in Fig. 17.

Table 16: Dataset statistics for Bio-Catalysis Monitoring of AXP.

Dataset	Task	No. Targets	Samples	Features	Wavelength (cm^{-1})	License	Ref.
Bio-Catalysis Monitoring of AXP	Regr.	4	344	2,048	-32–3385	CC BY 4.0	—

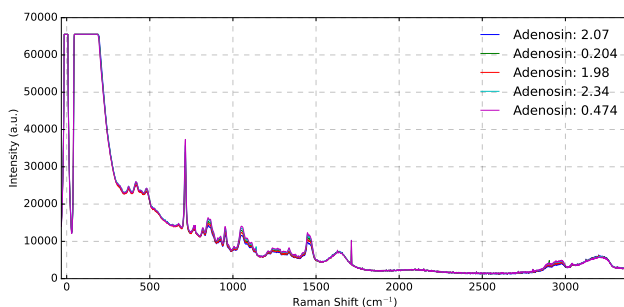


Figure 17: Representative Raman spectra from the Bio-Catalysis AXP dataset showing 5 random samples.

A.13.5 Ethanolic Yeast Fermentation

This dataset contains Raman spectra acquired during the continuous ethanolic fermentation of sucrose by *Saccharomyces cerevisiae* immobilized in calcium alginate beads, originally published by Legner et al. [77] without providing access to the dataset.

Instrument. Raman spectra were recorded online using a handheld ID Raman mini 2.0 spectrometer (Ocean Optics, Dunedin, FL, USA). The excitation wavelength was 785 nm. Spectra were acquired over the range 400–2300 cm^{-1} with a spectral resolution of 13 cm^{-1} . Measurements were performed in a flow-through configuration using a QS 0.5 mm quartz flow cell (Hellma Analytics, Müllheim, Germany) attached directly to the reactor apparatus.

Fermentation Setup. A BIOSTAT B fermenter with 1 L working volume (Sartorius AG, Göttingen, Germany) was used in continuous mode. *S. cerevisiae* cells were immobilized in calcium alginate beads (10 g L^{-1} sodium alginate, cross-linked with CaCl_2) to enable stable continuous processing and unobstructed optical access to the liquid phase. The sucrose-containing substrate solution was delivered from a storage vessel by a peristaltic pump at a defined flow rate.

Data Acquisition and Processing. Data acquisition was automated using MATLAB (R2016b; The MathWorks, Natick, MA, USA) with automated upload to cloud storage after each spectrum. A baseline correction based on a moving average over a 6-point interval was applied to the raw spectra. The selected analysis range was 400–2300 cm^{-1} . Reference concentrations for ethanol, fructose, glucose, and glycerol were determined by HPLC (Knauer EuroChrom 1.57).

Raman spectra of the continuous ethanolic fermentation of sucrose by immobilized *Saccharomyces cerevisiae* in calcium alginate beads. Four regression targets (glucose, fructose, glycerol, ethanol) capture the dynamic evolution of key metabolites during continuous operation. Statistics are given in Table 17; representative spectra are shown in Fig. 18.

Table 17: Dataset statistics for Yeast Fermentation.

Dataset	Task	No. Targets	Samples	Features	Wavelength (cm^{-1})	License	Ref.
Yeast Fermentation	Regr.	4	58	1,900	401–2300	CC BY 4.0	[77]

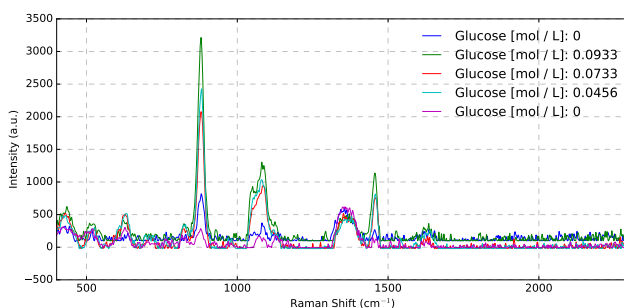


Figure 18: Representative Raman spectra from the Yeast Fermentation dataset showing 5 random samples.

A.13.6 *R. eutropha* Copolymer Fermentations

This dataset supports the monitoring of poly(3-hydroxybutyrate-co-3-hydroxyhexanoate) [P(HB-co-HHx)] copolymer synthesis in *Ralstonia eutropha* batch cultivations [78].

Fermentation Setup and Targets. Four independent cultivations were conducted over approximately 72 hours under varying fermentation conditions to generate a diverse dataset of Raman spectra and offline reference measurements. Two cultivations were performed using canola oil as the primary carbon substrate, while two cultivations used fructose. To further increase variability

in biomass formation and metabolite profiles, the experiments were initiated with different starting concentrations of residual cell dry weight (RCDW), fructose, and urea.

Instrument. Raman monitoring of all cultivations was performed in-line using a Multi-Spec[®] Raman spectrometer (Tec5) equipped with a 785 nm excitation laser operating at up to 500 mW. Spectra were recorded over a wavelength range of 365–3180 cm^{-1} using an in-line probe mounted to the bioreactor through a sapphire optical window (SCHOTT ViewPort[™], Schott AG, Mainz, Germany), minimizing the risk of probe fouling during cultivation.

Raman spectra from the cultivation of *Ralstonia eutropha* for biosynthesis of the biodegradable copolymer P(HB-*co*-HHx). The dataset uniquely combines experimental and high-fidelity synthetic spectra to address multicollinearity between correlated process variables such as biomass, substrate concentration, and monomer ratios. Six regression targets cover cell dry weight, substrate consumption, and copolymer fractions. Statistics are given in Table 18; representative spectra are shown in Fig. 19.

Table 18: Dataset statistics for *R. eutropha* Copolymer Fermentations.

Dataset	Task	No. Targets	Samples	Features	Wavelength (cm^{-1})	License	Ref.
R. eutropha Copolymer Fermentations	Regr.	6	82	2,776	405–3180	CC BY 4.0	[78]

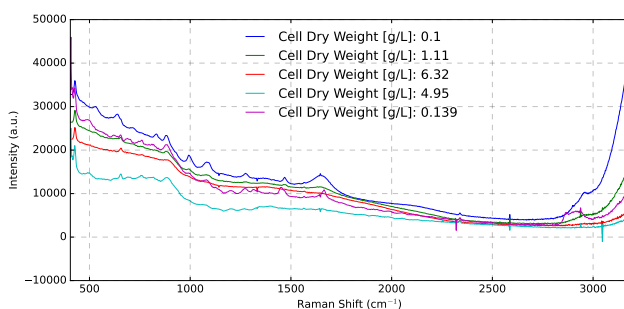


Figure 19: Representative Raman spectra from the *R. eutropha* Copolymer Fermentations dataset showing 5 random samples.

A.13.7 Gasoline Properties: Benchtop and Handheld Raman Measurements

These two datasets contain Raman spectra of the same commercial gasoline samples recorded with two different spectrometers for the prediction of Research Octane Number (RON), Motor Octane Number (MON), and oxygenated additive concentrations. The sample set comprised 130 refinery samples spanning RON 95–102.2 (covering Super, Super Plus, and premium quality grades) together with additional samples from petrol stations [79, 80].

Handheld Raman. Spectra were recorded using a handheld IDRaman mini 2.0 spectrometer (Ocean Optics, Dunedin, FL, USA; weight 380 g) with 785 nm excitation at 100 mW laser power. The spectral range was 400–2300 cm^{-1} with a resolution of 13 cm^{-1} . Samples were transferred into 2 mL glass vials for measurement; the spectrometer was powered by a laptop computer or AA batteries. Prominent spectral features include C–C stretching vibrations of branched paraffins (800–1100 cm^{-1}) and C–H deformation bands (1300–1700 cm^{-1}); oxygenate additives (MTBE, ETBE) contribute characteristic Raman bands that enable their quantification.

Benchtop FT-Raman. Offline analyses were performed using an NXR FT-Raman module (Thermo Fisher Scientific, Dreieich, Germany) with a 1,064 nm laser, coupled to a Nicolet 6700 FT-IR spectrometer (Thermo Fisher Scientific, Dreieich, Germany). For each measurement, 64 spectra were averaged at 900 mW over 100–3800 cm^{-1} with 8 cm^{-1} resolution. Analyses were carried out in 2 mL vials fixed in the optical bench. The 1064 nm excitation suppresses fluorescence from aromatic gasoline components that hinders measurements at shorter wavelengths.

Reference Analysis. Ground-truth RON values were measured using a Cooperative Fuel Research (CFR) motor according to ASTM D2699 and DIN EN ISO 5164. MON was determined according to ASTM D2885 and DIN EN ISO 5163. Oxygenate additive concentrations were verified against standard reference tables.

This dataset contains FT-Raman spectra (1064 nm excitation) of 179 commercial fuel samples for multi-target regression, predicting 12 physico-chemical properties including Research Octane Number (RON), Motor Octane Number (MON), ethanol content, oxygenate additives, and benzene content. Statistics are given in Table 19; representative spectra are shown in Fig. 20.

Table 19: Dataset statistics for Gasoline Properties (Benchtop).

Dataset	Task	No. Targets	Samples	Features	Wavelength (cm ⁻¹)	License	Ref.
Gasoline Properties (Benchtop)	Regr.	12	179	961	98–3801	CC BY 4.0	[79, 80]

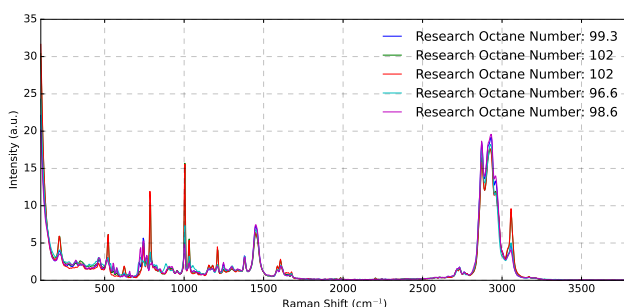


Figure 20: Representative Raman spectra from the Gasoline Properties (Benchtop) dataset showing 5 random fuel samples.

This dataset is the handheld-spectrometer counterpart (785 nm excitation) of the Gasoline Properties (Benchtop) dataset, comprising the same 179 fuel samples with the same 12 regression targets. Together, the two datasets enable evaluation of cross-instrument transferability between laboratory and portable form factors. Statistics are given in Table 20; representative spectra are shown in Fig. 21.

Table 20: Dataset statistics for Gasoline Properties (Handheld).

Dataset	Task	No. Targets	Samples	Features	Wavelength (cm ⁻¹)	License	Ref.
Gasoline Properties (Handheld)	Regr.	12	179	1,901	400–2300	CC BY 4.0	[79, 80]

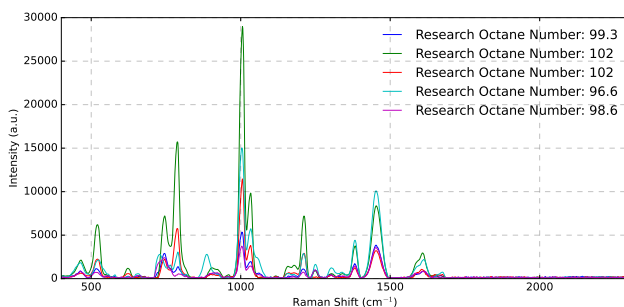


Figure 21: Representative Raman spectra from the Gasoline Properties (Handheld) dataset showing 5 random fuel samples.

A.13.8 Adenine SERS: European Multi-Instrument Interlaboratory Study

These four datasets originate from a large-scale European interlaboratory study (ILS) on quantitative Surface-Enhanced Raman Spectroscopy (SERS), conducted within the COST Action Raman4Clinics Working Group 1 [81]. The study was designed to assess the reproducibility and accuracy of SERS-based quantification across different laboratories, operators, and instrument configurations.

Study Design. Up to 18 European laboratories participated. Six SERS measurement methods were evaluated, distinguished by substrate type (colloidal vs. solid) and substrate material (Au vs. Ag), with Ag substrates measured at 532 nm and/or 785 nm excitation. The four benchmark datasets correspond to the 785 nm excitation methods: colloidal Au (cAu@785), solid Au (sAu@785), colloidal Ag (cAg@785), and solid Ag (sAg@785). Each method was independently evaluated by up to eight laboratories using the same standard operating procedure (SOP).

Instrumentation. Each participating laboratory used its own Raman spectrometer at 785 nm excitation; instruments from multiple manufacturers were represented (including Horiba, Renishaw, and others; see Figure 3 in Fornasaro et al. 81). The deliberate use of instruments from different manufacturers captures real-world inter-instrument variability within a controlled protocol.

Sample Preparation. A standard operating procedure and measurement kit were prepared by the organizing Laboratory (OL, University of Trieste, Italy) and distributed to all participants under the Raman4Clinics ILS framework. Each kit contained centrally assembled SERS substrates, adenine solution stocks, and reagents to ensure homogeneity. For colloidal substrates, citrate-reduced silver and gold nanoparticle suspensions were provided; for solid substrates, metal-coated nanostructured surfaces were included. Aqueous adenine solutions were prepared in phosphate-buffered saline (PBS, pH 7.4) at multiple concentration levels.

Part of a large inter-laboratory SERS trial across 15 European laboratories measuring adenine on colloidal SERS substrates (colloidal silver, cAg; colloidal gold, cAu). The two datasets differ in substrate metal and yield 855 spectra in total. Statistics are given in Table 21; representative spectra are shown in Fig. 22.

Table 21: Dataset statistics for Adenine Colloidal.

Dataset	Task	No. Targets	Samples	Features	Wavelength (cm ⁻¹)	License	Ref.
Gold	Regr.	1	225	534	400–1999	CC BY 4.0	[81]
Silver	Regr.	1	630	534	400–1999		

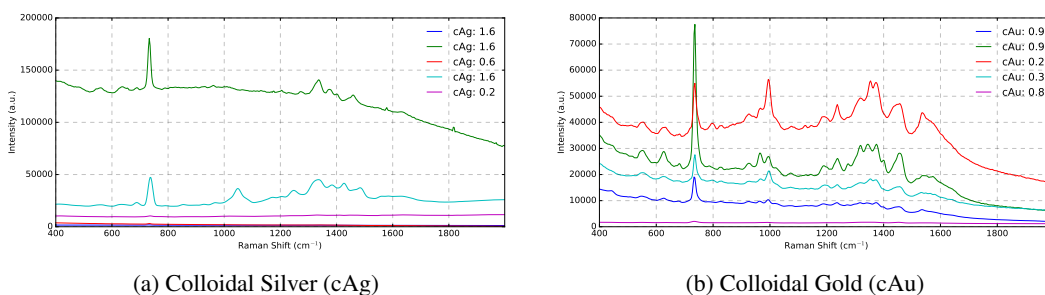


Figure 22: Representative SERS spectra from the Adenine (Colloidal) dataset, 5 random samples per substrate.

The sputtered-substrate counterpart of the colloidal adenine dataset from the same inter-laboratory trial, using sputtered silver (sAg) and sputtered gold (sAu) substrates. With 2,661 spectra, this is the larger of the two Adenine sub-collections. Statistics are given in Table 22; representative spectra are shown in Fig. 23.

Table 22: Dataset statistics for Adenine Solid.

Dataset	Task	No. Targets	Samples	Features	Wavelength (cm^{-1})	License	Ref.
Gold	Regr.	1	810	534	400–1999	CC BY 4.0	[81]
Silver	Regr.	1	1,851	534	400–1999		

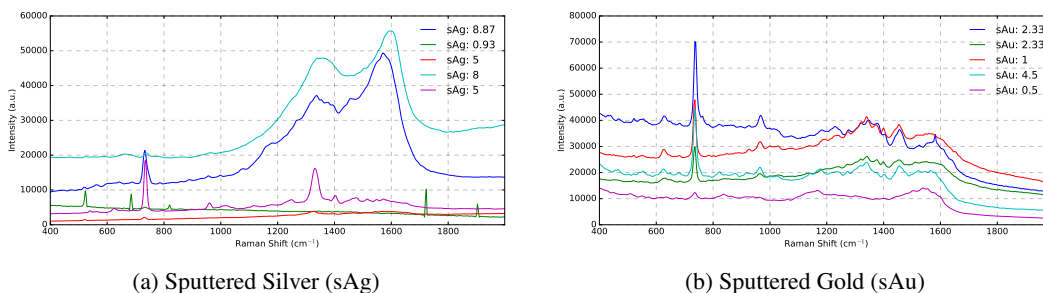


Figure 23: Representative SERS spectra from the Adenine (Solid) dataset, 5 random samples per substrate.

A.14 Dataset Descriptions

This section provides descriptions of all datasets in **RamanBench**, organized by application domain.

A.14.1 Material Science

ML Raman Open Dataset (MLROD) [16] The ML Raman Open Dataset is a large-scale public dataset designed to support autonomous mineral identification for planetary rover missions (NASA’s *Perseverance* and ESA’s *ExoMars*), where mechanical dust cleaning is not always feasible. It contains Raman spectra from rocks, pure minerals, and mineral mixtures measured under both clean and basaltic-dust-covered conditions (up to $\sim 50\%$ dust coverage) with varying dust obstruction and surface orientations to simulate Mars-like, low-SNR field conditions. Crucially, no traditional spectral preprocessing such as cosmic-ray or baseline removal was applied, making the dataset well-suited for evaluating end-to-end deep learning pipelines. With 130,061 spectra spanning $141\text{--}1100\text{ cm}^{-1}$, it is the largest single-source classification dataset in **RamanBench**. Statistics are given in Table 23; representative spectra are shown in Fig. 24.

Table 23: Dataset statistics for ML Raman Open Dataset (MLROD).

Dataset	Task	No. Classes	Samples	Features	Wavelength (cm^{-1})	License	Ref.
ML Raman Open Dataset (MLROD)	Class.	16	130,061	1,836	141–1100	BY-NC	[16]

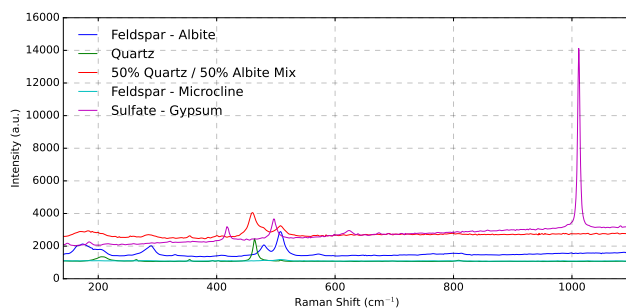


Figure 24: Representative Raman spectra from MLROD showing 5 random samples.

RRUFF Minerals (Raw)[†] [2] The RRUFF Database is the most comprehensive resource for reference Raman spectra of minerals [2], distinguished from other compilations by its consistent collection methodology: all spectra are acquired with the same instruments and procedures, and each mineral species is ideally represented by at least two samples from different localities to capture natural chemical variability. Every entry is corroborated by X-ray diffraction and, where possible, chemical analysis, ensuring reliable species assignments. **RamanBench** includes the raw (unprocessed) subset, which covers a variety of mineral species recorded under varying excitation conditions. The full dataset spans 1,685 mineral classes, of which 79 classes meet the minimum-sample threshold after rare-class filtering. Statistics are given in Table 24; representative spectra are shown in Fig. 25.

Table 24: Dataset statistics for RRUFF Minerals (Raw).

Dataset	Task	No. Classes	Samples	Features	Wavelength (cm ⁻¹)	License	Ref.
RRUFF Minerals (Raw)	Class.	79	1,162	1,142	303–853	Free access	[2]

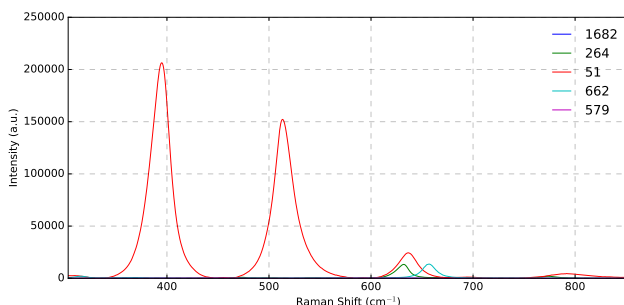


Figure 25: Representative Raman spectra from the RRUFF Database (raw subset) showing 5 random mineral samples.

Synthetic Organic Pigments (Raw) [82] The SOP (Synthetic Organic Pigments) Spectral Library from the Royal Institute for Cultural Heritage (KIK-IRPA, Brussels) was built to support conservation science and artwork authentication for modern and contemporary paintings, where the sheer number of commercially available synthetic pigments makes manual identification by flow charts impractical. Spectra were acquired with a Renishaw inVia dispersive Raman spectrometer using 785 nm near-infrared excitation, and the library was validated by identifying SOPs in four contemporary paintings from the Stedelijk Museum voor Actuele Kunst (Ghent, Belgium). **RamanBench** uses the raw (unprocessed) subset. **Note:** This dataset is not publicly hosted; interested users should contact KIK-IRPA (<https://soprano.kikirpa.be>) to obtain access. Statistics are given in Table 25; representative spectra are shown in Fig. 26.

Table 25: Dataset statistics for Synthetic Organic Pigments (Raw).

Dataset	Task	No. Targets	Samples	Features	Wavelength (cm ⁻¹)	License	Ref.
Synthetic Organic Pigments (Raw)	Regr.	1	325	561	1189–1651	research use only	[82]

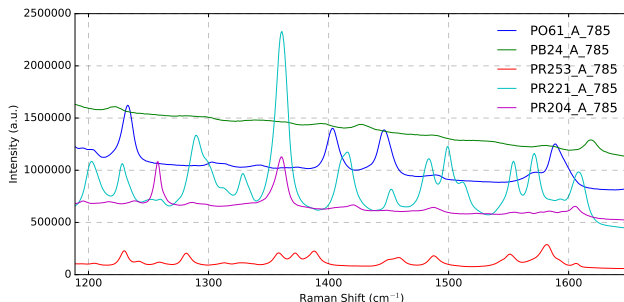


Figure 26: Representative Raman spectra from the SOP Spectral Library (raw subset) showing 5 random pigment samples.

Weathered Microplastics[†] [83] A collection of Raman spectra of microplastic particles weathered under natural environmental conditions [83], sampled from river sediments around waste-plastic recycling industries in Laizhou, Shandong Province, China. The central challenge motivating this dataset is that Raman spectra of naturally weathered microplastics differ substantially from standard library spectra due to weakened characteristic peaks and strong fluorescence interference caused by surface oxidation and organic matter adsorption. Spectra were acquired with a confocal micro-Raman microscope (WITec alpha300-R) using a 532 nm laser, and ATR-FTIR and SEM-EDS measurements were included to cross-validate polymer identification and characterise surface changes. After rare-class filtering, 3 of the original 10 polymer classes are retained. Statistics are given in Table 26; representative spectra are shown in Fig. 27.

Table 26: Dataset statistics for Weathered Microplastics.

Dataset	Task	No. Classes	Samples	Features	Wavelength (cm ⁻¹)	License	Ref.
Weathered Microplastics	Class.	3	77	1,144	202–3498	CC BY 4.0	[83]

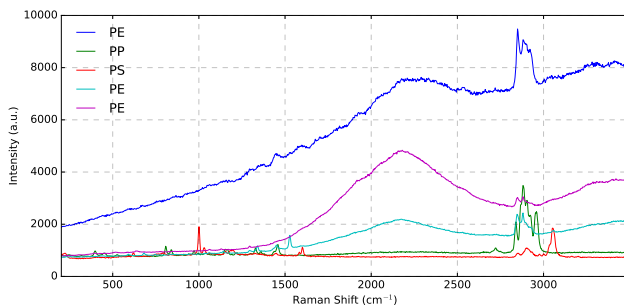


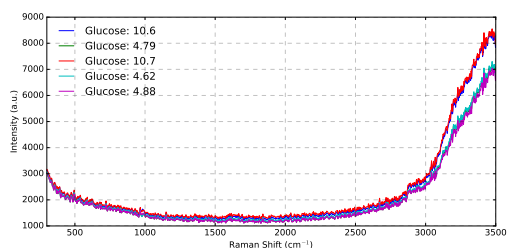
Figure 27: Representative Raman spectra from the Weathered Microplastics dataset showing 5 random samples.

A.14.2 Biological & Biotechnological

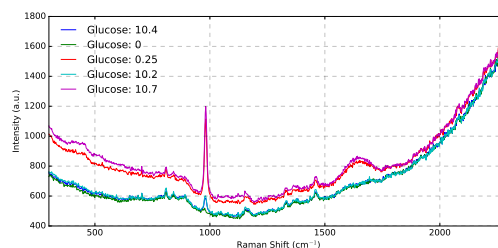
Bioprocess Analytes [22] A multi-spectrometer benchmark for bioprocess analyte quantification, in which the same aqueous solutions of glucose, sodium acetate, and magnesium sulfate were measured on eight spectrometers from seven different manufacturers (Anton Paar Cora 5001 at 532 nm and 785 nm, Kaiser RXN1 at 785 nm, Metrohm i-Raman Plus at 785 nm, Mettler Toledo React Raman 802L at 785 nm, Tec5 Multi-Spec, Timegate Pico-Raman M2, and Tornado HyperFlux Pro Plus). Statistics are given in Table 27; representative spectra are shown in Fig. 28.

Table 27: Dataset statistics for Bioprocess Analytes.

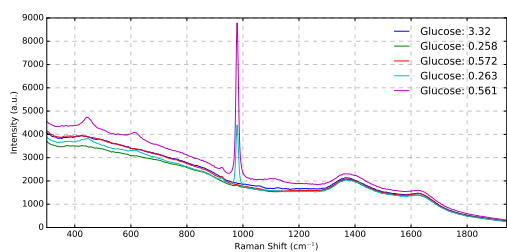
Dataset	Task	No. Targets	Samples	Features	Wavelength (cm ⁻¹)	License	Ref.
Anton 532	Regr.	3	270	1,601	300–3500	CC BY 4.0	[22]
Anton 785	Regr.	3	270	1,001	300–2300		
Kaiser	Regr.	3	134	5,472	300–1941		
Metrohm	Regr.	3	399	1,875	301–3349		
Mettler Toledo	Regr.	3	275	2,901	300–3200		
Tec5	Regr.	3	395	2,911	300–3210		
Timegate	Regr.	3	133	486	304–1998		
Tornado	Regr.	3	385	3,001	300–3300		



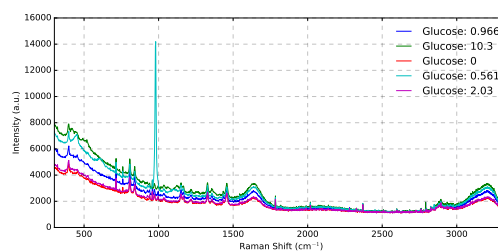
(a) Anton 532 nm



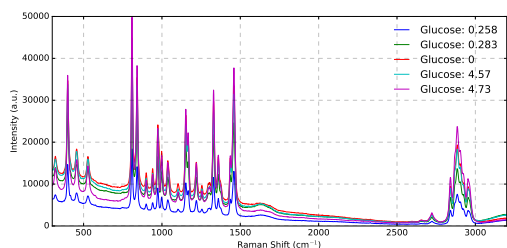
(b) Anton 785 nm



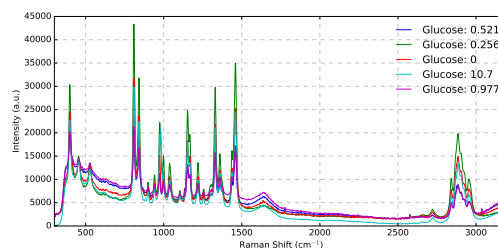
(c) Kaiser



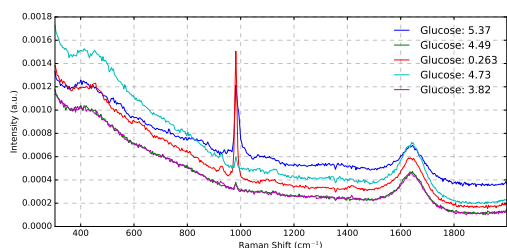
(d) Metrohm



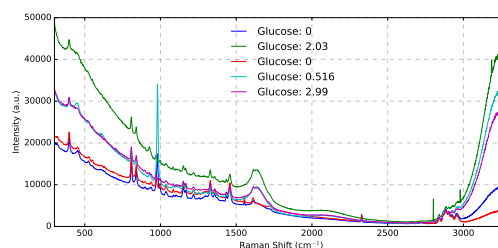
(e) Mettler Toledo



(f) Tec5



(g) Timegate



(h) Tornado

Figure 28: Representative Raman spectra from the Bioprocess Analytes dataset across all 8 spectrometers, 5 random samples each.

Bioprocess Monitoring [21] A dataset of aqueous solutions containing eight fermentation-relevant substrates (glucose, glycerol, acetate, nitrate, phosphate, sulfate, yeast extract, and antifoam), prepared with a liquid handling robot to ensure a broad and statistically independent concentration distribution. Mineral salt medium and antifoam are included at varying concentrations to simulate the turbidity and signal attenuation encountered in supernatants from real bioreactors. Statistics are given in Table 28; representative spectra are shown in Fig. 29.

Table 28: Dataset statistics for Bioprocess Monitoring.

Dataset	Task	No. Targets	Samples	Features	Wavelength (cm^{-1})	License	Ref.
Bioprocess Monitoring	Regr.	8	6,960	1,870	391–3385	CC BY 4.0	[21]

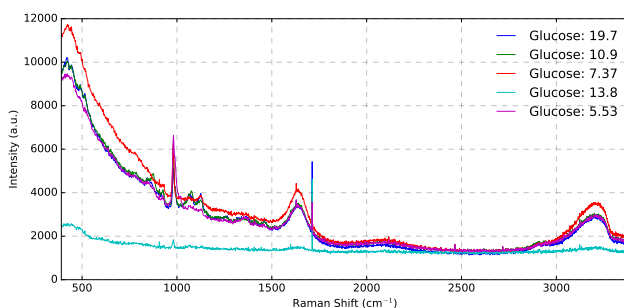


Figure 29: Representative Raman spectra from the Bioprocess Monitoring dataset showing 5 random samples.

Cancer Cell (SERS) [84] This dataset contains Surface-Enhanced Raman Spectroscopy (SERS) spectra of conditioned cell culture media, collected without direct cell contact, for rapid metabolic profiling of cancer and normal cells. Gold multibranched nanoparticles (AuMs, “gold nanourchins”) with sharp edges were functionalised with three different chemical moieties (COOH, NH_2 , and $(\text{COOH})_2$) to selectively entrap biomolecules from the cultivation medium; spectra were acquired with a ProRaman-L spectrometer at 785 nm excitation. The three datasets differ by substrate functionalisation; a Convolutional Neural Network (CNN) with multiple independent inputs (one per substrate) was used to achieve 100% classification accuracy on held-out data. Statistics are given in Table 29; representative spectra are shown in Fig. 30.

Table 29: Dataset statistics for Cancer Cell.

Dataset	Task	No. Classes	Samples	Features	Wavelength (cm^{-1})	License	Ref.
(cooh)2	Class.	12	627	2,090	100–4278	CC BY-NC-SA 4.0	[84]
Cooh	Class.	12	633	2,090	100–4278		
Nh2	Class.	12	632	2,090	100–4278		

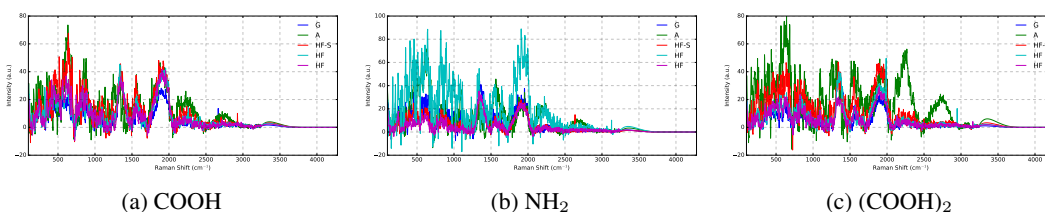


Figure 30: Representative SERS spectra from the Cancer Cell dataset, 5 random samples per functionalisation subset.

E. coli Fermentation [76] At-line Raman spectra were acquired during high-throughput fed-batch *Escherichia coli* fermentations. The spectra were recorded from the supernatant using an integrated automated measurement system that simultaneously handles eight parallel 50 μL samples via a liquid handling robot (Tecan EVO 200), completing measurement, cleaning, and concentration prediction within 45 s per sample. Spectra were recorded with a Metrohm i-Raman Plus 785 spectrometer (785 nm excitation) through a flow-through cuvette. Statistics are given in Table 30; representative spectra are shown in Fig. 31.

Table 30: Dataset statistics for E. coli Fermentation.

Dataset	Task	No. Targets	Samples	Features	Wavelength (cm^{-1})	License	Ref.
E. coli Fermentation	Regr.	2	379	1,870	391–3385	CC BY 4.0	[76]

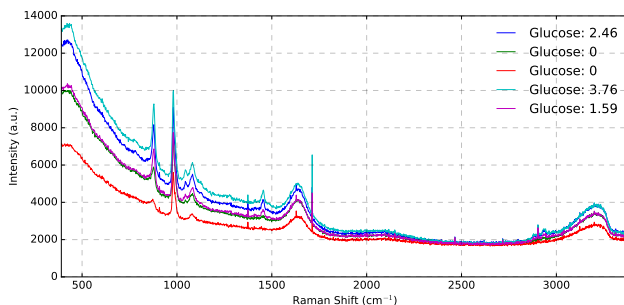


Figure 31: Representative Raman spectra from the E. coli Fermentation dataset showing 5 random samples.

Mutant Wheat [85] Raman spectroscopy was used to analyze leaf samples from salt-tolerant wheat plants. These plants belonged to the seventh generation of mutant lines of bread wheat (*Triticum aestivum* L. “Adana-99”), which were created using sodium azide (NaN_3). The results were compared with standard biochemical measurements, such as antioxidant enzyme activity, chlorophyll content, proline levels, ion concentrations, and gene expression (qPCR). The goal was to evaluate whether Raman spectroscopy could be used as a fast and efficient method to screen plant traits in breeding programs.

The Raman measurements showed clear differences between salt-tolerant plants and the original wheat variety. In particular, signals related to proteins (e.g., the Amide-I band and certain amino acid vibrational modes) were lower in the tolerant plants, while signals associated with beta-carotene (at 1,153 and 1,519 cm^{-1}) were higher. With 53,134 spectra, this is the largest classification dataset in **RamanBench** by sample count. Statistics are given in Table 31; representative spectra are shown in Fig. 32.

Table 31: Dataset statistics for Mutant Wheat.

Dataset	Task	No. Classes	Samples	Features	Wavelength (cm^{-1})	License	Ref.
Mutant Wheat	Class.	4	53,134	1,748	296–2043	CC BY 4.0	[85]

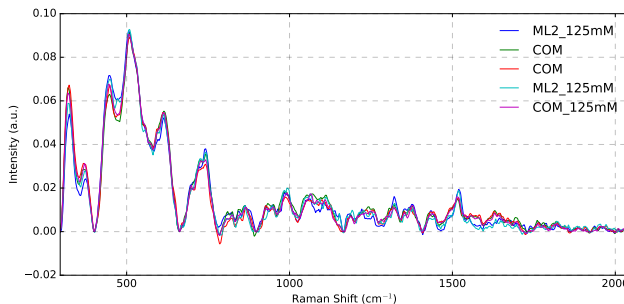


Figure 32: Representative Raman spectra from the Mutant Wheat dataset showing 5 random leaf samples.

A.14.3 Medical & Clinical

Alzheimer’s SERS Serum [25] SERS spectra of blood serum for Alzheimer’s disease classification, collected as part of a multi-disease study that developed a deep learning model for spectral analysis [25]. The dataset was used to demonstrate molecule-level metabolic profiling from SERS serum spectra, with nanoparticle background subtraction identified as a critical preprocessing step. The 3,417 spectra represent a binary (disease vs. control) classification task. Statistics are given in Table 32; representative spectra are shown in Fig. 33.

Table 32: Dataset statistics for Alzheimer’s SERS Serum.

Dataset	Task	No. Classes	Samples	Features	Wavelength (cm ⁻¹)	License	Ref.
Alzheimer’s SERS Serum	Class.	3	3,417	724	0–723	CC BY 4.0	[25]

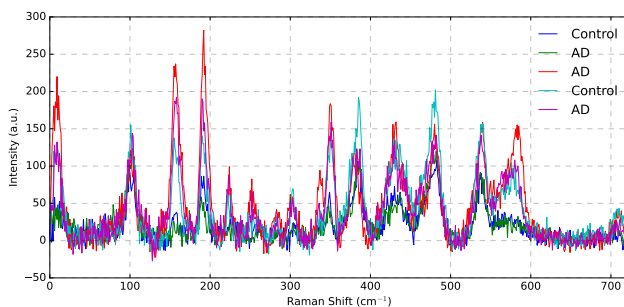


Figure 33: Representative SERS spectra from the Alzheimer’s Serum dataset showing 5 random samples.

Diabetes Skin [86] *In vivo* skin Raman spectra for non-invasive Type 2 Diabetes mellitus (DM2) screening, acquired to replace invasive finger-prick blood glucose tests with a low-cost, harmless optical alternative. Spectra were collected with a portable PEK-785 spectrometer (Agiltron, 785 nm, 90 mW) across four anatomical sites from 11 DM2 patients and 9 healthy controls, averaging five scans per location. Artificial neural networks (ANN) achieved 88.9–90.9% accuracy, outperforming conventional Principal Component Analysis (PCA)-Support Vector Machine (SVM) (76.0–82.5%). Statistics are given in Table 33; representative spectra are shown in Fig. 34.

Table 33: Dataset statistics for Diabetes Skin.

Dataset	Task	No. Classes	Samples	Features	Wavelength (cm ⁻¹)	License	Ref.
Ear Lobe	Class.	2	20	3,160	0–3159	Optica OAPA	[86]
Inner Arm	Class.	2	20	3,160	0–3159		
Thumbnail	Class.	2	20	3,160	0–3159		
Vein	Class.	2	20	3,160	0–3159		

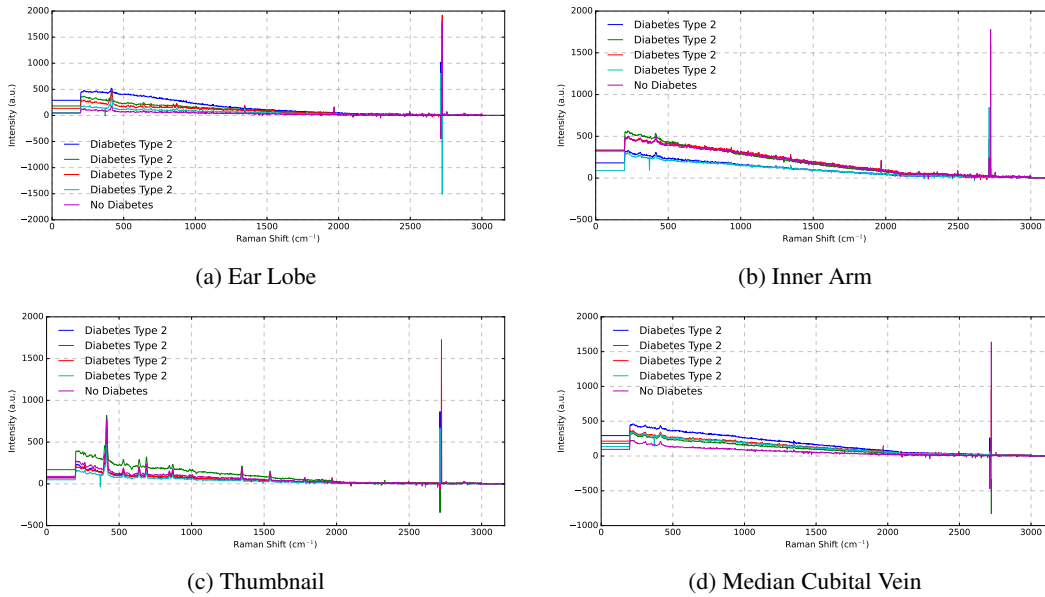


Figure 34: Representative Raman spectra from the Diabetes Skin dataset, 5 random samples per anatomical site.

Head & Neck Cancer A clinical liquid biopsy dataset of Raman spectra from blood plasma and saliva for binary Head & Neck squamous cell carcinoma (SCC) classification [87], collected from a 53-person cohort at the University of California, Davis. The key methodological finding was that fusing paired plasma and saliva spectra per patient substantially outperformed either biofluid alone, achieving 96.3% sensitivity, 85.7% specificity, and 91.7% accuracy, validated against GC-TOF-MS metabolomics. Spectra were acquired on a custom-built inverted scanning confocal Raman microscope (785 nm excitation, 65 mW) in both native and dried states. Statistics are given in Table 34; representative spectra are shown in Fig. 35.

Table 34: Dataset statistics for Head & Neck Cancer.

Dataset	Task	No. Classes	Samples	Features	Wavelength (cm ⁻¹)	License	Ref.
Head & Neck Cancer	Class.	4	111	1,004	789–910	CC BY 4.0	[87]

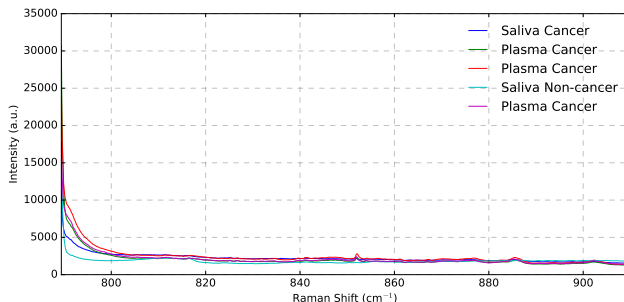


Figure 35: Representative Raman spectra from the Head & Neck Cancer dataset showing 5 random plasma and saliva samples.

Pathogenic Bacteria [4] A large-scale Raman dataset for culture-free, rapid clinical pathogen identification, in which bacterial cells are deposited onto gold-coated silica substrates and measured using confocal Raman microscopy with 1 s acquisition time, yielding very low SNR (≈ 4.1) spectra that are an order of magnitude noisier than conventional bacterial Raman data [4]. The 30 bacterial and yeast isolates cover 94% of the most common infections treated at Stanford Hospital (2016–17) and include both methicillin-resistant (MRSA) and susceptible (MSSA) *S. aureus* strains for antibiotic susceptibility classification. A CNN with 25 residual convolutional layers achieved 97.0% treatment-group accuracy and 89% MRSA/MSSA discrimination on held-out clinical patient isolates. Statistics are given in Table 35; representative spectra are shown in Fig. 36.

Table 35: Dataset statistics for Pathogenic Bacteria.

Dataset	Task	No. Classes	Samples	Features	Wavelength (cm^{-1})	License	Ref.
Pathogenic Bacteria	Class.	30	78,500	1,000	382–1792	MIT	[4]

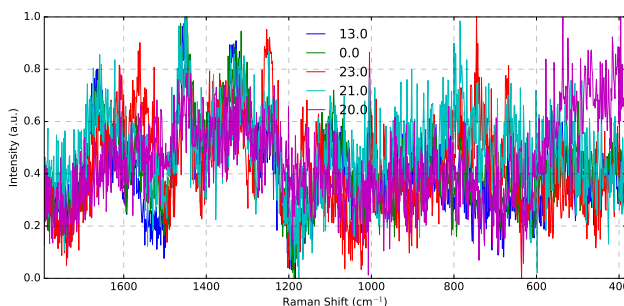


Figure 36: Representative SERS spectra from the Pathogenic Bacteria dataset showing 5 random bacterial isolates.

Pharmaceutical Ingredients [6] An open Raman spectral dataset of 3,510 spectra from 32 chemical substances (organic solvents and reagents used in active pharmaceutical ingredient (API) development), collected at the University of Galway using a Kaiser Rxn2 analyser (Endress+Hauser/Kaiser Optical Systems) with an Rxn-10 immersion probe at 785 nm excitation, spanning 150–3425 cm^{-1} . Samples were stored in 4 mL amber vials; automatic dark-noise subtraction and cosmic-ray filtering were applied to the spectra. Statistics are given in Table 36; representative spectra are shown in Fig. 37.

Table 36: Dataset statistics for Pharmaceutical Ingredients.

Dataset	Task	No. Classes	Samples	Features	Wavelength (cm^{-1})	License	Ref.
Pharmaceutical Ingredients	Class.	32	3,510	3,276	150–3425	CC BY 4.0	[6]

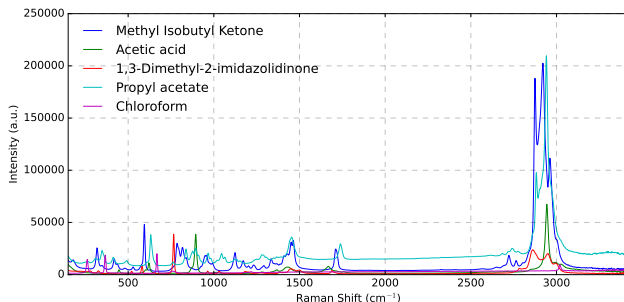


Figure 37: Representative Raman spectra from the Pharmaceutical Ingredients dataset showing 5 random samples.

Prostate Cancer SERS Serum [25] SERS spectra of blood serum for prostate cancer classification, from the same multi-disease study as the Alzheimer’s and Stroke serum datasets [25]. The dataset was collected from patients with prostate cancer and benign prostatic hyperplasia, and served as a benchmark for the Deep Spectral Component Filtering (DSCF) foundation model’s nanoparticle background subtraction and metabolic biomarker screening capabilities. Statistics are given in Table 37; representative spectra are shown in Fig. 38.

Table 37: Dataset statistics for Prostate Cancer SERS Serum.

Dataset	Task	No. Classes	Samples	Features	Wavelength (cm ⁻¹)	License	Ref.
Prostate Cancer SERS Serum	Class.	3	12,601	725	0–724	CC BY 4.0	[25]

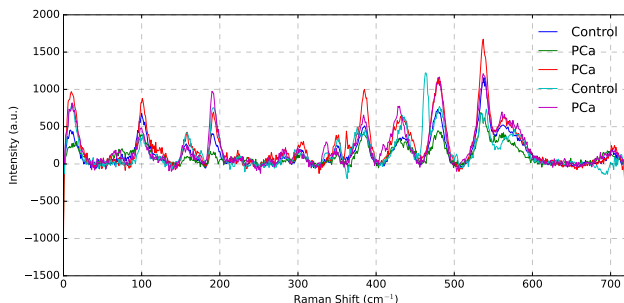


Figure 38: Representative SERS spectra from the Prostate Cancer Serum dataset showing 5 random samples.

Saliva COVID-19 [5] Raman spectra of dried saliva drops for non-invasive SARS-CoV-2 screening, collected as part of a study developing a diagnostic pipeline for salivary sample diagnostics. The 2,501 spectra cover positive, negative symptomatic, and healthy control groups from 101 subjects, with approximately 25 replicates per patient. Statistics are given in Table 38; representative spectra are shown in Fig. 39.

Table 38: Dataset statistics for Saliva COVID-19.

Dataset	Task	No. Classes	Samples	Features	Wavelength (cm ⁻¹)	License	Ref.
Saliva COVID-19	Class.	3	2,501	885	401–1598	Authors contacted ⁶	[5]

⁶<https://github.com/piazzam/Robust-SVM-Raman/issues/1>

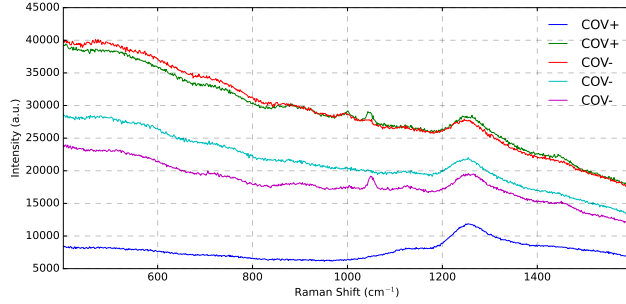


Figure 39: Representative Raman spectra from the Saliva COVID-19 dataset showing 5 random samples.

Saliva Alzheimer [5] Salivary Raman spectra for Alzheimer’s disease (AD) screening via liquid biopsy, from the same study as Saliva COVID-19 and Saliva Parkinson. The spectra were preprocessed via an aluminium substrate background subtraction. The 1,151 spectra cover Alzheimer’s disease patients and healthy controls. Statistics are given in Table 39; representative spectra are shown in Fig. 40.

Table 39: Dataset statistics for Saliva Alzheimer.

Dataset	Task	No. Classes	Samples	Features	Wavelength (cm ⁻¹)	License	Ref.
Saliva Alzheimer	Class.	2	1,151	885	401–1598	Authors contacted ⁷	[5]

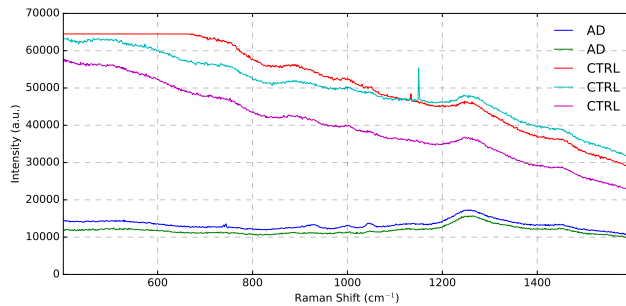


Figure 40: Representative Raman spectra from the Saliva Alzheimer dataset showing 5 random samples.

Saliva Parkinson [5] Salivary Raman spectra for Parkinson’s disease screening are from the same collection as Saliva COVID-19 and Saliva Alzheimer. The spectra were preprocessed via an aluminium substrate background subtraction. The 1,476 spectra cover PD patients and healthy controls. Statistics are given in Table 40; representative spectra are shown in Fig. 41.

Table 40: Dataset statistics for Saliva Parkinson.

Dataset	Task	No. Classes	Samples	Features	Wavelength (cm ⁻¹)	License	Ref.
Saliva Parkinson	Class.	2	1,476	885	401–1598	Authors contacted ⁸	[5]

⁷<https://github.com/piazzam/Robust-SVM-Raman/issues/1>

⁸<https://github.com/piazzam/Robust-SVM-Raman/issues/1>

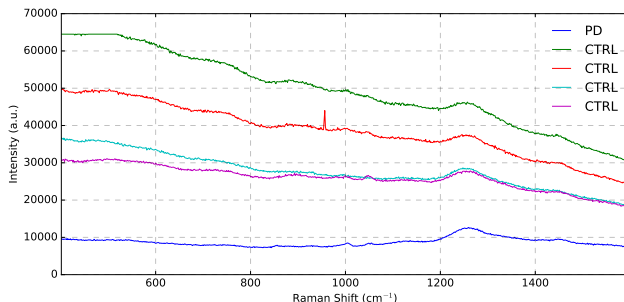


Figure 41: Representative Raman spectra from the Saliva Parkinson dataset showing 5 random samples.

Stroke SERS Serum [25] SERS spectra of blood serum for stroke classification, from the same multi-disease study as the Alzheimer’s and Prostate Cancer serum datasets [25]. The spectra were used to evaluate the DSCF foundation model’s zero-shot metabolic profiling ability, mapping serum metabolic phenotypes from stroke patients and demonstrating that nanoparticle background subtraction markedly improves downstream classification accuracy. The 4,020 spectra cover a broader spectral range (200–2000 cm^{-1}) than the other two serum datasets. Statistics are given in Table 41; representative spectra are shown in Fig. 42.

Table 41: Dataset statistics for Stroke SERS Serum.

Dataset	Task	No. Classes	Samples	Features	Wavelength (cm^{-1})	License	Ref.
Stroke SERS Serum	Class.	2	4,020	724	200–2000	CC BY 4.0	[25]

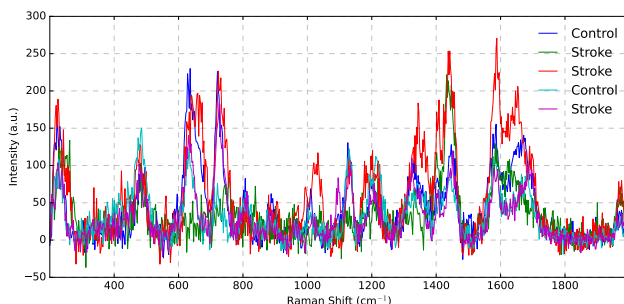


Figure 42: Representative SERS spectra from the Stroke Serum dataset showing 5 random samples.

A.14.4 Chemical & Industrial

Acetic Concentration [7] In-line Raman spectra from titration experiments for aqueous acetic acid systems, collected to demonstrate Indirect Hard Modeling (IHM) combined with Multivariate Curve Resolution (MCR) for quantifying dissociated carboxylic acid species [7]. The pKa values are estimated as part of the IHM calibration, which requires only ~ 4 calibration titrations, and IHM outperforms Partial Least Squares (PLS) for species discrimination. Two regression targets cover the acid (acetic acid, AA) and its conjugate base (acetate, AA^-) in varying proportions. Statistics are given in Table 42; representative spectra are shown in Fig. 43.

Table 42: Dataset statistics for Acetic Concentration.

Dataset	Task	No. Targets	Samples	Features	Wavelength (cm^{-1})	License	Ref.
Acetic Concentration	Regr.	2	42	11,084	100–3425	CC0 1.0	[7]

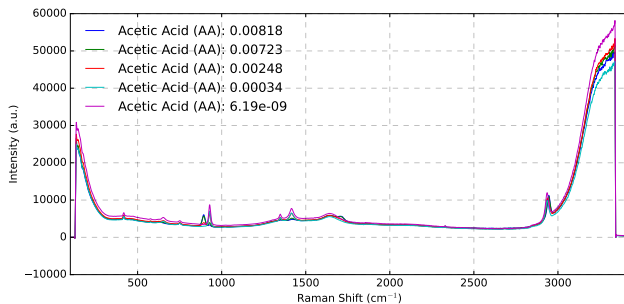
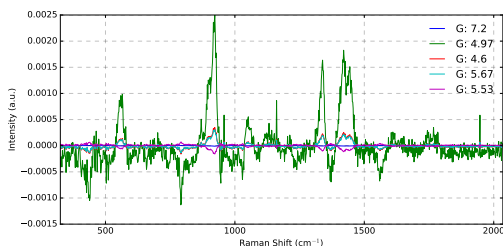


Figure 43: Representative Raman spectra from the Acetic Concentration dataset showing 5 random samples.

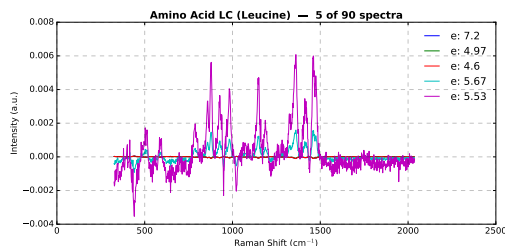
Amino Acid LC [88] Time-resolved Raman spectra collected during liquid chromatography (LC-Raman) elution of four amino acids (Glycine, Leucine, Phenylalanine, Tryptophan) using the vertical flow method, in which eluates flow past a Raman probe inside the column, enabling label-free analyte detection at millimolar concentrations in an H_2O /acetonitrile mobile-phase gradient [88]. Each amino acid constitutes a separate dataset of 90 spectra; the regression target is the elution concentration profile. Leucine and Phenylalanine are excluded from **RamanBench** due to failed learnability (see Section A.6); only Glycine and Tryptophan are included. The dataset license is not explicitly stated by the authors; we have contacted them for clarification (see <https://www.kaggle.com/datasets/sergioalejandrod/raman-spectroscopy/discussion/690923>). Statistics are given in Table 43; representative spectra are shown in Fig. 44.

Table 43: Dataset statistics for Amino Acids.

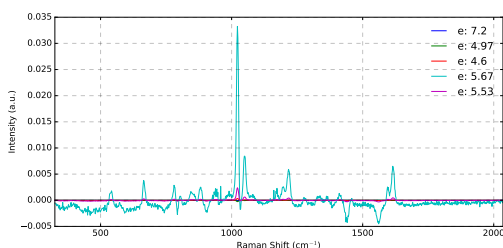
Dataset	Task	No. Targets	Samples	Features	Wavelength (cm^{-1})	License	Ref.
Glycine	Regr.	1	90	1,024	326–2035	Requested from authors	[88]
Tryptophan	Regr.	1	90	1,024	326–2035		



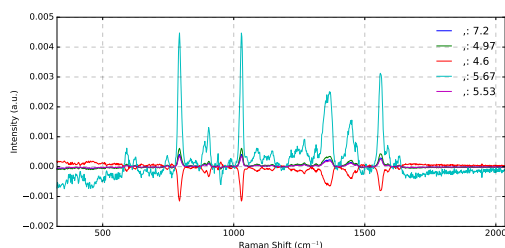
(a) Glycine



(b) Leucine



(c) Phenylalanine



(d) Tryptophan

Figure 44: Representative Raman spectra from the Amino Acid LC dataset, 5 random samples per amino acid.

Citric Concentration [7] In-line Raman spectra from titration experiments for aqueous citric acid systems, part of the same inline IHM+MCR multi-acid monitoring study as the Acetic, Formic, Itaconic, Levulinic, and Succinic Concentration datasets [7]. Two regression targets cover citric acid (CA) and its conjugate base (citrate, CA^-). Statistics are given in Table 44; representative spectra are shown in Fig. 45.

Table 44: Dataset statistics for Citric Concentration.

Dataset	Task	No. Targets	Samples	Features	Wavelength (cm^{-1})	License	Ref.
Citric Concentration	Regr.	2	45	11,084	100–3425	CC0 1.0	[7]

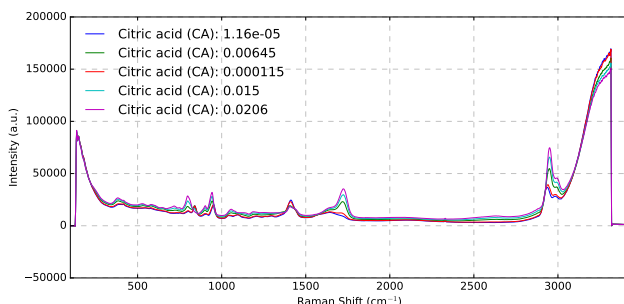


Figure 45: Representative Raman spectra from the Citric Concentration dataset showing 5 random samples.

Formic Concentration [7] In-line Raman spectra from titration experiments for aqueous formic acid systems, part of the IHM+MCR multi-acid inline monitoring study by Echtermeyer et al. [7], in which pKa estimation and species quantification from as few as ~ 4 calibration titrations were demonstrated. Three regression targets cover formic acid (FA), formate (FA^-), and water. Statistics are given in Table 45; representative spectra are shown in Fig. 46.

Table 45: Dataset statistics for Formic Concentration.

Dataset	Task	No. Targets	Samples	Features	Wavelength (cm^{-1})	License	Ref.
Formic Concentration	Regr.	3	24	11,084	100–3425	CC0 1.0	[7]

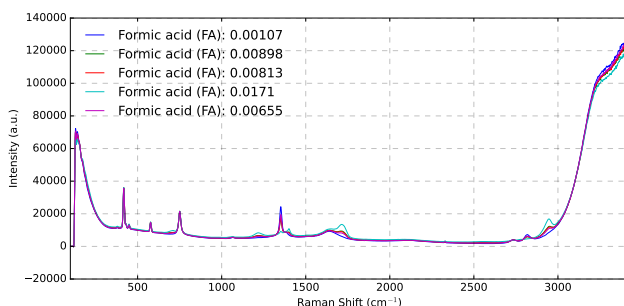


Figure 46: Representative Raman spectra from the Formic Concentration dataset showing 5 random samples.

Hair Dyes SERS SERS spectra of human hair colored with 33 commercial hair dyes from four brands (Ion, Wella, Clairol, L'Oréal), motivated by the lack of robust forensic methods for confirmatory identification of artificial colorants at crime scenes [89]. Gold nanorods (AuNRs) were deposited on hair samples and spectra were acquired with a TE-2000U Nikon inverted confocal microscope at

785 nm (1.8 mW, ~ 60 s acquisition); PLS-DA achieved 97 % average accuracy for individual colorant identification, with brand-level accuracy of 99.3–100 % and colorant-type accuracy (semi-permanent, demi-permanent, permanent) near 100 %. The dataset contains 1,713 spectra covering a broad fingerprint region; the classification target in **RamanBench** is the brand (4 classes: Ion, Wella, Clairol, L'Oréal). Statistics are given in Table 46; representative spectra are shown in Fig. 47.

Table 46: Dataset statistics for Hair Dyes SERS.

Dataset	Task	No. Classes	Samples	Features	Wavelength (cm^{-1})	License	Ref.
Hair Dyes SERS	Class.	4	1,713	1,340	309–1952	CC BY 4.0	[89]

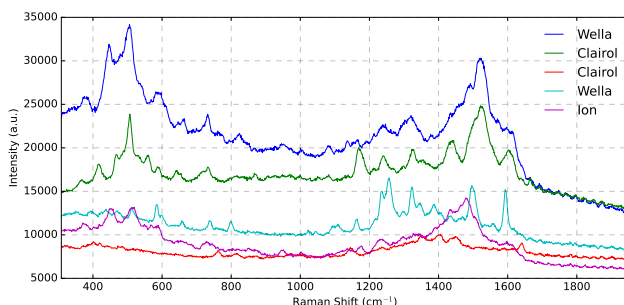


Figure 47: Representative SERS spectra from the Hair Dyes dataset showing 5 random samples.

Itaconic Concentration [7] This dataset contains in-line Raman spectra from titration experiments for aqueous itaconic acid systems [7]. Three regression targets cover itaconic acid (IA), itaconate 1 (IA^-), and itaconate 2 (IA^{2-}), each comprising 4 calibration titration levels. Statistics are given in Table 47; representative spectra are shown in Fig. 48.

Table 47: Dataset statistics for Itaconic Concentration.

Dataset	Task	No. Targets	Samples	Features	Wavelength (cm^{-1})	License	Ref.
Itaconic Concentration	Regr.	3	21	11,689	-37–3470	CC0 1.0	[7]

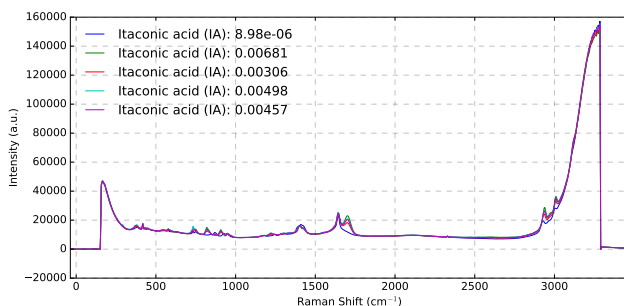


Figure 48: Representative Raman spectra from the Itaconic Concentration dataset showing 5 random samples.

Levulinic Concentration [7] This dataset contains in-line Raman spectra from titration experiments for aqueous levulinic acid systems [7]. Two regression targets cover pH and the mass of NaOH added during titration. Statistics are given in Table 48; representative spectra are shown in Fig. 49.

Table 48: Dataset statistics for Levulinic Concentration.

Dataset	Task	No. Targets	Samples	Features	Wavelength (cm ⁻¹)	License	Ref.
Levulinic Concentration	Regr.	2	36	11,084	100–3425	CC0 1.0	[7]

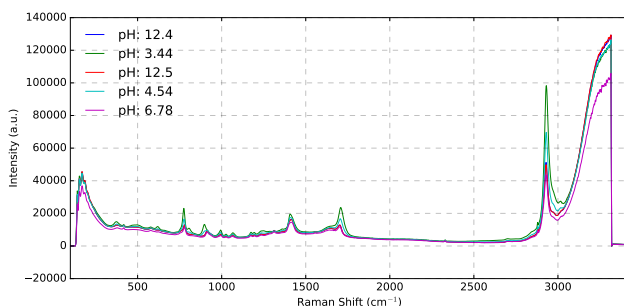


Figure 49: Representative Raman spectra from the Levulinic Concentration dataset showing 5 random samples.

Microgel Size [90] Raman spectra of 235 *N*-isopropylacrylamide (NIPAM) microgel samples with particle diameters ranging from 208 to 483 nm as determined by Dynamic Light Scattering (DLS), collected offline at 20 °C using a Kaiser RXN2 Raman Analyzer (40 s acquisition, cosmic-ray correction) [90]. The paper proposes nonlinear manifold learning workflows combining diffusion maps (DMAPs) with alternating DMAPs or Y-shaped conformal autoencoders, which substantially outperform PLS and IHM+PLS for polymer size prediction from Raman spectra. **RamanBench** includes 14 datasets across two spectral ranges (global: 100–3425 cm⁻¹; fingerprint: 800–1850 cm⁻¹). Statistics are given in Table 49; representative spectra are shown in Fig. 50.

Table 49: Dataset statistics for Microgel Size.

Dataset	Task	No. Targets	Samples	Features	Wavelength (cm ⁻¹)	License	Ref.
Lf Fingerprint	Regr.	1	235	3,500	800–1850	CC BY-NC 3.0	[90]
Lf Global	Regr.	1	235	11,084	100–3425		
Mm Lf Fingerprint	Regr.	1	235	3,166	850–1800		
Mm Lf Global	Regr.	1	235	11,084	100–3425		
Mm Rb Fingerprint	Regr.	1	235	3,500	800–1850		
Mm Rb Global	Regr.	1	235	11,084	100–3425		
Raw Fingerprint	Regr.	1	235	3,500	800–1850		
Raw Global	Regr.	1	235	11,084	100–3425		
Rb Fingerprint	Regr.	1	235	3,500	800–1850		
Rb Global	Regr.	1	235	11,084	100–3425		
Snv Lf Fingerprint	Regr.	1	235	3,500	800–1850		
Snv Lf Global	Regr.	1	235	11,084	100–3425		
Snv Rb Fingerprint	Regr.	1	235	3,500	800–1850		
Snv Rb Global	Regr.	1	235	11,084	100–3425		

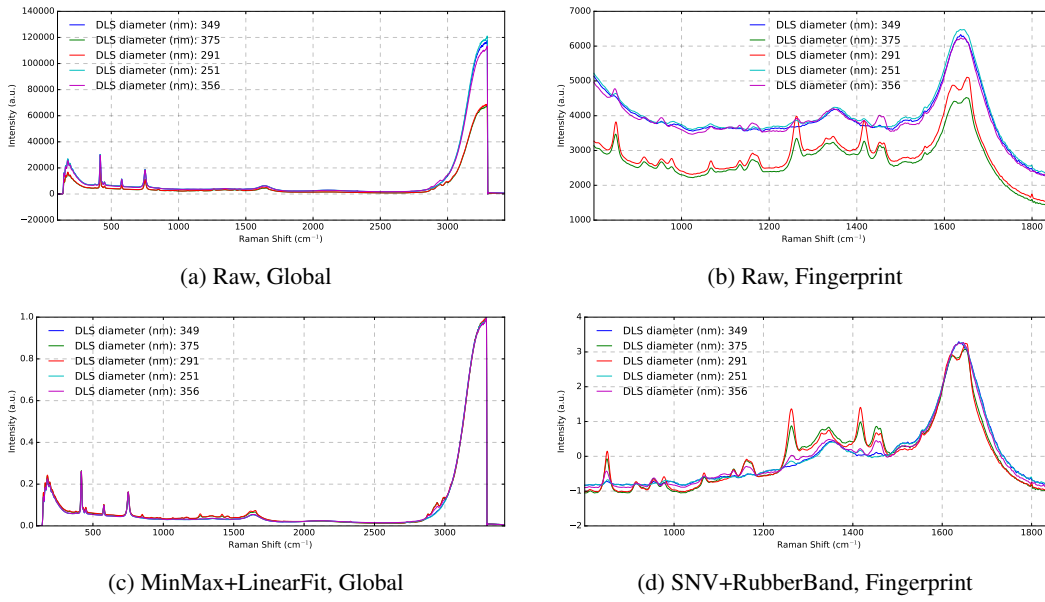


Figure 50: Representative Raman spectra from the Microgel Size dataset for four representative pre-treatment/range combinations, 5 random samples each.

Microgel Synthesis Flow vs. Batch [53] In-line Raman spectra from a tubular flow reactor monitoring the synthesis of *N*-isopropylacrylamide microgels under varying residence times and calibration strategies. This tiny dataset ($N = 14$) targets the microgel hydrodynamic radius as a single regression target. Statistics are given in Table 50; representative spectra are shown in Fig. 51.

Table 50: Dataset statistics for Microgel Synthesis Flow vs. Batch.

Dataset	Task	No. Targets	Samples	Features	Wavelength (cm ⁻¹)	License	Ref.
Microgel Synthesis Flow vs. Batch	Regr.	1	14	11,084	100–3425	CC BY 4.0	[53]

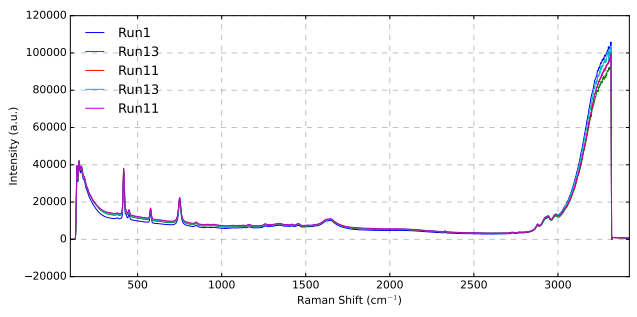


Figure 51: Representative Raman spectra from the Microgel Synthesis Flow vs. Batch dataset showing 5 random samples.

Microgel Synthesis in Flow [91] In-line Raman spectra from continuous-flow synthesis of NIPAM-based microgels in a tubular glass reactor, collected as part of a data-driven hardware-in-the-loop study using Thompson-sampling efficient multi-objective Bayesian optimization (TS-EMO) to simultaneously maximize product flow and achieve a targeted hydrodynamic radius of 100 nm [91]. Spectra were recorded with a Kaiser RXN2 Raman Analyzer (HoloGRAMS, 40 s acquisition, cosmic-ray correction); synthesis was controlled via initiator flow, monomer flow, CTAB surfactant concentration, and reactor temperature (60–80 °C). DLS-measured hydrodynamic radii at 20 °C and 50 °C serve as the regression targets. Statistics are given in Table 51; representative spectra are shown in Fig. 52.

Table 51: Dataset statistics for Microgel Synthesis in Flow.

Dataset	Task	No. Targets	Samples	Features	Wavelength (cm ⁻¹)	License	Ref.
Microgel Synthesis in Flow	Regr.	1	86	11,084	100–3425	CC BY 4.0	[91]

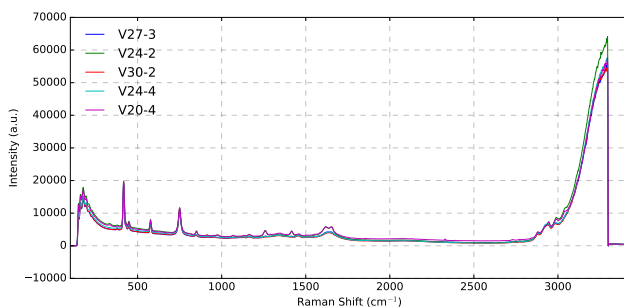


Figure 52: Representative Raman spectra from the Microgel Synthesis in Flow dataset showing 5 random samples.

Succinic Concentration [7] In-line Raman spectra from titration experiments for aqueous succinic acid systems [7]. Two regression targets cover pH and the mass of NaOH added during titration. Statistics are given in Table 52; representative spectra are shown in Fig. 53.

Table 52: Dataset statistics for Succinic Concentration.

Dataset	Task	No. Targets	Samples	Features	Wavelength (cm ⁻¹)	License	Ref.
Succinic Concentration	Regr.	2	70	11,567	-20–3450	CC0 1.0	[7]

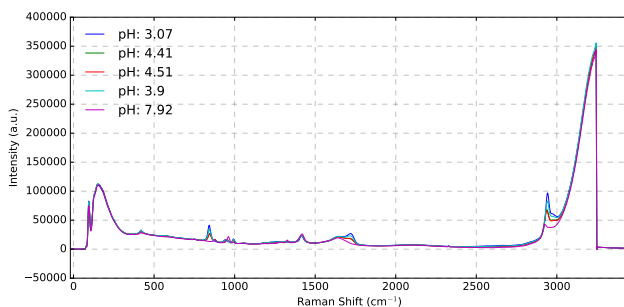
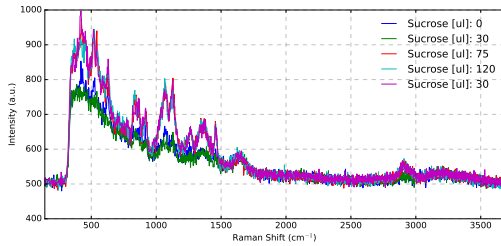


Figure 53: Representative Raman spectra from the Succinic Concentration dataset showing 5 random samples.

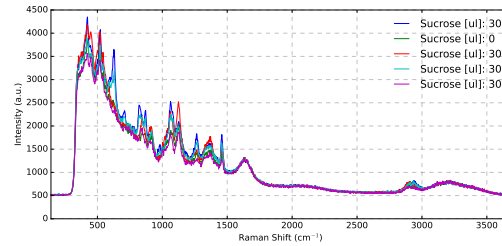
Sugar Mixtures [92] Aqueous mixtures of five components (sucrose, fructose, maltose, glucose, water) prepared in a 240-sample combinatorial library for benchmarking hyperspectral Raman unmixing methods [92]. Spectra were acquired on a custom Raman microspectroscopy platform at two integration times (5 s and 0.5 s) to produce high and low SNR conditions. Two datasets cover a high SNR (1,960 spectra) and low SNR (7,840 spectra) setting, with five concentration targets each; the water target is excluded from **RamanBench** due to failed learnability (see Section A.6), leaving four targets per dataset and eight regression targets in total. Statistics are given in Table 53; representative spectra are shown in Fig. 54.

Table 53: Dataset statistics for Sugar Mixtures.

Dataset	Task	No. Targets	Samples	Features	Wavelength (cm^{-1})	License	Ref.
High Snr	Regr.	4	1,960	2,000	142–3685	CC BY 4.0	[92]
Low Snr	Regr.	4	7,840	2,000	142–3685		



(a) Low SNR



(b) High SNR

Figure 54: Representative Raman spectra from the Sugar Mixtures dataset, 5 random samples per SNR subset.